INVESTIGATIONS OF THE

STRUCTURE–FUNCTION RELATIONSHIP OF

CRYPTOCHROME IN UNICELLULAR ORGANISMS

by

Hande Asımgil

A Thesis Submitted to the

Graduate School of Sciences and Engineering

in Partial Fulfillment of the Requirements for

the Degree of

Doctor of Philosophy

in

Material Science and Engineering

Koç University

December, 2012

Koç University

Graduate School of Sciences and Engineering

This is

To certify that I have examined this copy of Ph.D thesis by

Hande Asımgil

and have found that it is complete and satisfactory in all respects,

and

that any and all revisions required by the final

examining committee have been made.

Committee Members:

_____

İ. Halil Kavaklı, Ph. D.(Advisor)

_____

Özlem Keskin, Ph. D.

_____

Metin Türkay, Ph. D.

_____

Necla Birgül-İyison, Ph. D.

_____

Funda Şar, Ph. D.

Date: _____

To my lovely family …

ABSTRACT

Photoreceptors allow living organisms to gain information about their external world and thus adapt themselves and optimize their metabolism to changes in the nature. The photolyase/cryptochrome (PHR/CRY) family is a large and diversified gene family that encodes DNA repair enzymes and blue-light photoreceptors. They exist widespread in three kingdoms of life. There are 3 major categories of proteins represented by this family: 1) The cyclobutane pyrimidine dimer (CPD) Phr, 2) the [6-4] Phr, and 3) the cryptochromes (Cry). Photolyases are enzymes that utilize light energy for repair of UV lesion on DNA. Cryptochromes, in contrast, function as signaling molecules that regulate diverse biological responses such as entrainment of circadian rhythms in plants and animals. Nevertheless, the role of the Crys is ill-defined especially in unicellular organisms. From the evolutionary point of view, the Crys in such lower organisms hold the potential to be the ancestors of animal and plant cryptochromes. Hence, identification of new members of PHR/CRY family encoded by the genomes of different unicellular organisms is important to understand functional diversity of Cry family and also to know how structure influences cryptochrome function. Towards this aim, this dissertation concentrates on the analysis of structure-function and kinetics of cryptochromes in unicellular organisms via biochemical complementation and SPR spectroscopy methods. Here, seven new members of the PHR/CRY family of a red algae *Cyanidioschyzon merolae* were identified. Evolutionary relationships of algal Phr-like genes revealed that one gene is close to the [6-4] photolyase, three to the single strand DNA repairing subfamily of cryptochromes; called Cry-DASHes. Also, two plant type cryptochromes and one blue light photoreceptor as an independent clade between photolyase and plant type cryptochrome were found. Both, biochemical and complementation data provide evidence that *C. merolae* harbors two functional Cry-DASHes in addition to the one without DNA repair property. Functional characterization of photolyase/cryptochrome family from such a primitive algae provides insights into the evolution and the origin of plant cryptochrome lineages back

to early eukaryotes. Secondly, the repair kinetics of a *Vc*Cry-DASH and a *Vc*Phr were investigated using Surface Plasmon Resonance (SPR). To our knowledge for the first time, we quantified the affinity of *Vc*Cry-DASH to ssDNA and dsDNA containing CPD UV lesion. Moreover, we showed that DNA repair assays can be made by SPR spectroscopy by real time monitoring DNA repair.

ÖZET

Işık algı reseptörleri canlılarda çevreden gelen ışık bilgisini almakla görevlidirler. Canlılar, doğada gerçekleşen ışık değişimlerine kendilerini adapte edip, metabolizmalarını optimize ederler. Işık algı reseptörü olarak görev alan proteinleri kodlayan genlerden bir tanesi de fotoliyaza benzerlik gösteren kriptokrom proteinleridir. Genel olarak, fotoliyaz /kriptokrom genleri, DNA tamiri ve mavi ışık reseptörü olarak çalışan geniş ve farklılaşmış bir gen ailesidir. Bu aile yaşamın üç alemindeki canlılarda yaygın olarak bulunur. Üç ana kategoriden oluşan bu aile; 1) Siklobütan pirimidin dimer fotoliyaz (CPD-Fl), 2) [6-4] fotoliyaz ([6-4] Fl) ve 3) kriptokrom (Kri) proteinlerinden oluşur. Fotoliyazlar ışık enerjisini kullanarak DNA üstündeki ultraviyole ışının yarattığı hasarları tamir eden enzimlerdir. Buna karşın kriptokromlar, bitki ve hayvanlarda sirkadyen ritmi düzenlemek gibi çeşitli biyolojik olayları kontrol eden sinyal molekülleri olarak çalışırlar. Yüksek canlılarda fonksiyonları tanımlanmış olsa da, kriptokromların tek hücreli canlılardaki rolleri belirli değildir. Evrimsel açıdan bakıldığında, basit canlılardaki kriptokromlar bitki ve hayvanlardaki kriptokromların atası olabilme ihtimalini taşımaktadırlar. Sonuç olarak, fotoliyaz/kriptokrom ailesine ait genleri kodlayan tek hücreli genomlarından bu aileye ait yeni proteinler kodlayan genleri keşfetmek, kriptokromun yapı-işlev ilişkisini ve farklı canlılarda farklı fonksiyonlara sahip olabilmesinin altında yatan yapısal değişiklikleri anlamak açısından önem taşır. Bu amaçla, bu tezde tek hücreli canlılarda bulunan kriptokromlar yapı-işlev ve kinetik ilişkisi yönünden biyokimyasal, komplementasyon ve yüzey plasmon rezonans spektroskopi yöntemleri kullanılarak incelenmiştir. Bu çalışmada, bir kırmızı alg olan *Cyanidioschyzon merolae*'ye ait fotoliyaz/kriptokrom ailesine ait yedi tane yeni gen tanımlanmıştır. Filogenetik sınıflandırmada kırmızı alge ait fotoliyaz benzeri bu genlerden bir tanesi [6-4] fotoliyaza benzerlik gösterir. Üç tanesi tek zincir DNA üstündeki UV ışının yarattığı hasarları tamir eden ve kriptokromun alt bir grubu olarak sayılan KRİ-DASH proteinleriyle aynı ailedendirler. Bunun yanında iki tane genin bitki kriptokromlarıyla

sınıflandığı ve son olarak bir tanesinin de bitki kriptokromuyla fotoliyaz arasında bağımsız olarak evrimleştiği belirlenmiştir. Biyokimyasal ve komplementasyon verileri *C. merolae*'nin iki tane işlevsel Kri-DASH proteinine ve bir tane de DNA tamir işlevi olmayan Kri-DASH'e sahip olduğunu kanıtlamıştır. Fotoliyaz/kriptokrom ailesine ait olan ve ilkel bir canlıda bulunan bu yeni fotoliyaz/kriptokrom benzeri genler için yapılan böyle bir fonksiyonel karakterizasyon çalışması, bitki kriptokrom ailesinin ilk ökaryotlardan itibaren oluşumuna, orijinine ve evrimine ışık tutması açısından önemlidir. İkinci olarak, bu tezde *V.cholerae* Kriptokrom-DASH ve *V.cholerae* Fotoliyaz enzimlerinin DNA tamiri kinetiği yüzey plazmon rezonans spektroskopisi ile incelenmiştir. Bildiğimiz kadarıyla ilk defa bu çalışmayla *V.cholerae* Kriptokrom-DASH'in siklobutan pirimidin dimer içeren tek zincir ve çift zincir DNA'ya olan bağlanma isteği sayısal olarak ölçülmüştür. Buna ek olarak, DNA tamir deneylerinin, yine bu çalışmada ilk defa, yüzey plazmon rezonans spektroskopisi tekniği ile gerçek zamanlı olarak gözlenebildiği gösterilmiştir.

ACKNOWLEDGEMENTS

I consider it an honor to work with all my colleaques in Prof.Kavaklı's lab during my doctoral study. I am very thankful to Natali Özber for her genuinity, invaluable advises and her friendship. First few years of my Ph.D were easier and more enjoyable with you and Gökhan Hatipoğlu. Acknowledgement section would be incomplete if I would not mention Şule Özdaş and Seda Kılınç Avşaroğlu. I would like thank them for their willingness to help me any time and surely for their nice friendship. I am grateful to my friend Dr. İbrahim Barış who I consulted in the first place whenever I had questions about academic issues. Many thanks go to all the members of Prof. Kavaklı Research group, Kaan Koper, Elif Muku, Ehsan Sarayloo, and Mehmet Tardu, İbrahim Gür, Oytun Aygün, Onur Dağlıyan, Onur Öztaş and Bilal Çakır. It was a pleasure for me to get to know them and to have a chance to work with them.

Lastly, I am deeply thankful to my lovely friends and also my colleagues Selma Bulut and Bengisu Seferoğlu. Two of you have become like sisters to me. During writing this dissertation, without your moral and mental support, everything would be much more difficult for me but you turned it to unforgettable and enjoyable moments. I feel so lucky to have both of you.

Last but not the least, I dedicate my dissertation to my lovely family, my father Zeki Asımgil, my mother Ümran Asımgil and my sister Merve who always stand behind me and my decisions. They have tried to give me the best of everything so I feel special and lucky. Their support, love and trust always make me feel strong enough to pursue whatever I want to do. I also dedicate this thesis to my grandfather Abdullah Asımgil and my grandmother Sevim Aksu who always proud of me and wanted to see me as a doctor.

TABLE OF CONTENTS

LIST OF TABLES

LIST OF FIGURES

NOMENCLATURE

[6-4] PP	[6-4] photoproduct
8-HDF	8-hydroxy-7, 8-didemethyl-5-deazariboflavin
BLUF	Blue Light Using FAD
BMAL	Arnt-like protein-1
CRY	Cryptochrome
Cm	*Cyanidioschyzon merolae*
CPD	Cyclobutane pyrimidine dimer
CLOCK	Circadian Locomotor Output Cycles Kaput
CYC	CYCLE protein
DNA	Deoxyribonucleic acid
EMSA	Electro Mobility Shift Assay
FAD	Flavin Adenine Dinucleotide
FRET	Forster Resonance Energy Transform
GABA	Gamma-AminoButyric Acid
K_d	Equilibrium dissociation constant
LOV	Light-Oxygen-Violet
MTHF	5, 10-Methylenetetrahydrofolate
PER	Period protein
PHR	Photolyase
PHY	Phytochrome
PYP	Photoactive Yellow Protein
Pyr<>Pyr	Pyrimidine-Pyrimidine dimer
RHT	*Retinohypothalamic Tract*
RU	Response/Resonance Unit
SCN	Supra Chiasmatic Nucleus
SPR	Surface Plasmon Resonance
TIM	Timeless protein
UVR	Ultraviolet radiation

Vc	*Vibrio cholera*
VP	Vasopressin
VIP	Vasoactive intestinal peptide

Chapter 1

INTRODUCTION

Photoreceptors allow living organisms to gain information about their external world and thus to optimize their metabolism by percepting of light in the natural environment. There are three main types of photoreceptor families that can sense different ranges of wavelengths in the visible spectrum. These are grouped as blue light, green light and red/far-red light sensing photoreceptors. The organisms in all biological kingdoms evolved to sense and response to the wavelengths in the blue region of the optical spectrum by a number of blue light photoreceptors that act as the environmental sensors and the signaling molecules controlling diverse biological responses. Photolyases and cryptochromes constitute one of the major blue-light sensing protein families that exist in almost all domains of life. The photolyase/cryptochrome family is a large and diversified gene family that encodes blue-light photoreceptors found in the biological kingdoms, from archaebacteria to mammals. There are 3 major categories of proteins represented by this family; 1) The cyclobutane pyrimidine dimer (CPD) photolyases, 2) the [6-4] photolyases, and 3) the cryptochromes (CRY). Photolyases are enzymes that utilize light energy for repair of UV-damaged DNA i.e, either of [6-4] photoproducts or of cyclobutane pyrimidine dimers. Cryptochromes, in contrast, function as signaling molecules that regulate diverse biological responses such as entrainment of circadian rhythms in animals and the growth and development in plants.

Aforementioned the roles of CRYs are not well-defined especially in unicellular organisms. From the evolutionary point of view, the cryptochromes in such lower organisms holds the potential to be the ancestors of CRYs of higher organisms that could provide more insight about structure-function relationship of CRYs. Presently, only few studies on the roles of cryptochromes of unicellular organisms are available and they open up a debate related to dual or triple functions cryptochromes [1, 2] [3].

Hence, the identification of the new members of PHR/CRY family that are encoded by the genomes of different unicellular organisms is important to understand functional differentiation during evolution and the diversity of cryptochrome in the nature.

This dissertation focuses on the analyses of structure-function and the kinetics of cryptochromes from a prokaryotic bacterium and from a photosynthetic eukaryote via biochemical, complementation and SPR spectroscopy methods.The dissertation consists of independent chapters; however, all the chapters attempt to provide more insights on the role and kinetics of cryptochromes that may serve as pioneering model for all cryptochrome proteins.

The outline of this dissertation is as follows:

Chapter 3 includes the analyses of real-time interactions between *Vibrio cholerae* Cry-DASH (*Vc*Cry-DASH) and ss/dsDNA as well as the interactions between *Vibrio cholerae* photolyase (*Vc*Phr) and ss/dsDNA using Surface Plasmon Resonance (SPR). The interactions were then characterized and compared in order to investigate the effect of different types of flavoprotein on UV damaged ss/dsDNA.

Chapter 4 covers the study in which new genes belonging to PHR/CRY family were discovered in one of the most primitive unicellular organism and characterized using biochemical and complementation approaches.

Chapter 5 comprehends the results that are put forward in this dissertation and the major conclusions about the topics as well as the future directions.

Chapter 2

LITERATURE REVIEW

Sun light is the ultimate source of energy on the Earth and influences all aspects of life directly or indirectly by regulating various processes at molecular level. Therefore, the living organisms must adapt themselves to environmental conditions and sense the visible light through proteins called photoreceptors. Photoreceptors allow living organisms to gain information about their external world and thus to optimize their metabolism by receiving light input from the natural environment. Such that, the living organisms should perceive light to avoid and reverse the harmful effects of light, to adapt themselves to the available light conditions for growth, develop and reproduce as well as to make orientation, movement and migration. There are different photoreceptors that can sense different ranges of the visible spectrum. Red/far- red light are sensed by phytochrome receptors that mediate variety of biological processes from phototaxis, pigmentation in cyanobacteria and eubacteria, as well as photomorphogenesis, chloroplast movement in plants and algae. Green light is sensed by rhodopsins in vertebrate's retina and a novel phytochrome like chromoprotein called cyanochromes sensing green light is found in cyanobacteria that might be a hybrid receptor integrating light and hormone signals[4]. The organisms also evolved to sense and response to the wavelengths in the blue visible region of electromagnetic spectrum. There are a number of blue light sensing proteins which include primarily; photoactive yellow protein (PYP), blue light using FAD domain (BLUF), light, oxygen and voltage sensing LOV domain and the photolyase/cryptochrome family [5]. All these photoreceptors have arisen in living organisms to survive and adapt themselves as a result of selective pressure of the solar irradiation in the beginnings of life on the Earth. Photolyases and cryptochromes constitute one of the major blue-light protein families existing in almost all domains of life.

2.1 Photolyase

Ultraviolet light (UV) (200-300nm) is the primary cause of mutations on DNA which result in inhibition of replication, transcription, translation. The misreplicated and mismatched photolesions on DNA are prone to develop skin cancer in human [6]. Photolyases are found in most prokaryotes and in eukaryotes. Also, there are some certain viruses whose genome encodes putative photolyases. Upon UV irradiation, the adjacent pyrimidines on one strand of DNA can form four types of dimers as shown in Figure 2.1; thymine-thymine cyclobutane dimers can be formed as two isoforms; Cis-Syn and Trans-syn-I, the other types of dimers are [6-4] photoproducts ([6-4]PP) and its DEWAR isomer [7]. Cis-Syn and Trans-syn-I isomers together constitute approximately 80-90% and [6-4] PP's constitute 20-10% of total photoproducts and all photoproducts cause large structural distortions in DNA. Several molecular mechanisms are available in a cell to repair or remove Pyr<>Pyr dimers such as nucleotide excision repair and base excision repair systems. Yet, those mechanisms provide indirect elimination of DNA lesions. Only DNA photolyase enzyme directly repairs photoproducts on DNA through photoreactivation process.

DNA photolyase (EC 4.1.99.3) carries out *in situ* repair of UV lesions by using the blue light as energy source. Photolyase has higher binding affinity to a DNA damaged site than to an undamaged site due to the bending of DNA towards the major groove and it binds to a photolesion site light independent manner. Photoreactivation process starts with the available blue light in the environment. The DNA bound enzyme uses blue light (320-600nm) photon energy to convert cyclobutane dimer into two separate pyrimidines [8, 9].

Photolyase enzyme was first found by Rupert et al in 1950's as a DNA photoreactivating enzyme in *E.coli* [8]. This enzyme was found to repair only cyclobutane pyrimidine dimer (CPD) which is the major photolesion caused by UV irradiation but not [6-4] product. Forty years later, another enzyme was identified for

the repair of second major photolesion, [6-4] pyrimidine-pyrimidone photoproduct, and called [6-4] photolyase [10]. In literature, the term "photolyase" is generally used for CPD photolyase unless stated.

From an evolutionary point of view, all photolyases are hypothesized to have arisen from a single ancestor of CPD photolyase due to its existence in viruses, archae, eubacteria, parasites and eukaryotes. This ancestral protein gave rise to other subgroups (Class I, Class II and Class III) of photolyases. In an evolutionary development, Class I CPD photolyase evolved to [6-4] photolyase.
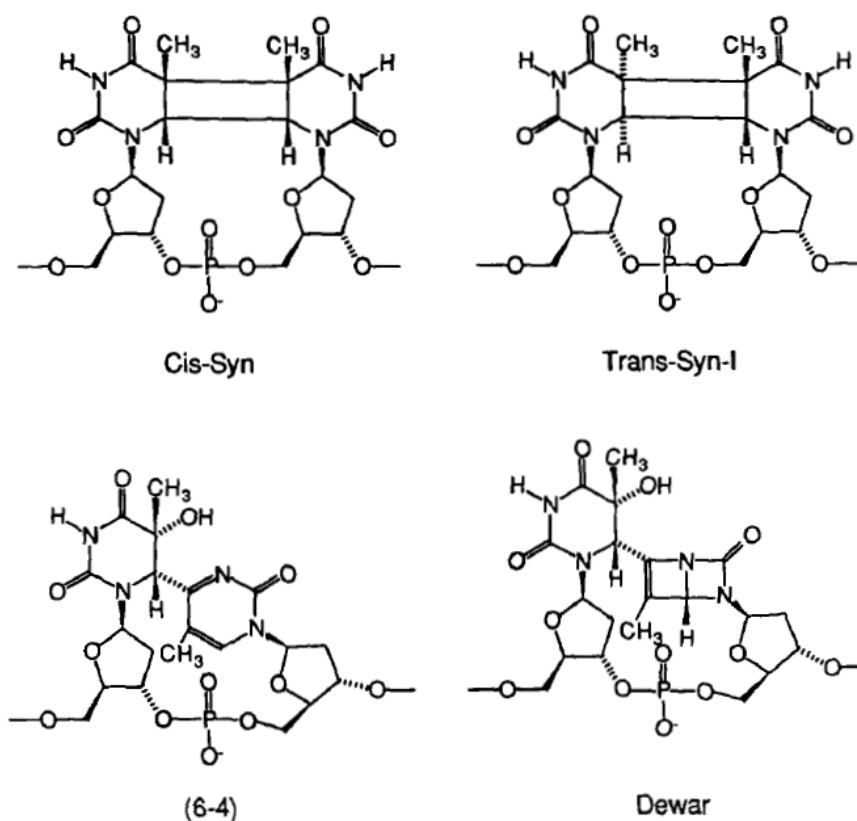
Figure 2.1 The structures of UV caused photoproducts on DNA. UV light causes the formation of cyclobutane thymine dimers by inducing the bond generation between the atoms C5-C5 and C6-C6 majorly in cis-Syn and Trans-Syn-I isoforms. 20% UV lesions

are formed as [6-4] thymine pyrimidine pyrimidone photoproduct which can sometimes converted to Dewar valence isomer by UV-B irradiation [7]

2.1.1 CPD Photolyase

CPD photolyase is a 45−70 kDa monomeric protein. It bounds to two chromophore/cofactors noncovalently. One of them is flavin adenine dinucleotide (FAD) that is the catalytic cofactor for photoreactivation process and it always existed in almost all identified photolyases. The second chromophore called photoantenna is either methenyltetrahydrofolate (MTHF) or 8-hydroxy-7, 8-didemethyl-5-deazariboflavin (8-HDF). Based on the type of the second chromophore, CPD photolyases have been classified into two categories as deazaflavin and folate classes. Photolyases can be further classified according to primary amino acid sequences. To date, there are three subfamilies identified in photolyase family. The proteins in all subfamilies are able to repair CPD lesions but the kingdoms they exist frequently are different. Class I photolyases are mostly found in microbial organisms, Class II photolyases are identified mostly in higher organisms; animals and plants [11]. In recent studies, another class was defined as Class III mostly in bacteria which is more likely the ancestor of plant cryptochromes.

CPD photolyases have been studied extensively over 50 years from different sources. Therefore, the crystal structure and the photoreactivation mechanism of are available. Structures of a number of CPD photolyases isolated from various sources have been determined by X-ray crystallography. Three-dimensional structures of the studied photolyases are highly similar but the conserved motifs in DNA binding sites among classes exhibit differences such as the conserved motifs in Class I are not retained in ClassII [9, 12, 13]. The more genome sequences are revealed, the more classes of photolyase with distintive properties are being exploitable. Recently, a new sequence of photolyase with unique Fe-S chromophore was identified in 350 bacterial organisms including plant and animal pathogens [14].

In addition to DNA repair function, photolyase is found to have 'dark function' which involves in repair of UV lesion by recruiting the other repair proteins at dark. Indeed, UvrABC excision repair mechanism of *E.coli* is stimulated by the binding of *E.coli* photolyase to DNA damage site at dark [15].

E.coli photolyase is a well-studied enyzme among all other photolyases. Conserved domains, 3-D structure, chromophore/cofactor content, photochemistry and photoreactivation mechanism of *Ec*Phr are accesible in the literature which draw a general frame for other photolyases. In the same chapter in the Ssection 2.3, the structural and photochemical properties of CPD photolyases will be presented in detail based on *Ec*Phr studies.

2.1.2 [6-4] Photolyase

[6-4] photoproduct lesions are the second major DNA lesions generated upon UV irradiation. [6-4]PP's are formed through the binding of C4 carbonyl of a pyrimidine with the C5–C6 double bond of a neighboring pyrimidine via photoaddition. Figure 2.1C shows the chemical stucture of [6-4] pyrimidine-pyrimidone photoproduct due to the generation of C4-C6 bonds between adjacent thymines. In the cell, those [6-4]PPs are removed by nucleotide excision repair and direct photoreactivation mechanism [11]. [6-4] photolyase (EC 4.1.99.13) plays a role in direct photoreversal of [6-4] pyrimidine–pyrimidone photoproducts. Primary amino acid sequence of [6-4] photolyase exhibits %20-25 similarity to CPD photolyase but it has distinctive substrate speficity.

[6-4] photolyase was identified in *Drosophila melagonaster* (fruit fly) by Todo et al. in 1993 [10]. Later, [6-4] photolyases have been found in a number of eukaryotic organisms including *Arabidopsis thaliana, Xenopus laevis, Gallus gallus, Danio rerio, Anophele gambia, Dunaliella salina* [16]. In contrast, [6-4] photolyase in prokaryotes have not been functionally identified yet. Therefore, the existence of [6-4] Phr is mostly restricted to higher eukaryotic organisms such as plants and animals [17-20].

During evolution, [6-4] photolyases are assumed to evolve to cryptochromes by gene duplication events since these two proteins share a high degree of homology by 40-60%

similarity. However, Cry's lost the DNA repair feature while evolving to a signaling molecule [21]. In the next section, cryptochromes will be explained in detail.

2.2 Cryptochrome

The living organisms from bacteria to human have been evolve to synchronize their metabolism to the 24-hour of solar day to anticipate daily and seasonal changes so that they optimize their energy to find food, mate and survive. The rhythmic changes in the physiology, behaviour and biochemistry of an organism with an approximately 24-hour period are called endogenous circadian rhythm. Each organism has a slightly different period of endogenous rhythm. In human, the endogenous clock sustains a period of almost 24.5 hours whereas mice have 23.4 hours. For that reason, each endogenous circadian oscillator is synchronized (entrained) by light stimulus to light/dark cycles of solar day by a photoreceptor.

The presence of several photoreceptor families allows the correct interpretation of different light cues from the Sun. Blue light is the major stimulus that allows the circadian clocks to tune (entrain) themselves to exact 24-hour solar day rhythm. For more than a century, biological response of the plants to blue light has taken interest of the biologists after Charles Darwin (1881) showed that plants did not respond to red light but to blue light [22].

Flavoproteins with an action spectrum that overlaps with blue light responses of plants are the most probable candidates for the regulation of blue light dependent changes in physiology and behaviour. A gene called *hy4* that expresses flavoprotein was identified in *Arabidopsis thaliana* [23]. HY4 protein was showing homology to bacterial photolyase enzyme but it was unable to repair DNA. HY4 then renamed as cryptochrome1 (CRY) that function as a blue light photoreceptor which mediates blue light responses in plants [23, 24].

Cryptochromes are proteins involved in the regulation of diverse biological responses in various organisms. They play role in the regulation of circadian rhythm in plants and animals as blue light photoreceptor and function as transcriptional repressor in

mammals. Cryptochromes are flavin containing proteins that exhibit 25-40% sequence identity to [6-4] photolyases. In terms of primary amino acid structure and photoactive pigment content, cryptochromes are very similar to photolyases. Only difference is their 50-250 amino acid long, unstructured C-terminal extension. Cryptochromes do not possess DNA repair function, instead these proteins have gained novel functions throughout evolution in various organisms [25] and the C-terminal tail is believed to have roles in signal transduction and protein-protein interactions [26].

Most of the knowledge about the function of cyptochromes acquired from the genetic studies of many organisms from bacteria to human. As there is a lack of direct biochemical analysis that can determine CRY function directly *in vivo* or *in vitro*. Based on the sequence homology, cryptochromes from a range of organisms are classified into three subfamilies; plant cryptochromes (Cry1, Cry2, and homologs), animal cryptochromes (insect- type I, mammalian- type II), and cryptochrome-DASH proteins. Those subgroups of cryptochrome are believed to have arisen from the separate photolyase ancestors [26]. Indeed, CRY-DASH may be the intermediate form between photolyase and cryptochrome due to its structural and photochemical properties highly similar to photolyases but it cannot repair DNA. It may play a role in signaling [17, 27].

Genetic studies showed that plant cryptochromes are blue light photoreceptors and they regulate plant growth and development. They have widespread and divergent roles in plants such as pigment production, flowering, hormone signaling, defense response, stress response, photosynthesis, and metabolism. As a circadian photoreceptor, they also involve in the signal transduction cascade for plant circadian clock [28, 29].

Animal cryptochromes are divided into two distinct groups based on their function in circadian clock. Insect type I cryptochrome functions as circadian photoreceptor and directly involves in the regulation of circadian rhythm at molecular level. Whereas mammalian type II cryptochrome is one of the main components of core circadian clock mechanism but not directly involve in photoreception, instead it plays a role as transcriptional repressor in circadian clock [26, 30]. In human, circadian rhythm is regulated by a region in the brain called Supra Chiasmatic Nuclei (SCN). It consists of

20,000 neuronal cells that lie in either side of the brain near hypothalamus. SCN controls master clock which receives blue light signal by such a signal transduction mechanism that blue light coming to the retina is perceived by photosensitive retinal ganglion cells retaining specialized photoreceptor molecules. Then, the light signal is projected to SCN via retinohypothalamic tract (RHT) via PACAP, glutamate. The cells in the core region in SCN start to synchronize and send neuronal signals like GABA and VP to the other cells in the shell region of SCN.

Rhythmic synchronization of all SCN cells result in the release of both neuronal and humoral output signals that are sent to other sides of the brain and the peripheral organs through GABA, VP,VIP,PK, Glutamate [31]. Thus, physiology, behavior and biochemistry of the whole body are synchronized with day/night cycles such that the enzymatic activities of internal organs, beat rate of heart, renal functions, glucogenesis, and insulin secretion and so on show rhythmic oscillations. In figure 2.2, signal transduction of light input from retina to peripheral organs is shown. SCN that receives light signal sustain human circadian rhythm through neuronal and humoral signal.

Apart from master clock, almost all organs such as liver, kidney, heart and skin have an individual endogenous clock called "the peripheral clock" and the circadian rhythm of each organ or tissue is influenced by the metabolic cues including feeding, body temperature, and social activity in addition to humoral and neuronal signals coming from the main oscillator, SCN that synchronize the whole body [32].

The third class is DASH type cryptochromes that arer found in both prokaryotes and eukaryotes. It is structurally and photochemically very similar to photolyase. Interestingly, this protein subfamily is able to repair single stranded DNA *in vitro* whose physiological relevance is undetermined [33]. However, it is believed that CRY-DASH play a role in signaling but has not been clearly identified, yet. It is probable that DASH group may be an evolutionarily intermediate form between cryptochromes and photolyases.

In recent years, cryptochromes have been proposed to be the most probable candidate molecules that can sense magnetic field of the Earth in migratory birds. It is known that

that the birds and butterflies use magnetic compass to find their way during migration. Unlike the other magnetoreception mechanisms, the birds' magnetic orientation is shown to be wavelength dependent and their migratory behavior can only be sustained by blue light but not red light [34]. Besides, of the known photoreceptors in birds and in other magnetosensitive animals, only cryptochromes are known to form the radical pair molecule that is magneto- sensitive and responsive to the Earth's magnetic compass. It has been proposed that during the photoreductive process of FADox to FADH^o through the protein's electron transfer pathway, the magnetic field of the Earth can interact with the radical pair state of FAD. Indeed, the lifetime of radical pair state should be longer than hundreds of nanosecond to sense the magnetic field and the avian CRY is theoretically met the criteria for magnetosensation. Therefore, avian CRY is suggested to have such kind of signaling and magnetosensory mechanisms [35, 36]. In fruit flies and plants, it was experimentally proved that cryptochromes involved in magnetoreception [33, 37]. Interestingly, a recent study of Reppert et. al, showed that human cryptochrome could also sense magnetic field in a light dependent manner when over-expressed in the retina of fruit fly [38]. This result may also challenge generally accepted view that hCRY2 that is highly expressed in human retina is not a photoreceptors [39].
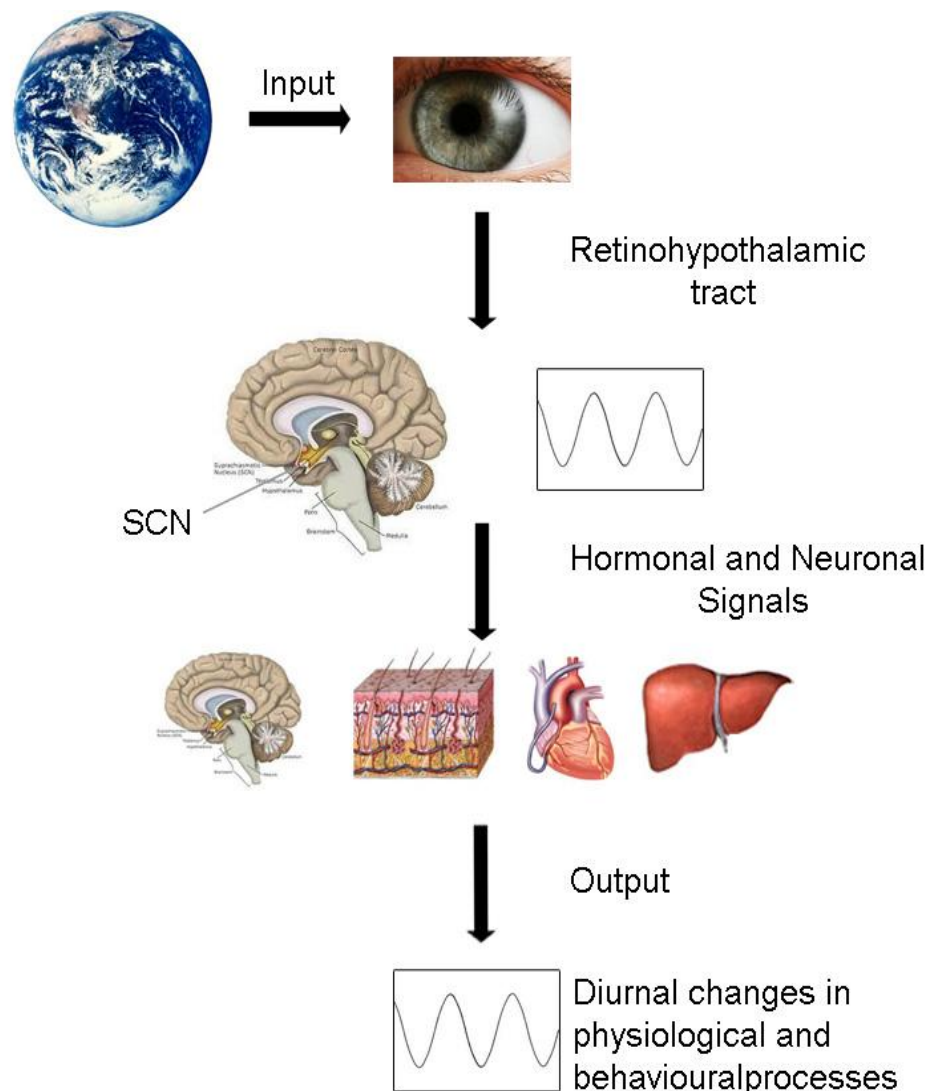
Figure 2.2 Signaling pathway of human circadian clock. Light input is received by the retinal ganglion cells in the retina of human eye. Light signal is projected to SCN in the brain through retinohypothalamic tract. Clock gene expressions start to oscillate and SCN cells synchronized. Then SCN cells send signals to the other part of the brain via neurotransmitters. Peripheral organs and the brain are synchronized to daily changes on the Earth by humoral and neuronal signals. Figure is adapted from Geyfman et al, 2009 [40] .

2.2.1 Plant Cryptochrome

The plants are very sensitive to daily and seasonal environmental light cues. Photoreceptors are playing a vital role in the survival and adaptation of plants. Blue light reception by cryptochrome results in the activation of many genes including transcriptional factors related to photomorphogenesis, flowering, leaf movement, photosynthesis that gives a plant selective advantage.

Plant cryptochromes are 70–80-kDa proteins with two recognizable domains, an N-terminal PHR domain that shares sequence homology with photolyases, and a C-terminal extension that shows little sequence similarity to any known protein domain [41]. First plant cryptochrome was identified in *Arabidopsis thaliana* (*At*CRY1) when *hy4* mutant showed inhibited hypocotyl elongation was rescued by *hy4/CRY1* gene under blue light during development [24]. Physiologically, *At*CRY1 was determined to regulate photomorphogenesis in *Arabidopsis*. Another homolog of *AtCRY1* called *At*CRY2 was also identified based on sequence similarity. *At*CRY2 structurally differs from *At*CRY1 with its shorter and poorly conserved C-terminal tail (120 amino acids) [23]. Functionally, both CRY proteins mediate numerous blue light induced responses including inhibition of hypocotyl elongation, increase in anthocyanin production, de-etiolation and photoperiodic flowering etc, [24, 42]. Genetic studies carried out with single $Cry1^{-/-}$ and $Cry2^{-/-}$ mutants and double $Cry1^{-/-}/Cry2^{-/-}$ mutants of *Arabidopsis thaliana* revealed that photomorphogenic responses are regulated by both cryptochromes that act redundantly. However, CRY2 also undertakes distinct roles such as the initiation of flowering response [43]. In addition, stabilities and sensitivities of these two receptors to different intensities of blue light are very different. CRY2 senses and mediates the responses to blue light at low intensities (up to 5 $\mu m^{-2}\,s^{-1}$) after which the protein undergoes blue light dependent phosphorylation and degradation whereas CRY1 remains stable and senses higher intensities (approximately 80-100 $\mu m^{-2}\,s^{-1}$) [27, 44]. Even though most of the knowledge about plant cryptochromes have been established from *Arabidopsis* studies, numerous plant type cryptochromes are being identified from various plants including tomato[45], rice[46], and pea [47]. Actually,

they contain several cryptochromes; for instance, tomato harbours three, rice has two cryptochromes. The roles of CRY1 in those plants are similar to the function of *At*CRY1 which regulates growth and development. Also, the CRY2s in other plants mediate the induction of flowering like in *Arabidopsis* [48]. Figure 2.3 summarizes the function of plant CRYs. In the figure, CRY is shown to regulate hypocotyl elongation, seedling development and flowering by transducing blue light signal and inducing the expression of related genes as well as by changing the stability of the proteins it interacts with.

An endogenous circadian clock helps the plants to anticipate daily and seasonal rhythmic changes and gives them an adaptive advantage depending on the incoming light intensity. Photoentrainment of circadian clock was initially thought to be carried out by cryptochromes since a study in *Arabidopsis* showed that *At*CRY mediated the shortening of the period length in the constant light conditions [28]. Nevertheless, genetic studies carried out by double Cry mutants indicated that plant cryptochromes do not play an essential rhythmic and central role in clock oscillatory mechanism, since double Cry mutants were fully conditioned [49]. Plant CRY1 and CRY2 are nuclear proteins but they do not activate gene expression directly because they are unable to bind DNA [50]. Instead, they exert their effects by mediating protein-protein interactions, blue light dependent posttranslational modifications and by the induction of certain genes. In *Arabidopsis*, the gene expression of many transcription factors induced in high light stress like APX, and ELIP1/2 and CO, flowering associated transcription factors, are induced through plant CRYs [29, 44, 51]. Also, flowering is regulated by the interaction of *At*CRY2 with red light receptor phytochrome (PHY) and its upstream regulators like COP1 and SPA [29, 52-54]. Furthermore, posttranslational modifications; phosphorylation, ubiquitylation of plant CRYs lead to function and /or degradation of the CRYs themselves or their interacting proteins.
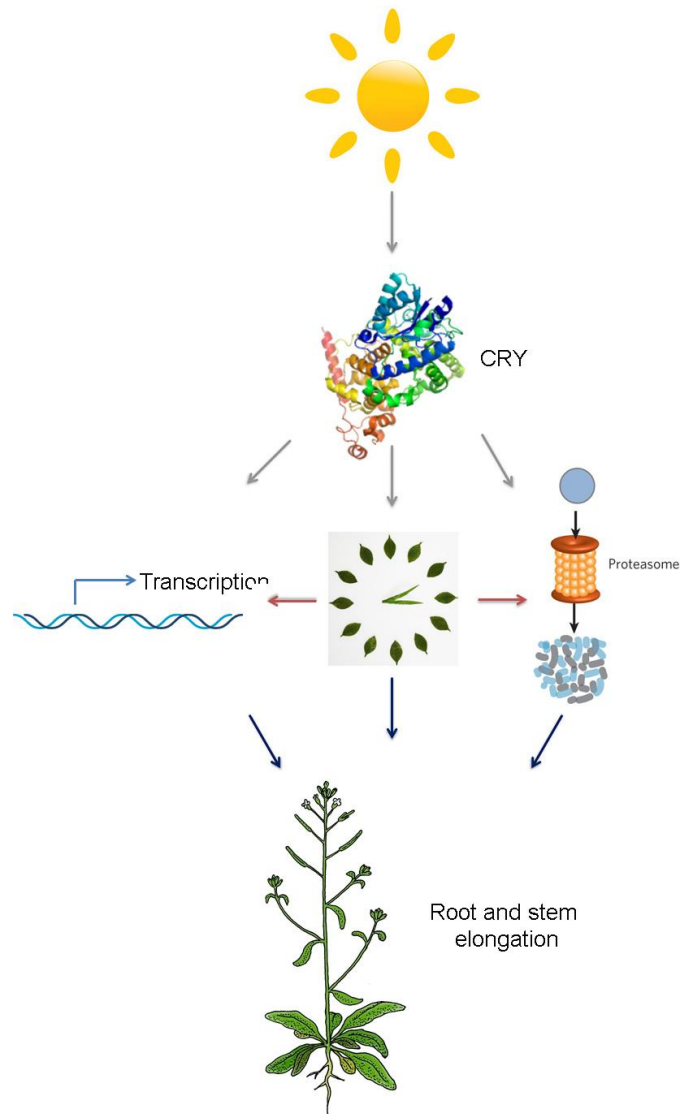
Figure 2.3 Schematic diagram for the functioning mechanism of plant CRYs. They sense sun light and regulate growth and development by activating the associated transcription factors or undergo proteosomal degradation depending on the circadian rhythm or the intensity of incoming light to the plant.

2.2.2 Animal Cryptochrome

Animal cryptochrome establish a distinct class from plant cryptochromes. Gene duplication events are believed to result in the evolution of animal cryptochrome from [6-4] photolyase which is supported by the fact that primary amino acid sequence of *Drosophila* [6-4] photolyase is highly similar to the sequence of animal CRY. On the other hand, plant cryptochrome is suggested to evolve from CPD photolyase. The knowledge on animal cryptochromes has been acquired from various sources including frog, zebra fish, mice, and insects. Animal CRYs are subdivided into two groups based on the role they play in the cell. CRYs in *Drosophila* and other insects function as circadian photoreceptors and whereas in mouse and in other vertebrates they function as core component of the molecular clock that repress the transcriptional activation of BMAL1/CLOCK independent of light [55].

Interestingly, the animals can possess more than one cryptochrome that belongs to functionally different subgroups. For instance, zebra fish contains one [6-4] photolyase and six cryptochromes including insect type CRY, CRY-DASH and mammalian type CRY genes [56, 57]. On the other hand, some insects such as the honeybee holds only a mammalian type cryptochrome and the others such as the monarch butterfly possess both insect and mammalian type CRYs [58, 59].

2.2.3 Insect Cryptochrome

The insects possess two types of cryptochromes; one of them is insect Type I and the other Type II cryptochrome. Insect CRY was discovered in fruit fly *Drosophila melanogaster*. Type II cryptochrome is found later in non-drosophilid insects. Insects can carry either one type of CRY or both types of CRYs. Figure 2.4 shows that fruit fly *Drosophila melanogaster* (*Dm*) has only TypeI cryptochrome whereas monarch butterfly holds both Type I and Type II CRYs [60]. Nevertheless, the genomes of the honeybee *Apis mellifera* and the beetle *Tribolium castaneum* contain only Type II CRYs. [39, 60]. *Drosophila* cryptochrome functions as a circadian photoreceptor. It was first discovered when a mutant allele, cry^b, of the flies showed attenuated rhythmic

behavioral photoresponses and strongly reduced synchronization to light/ dark cycles. Circadian rhythm is important for timing or regulating key biological events in insects. For example, the time of day of egg hatching, the time of day of adult eclusion, the seasonal timing of adult development, and time-compensated sun compass navigation are developmental incidents regulated by circadian rhythm of insects [39, 61] .

Circadian clock proteins Clock (CLK) and Cycle (CYC) forms a heterodimer and binds to E-box promoter of other clock genes *Period* (*Per*), *Timeless* (*Tim*) and *Cryptochrome* (*Cry*). After transcription, the proteins are localized mostly in cytoplasm. At dark, PER-TIM heterodimer enters the nucleus and prevent the binding of CYC-CLK transcription factors to the E-Box sequence of their own promoters. However, in the light, the Type I CRY interacts with TIM in light-dependent manner. The interaction results in ubiquitylation of TIM and proteosomal degradation of both TIM and CRY itself. TIM degradation leads to the de-repression of *Per* and *Tim* gene expression and also allow the circadian clock reset itself [62]. In addition, *Dm*CRY is responsible for entrainment of the clock in peripheral organs [63].

The knowledge of insect type I cryptochrome is not limited to *Drosophila* CRY. There are numerous publications reporting characterization of cryptochromes from various sources for example, monarch butterfly, mosquito and Chinese oak silk moth. Spectroscopic, photochemical and photobiological properties of those cryptochromes display notable similarities to *Drosophila* CRY [64].

Insect TypeII CRY functionally differs from TypeI CRY with its potential transcriptional repressor activity and its insensitivity to light. It behaves much like vertebrate CRY. Unlike *Dm*CRY, monarch butterfly *Dp*CRY2 represses CLK-CYC-mediated transcription and it does not undergo light dependent proteosomal degradation [39]. In Figure 2.4, functional differences of insect Type I (*Dm*CRY) and Type II (*Dp*CRY2) in the circadian clock of both insects are shown schematically.

Both types of insect cryptochromes (*Dm*CRY and *Dp*CRY2) have shown to function as a magnetoreceptor in *Drosophila* system in which magnetosensitive behavioral assays are available with Cry^b mutant background in the presence of light. However, that

photochemical mechanism for light dependent magnetoreception is not clear and suggested to be different from photoreception mechanism [65].
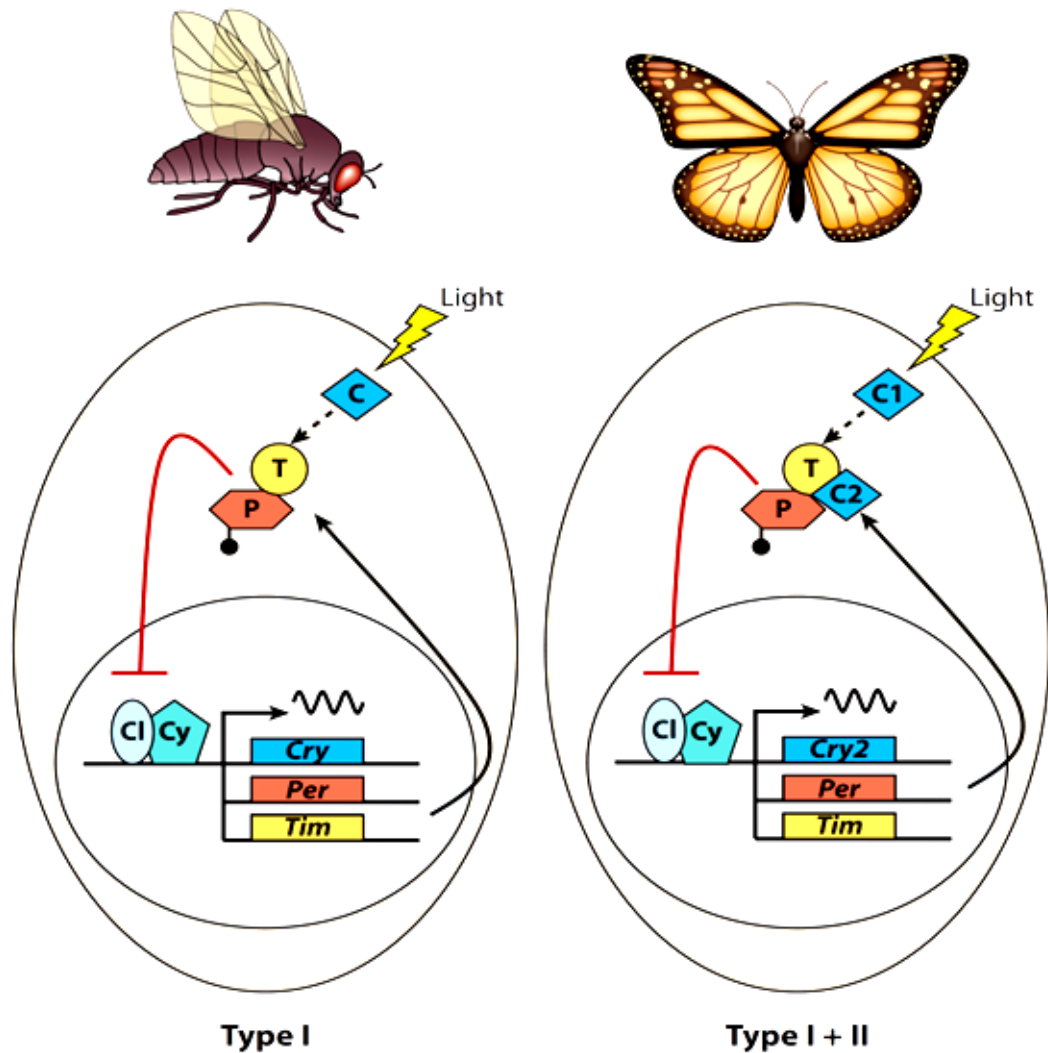
Figure 2.4 The roles of insect Type I and TypeII cryptochromes in circadian oscillatory mechanisms of fruit fly and monarch butterfly. Type I CRYs (DmCRY and DpCRY1) in both organisms act as a circadian photoreceptors. However, Type II CRY (DpCRY2) only involves in the regulation of circadian clock independent of light. The figure is adapted from Chaves et al, 2012 [27].

2.2.4 Mammalian Cryptochrome

In the mid 90's, photolyase orthologous genes as an expressed sequence tags in the human genome data base was reported [66] so such a controversial issue that the repair of UV damage by a photolyase in humans ended. It was Hsu et al, [67] who first purified and characterized two human [6-4] photolyase orthologous proteins. Unexpectedly, neither of these proteins had found to display CPD or [6-4] photolyase activity despite being structurally very similar to photolyase and having flavin cofactor [67]. Therefore, those proteins are classified as human blue light photoreceptors and named hCryptochrome1 (hCRY1) and hCryptochrome2 (hCRY2). The function of human cryptochromes in circadian rhythm has been investigated over years; one possibility is that cryptochromes may serve as circadian photoreceptors [68] but this issue had retained controversial in many years until melanopsin was found to be the major circadian photoreceptor molecule in mammals [69]. However, the contribution of hCRYs, especially hCRY2 in the retina, to photoreception still remains unclear.

The functions of mammalian cryptochromes are found by genetic studies for which mouse is used as a model organism to understand the role of cryptochrome. For this, cryptochrome genes in SCN of mouse brain were knockdown and behavioral and metabolic rhythms were observed. Figure 2.5 shows circadian behavior of Cry mutant mice in free running mode in which light entrainment is removed. Strikingly, the double $Cry1^{-/-}Cry2^{-/-}$ mutant mice become totally arrhythmic. Whereas, when $Cry1^{-/-}$ or $Cry2^{-/-}$, are knockdown, the circadian period of mice seemed to shorten or lengthen, respectively. The observation of partial circadian rhythmicity in the single Cry knockout mice indicates that cryptochromes in mammals have functional redundant roles in the regulation of circadian rhythm [70]. Thus, vertebrate cryptochromes including human and mice, function as one of the major components of their circadian clocks.

Biochemical analyses elucidate the function and the mode of action of mammalian cryptochromes in the circadian clock based on protein-protein interactions. All cell types have autonomous circadian clock which consists of the autoregulatory negative

feedback loop composed of several integral proteins [71]. Figure 2.6 exhibits circadian clock mechanism of mammals. The core proteins making up the core clock in all cell types are as follows; the brain and muscle Arnt-like protein-1 (BMAL1), Circadian Locomotor Output Cycles Kaput (Clock), Cryptochrome1(CRY1), Cryptochrome2(CRY2), Period1 (PER1), Period2 (PER2), Period3 (PER3). There are also complementary proteins like kinases and transcription factors that affect the function, expression and the localization of core clock proteins [72].

The two basic helix-loop-helix (bHLH)/PAS domain-containing transcription factors, BMAL1 and CLOCK, that form a heterodimeric transcriptional complex to activate target gene expression via E/E'-box (CACGTG) enhancer elements. Periods (PER1, PER2 and PER3) and Cryptochromes (CRY1 and CRY 2) constitute the negative components of the loop. PER2 by interacting with CRY in cytoplasm escapes from ubiquitin mediated proteosomal degradation and PER-CRY complex together translocates into nucleus. Then, the PER-CRY complex represses transcription of target genes, by directly interacting with and inhibiting BMAL1/CLOCK complex activity. In particular, the PER and CRY genes themselves are targets of BMAL1/CLOCK so PER-CRY in turn represses their own transcriptions and, thereby forming the autoregulatory negative feedback loop [56].

Post-translational modifications also effects stability, subcellular localization, and function of cryptochrome in circadian clock mechanism. Both CRY1 and CRY2 can be ubiquitylated by FBXL3 ubiquitin ligase and directed to proteosome for degradation [73]. Also, acetylation of CRY is another modification that affects the stability of those proteins [27]. hCRY1 and hCRY2 are able to carry out autophosphorylation but the correlation of autophosphorylation activity with light and the redox states of FAD as well as its role in signaling are unknown[74]. Type II cryptochromes do not only exist in mammals but in other vertebrates like *Danio rerio*, *Xenopus laevis*, zebra fish, chicken which play role in transcriptional-translational negative feedback loop [17].
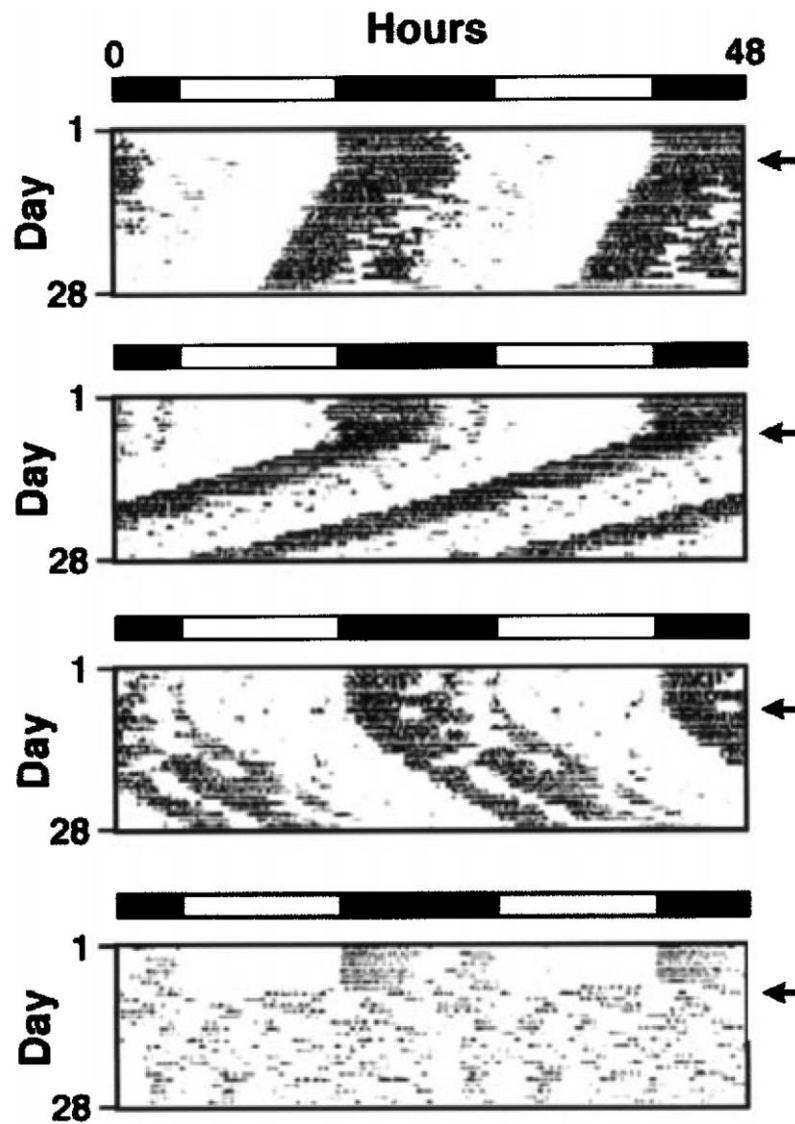
Figure 2. 5 Activity/rest behavior of a) Wild type, b) Cry1-/- mutant, c) Cry2-/- mutant, d) Cry1-/-Cry2-/- mutant mice. The actogram shows the rhythmic activity of wild type and mutant mice under 12:12 light and under constant dark. Figure is taken from Thompson et al, 2002.[26]
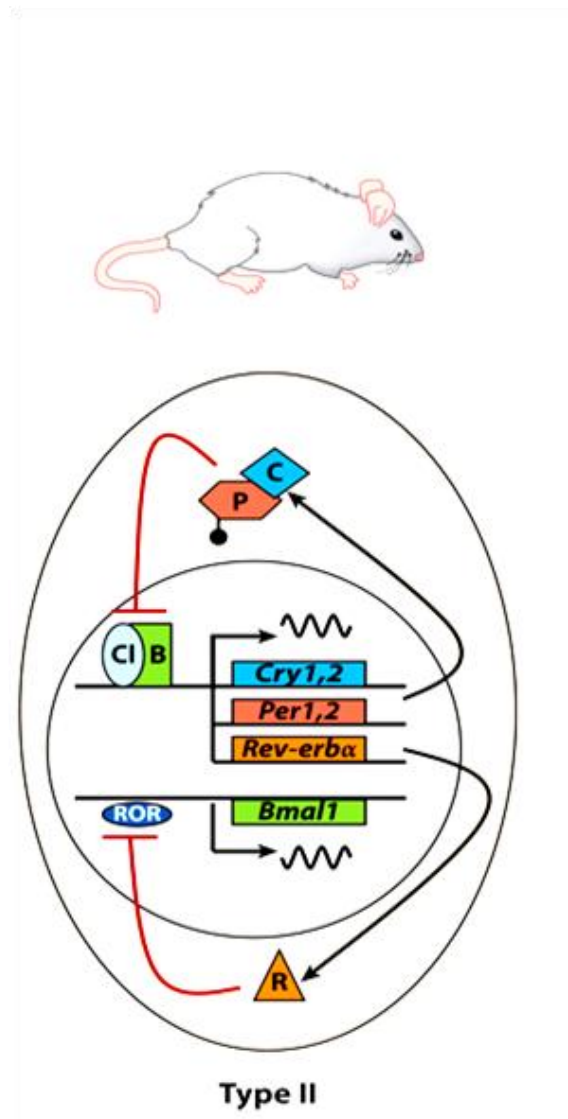
Figure 2. 6 Mammalian molecular clock. The bHLH-PAS domain-containing proteins Clock and BMAL1 dimerizes and then binds to the E-boxes in the promoters of clock controlled genes (CCG) and the promoters of Per and Cry genes. The CRY and PER proteins dimerize in cytoplasm and enter the nucleus. CRY-PER heterodimer inhibits Clock-BMAL1 activated transcription of theirown genes as well as of those of clock-controlled genes, thus generating an oscillatory pattern of gene expression. Figure is adapted from Chaves et al, 2012 [27, 75]

2.2.5 DASH Cryptochrome

The third class of cryptochromes is the DASH type cryptochrome. It was first identified in photosynthetic bacteria *Synechocystis*. Then, the members of that family were found showing higher sequence homology to <u>D</u>*rosophila*, <u>A</u>*rabidopsis* and <u>H</u>*uman* than bacterial photolyase. Taking the first letters of the organisms above, this family was named as Cryptochrome-DASH. DASH family members were not only identified in photosynthetic bacteria but also characterized in non-photosynthetic bacteria, plants, fungi and animals [76].

The first information related to the function of this relatively newer subgroup is gained from microarray studies of *Synechocyst*is. Transcriptional profile of CRY-DASH knockout mutant of *Synechocystis* reveals that CRY-DASH function as a transcriptional repressor [77]. Biochemical studies to find other functional aspects of Cry-DASHes taken from *Arabidopsis, Vibrio* and *Xenopus, Synechocystis* reveal that they repair CPD lesion on single stranded DNA [78]. In addition, CPD damages on dsDNA can be repaired by Cry-DASH if the damage site is in loop structure. Recently, it was shown that *Vc*Cry-DASH repaired UV lesions on $p(dA)_{10}$:$p(dT)_{10}$ duplex compared to *Ec*Phr [79]. Physiological significance of ssDNA repair should be elucidated but these results indicate that VcCry-DASH can disrupt short stretches of dsDNA.

In the sense of the transcriptional repression activity, Daiyasu et al, showed that Cry-DASHes from vertebrates are not able to suppress BMAL1-CLOCK mediated gene transcription although DASH-CRYs are relative of animal cryptochromes. It demonstrates that animal CRYs and Cry-DASHes are functionally different despite their close evolutionary relationship [76].

Having the structural similarity to animal CRYs with a residual DNA repair activity, CRY-DASH subfamily is presumed to be the missing link between functional differentiation of cryptochrome and photolyase. Supportively, photolyase/cryptochrome family proteins including CRY-DASHes isolated from fungi, diatom and algae were observed to perform dual functions. Both CRY-DASHes of *Aspergillus nidulans* were

found to regulate both sexual developments and to repair ssDNA [1, 80]. In plant pathogen fungus, *Sclerotinia sclerotiorum,* CRY-DASH protein was shown to mediate UV-A specific development [81]. *Cercospora zeae-maydis* PHL1 and *Trichoderma atroviride* PHL1 involve in gene regulation and also exhibit DNA photorepair activity [82] [83]. Presently, a universal role for CRY-DASH has been clearly defined despite its *in vitro* DNA repair ability. Therefore, the biological role and the signaling mechanism of CRY-DASH are needed to be more elucidated by the identification of its signaling partner and the biological responses it causes.

2.2.6 Photolyase/Cryptochrome in Unicells

Microorganisms are able adapt themselves to environmental conditions to survive and reproduce fast. Environmental light conditions influence the metabolism of microorganisms as much as the higher organisms [84]. Microorganisms sense the light through photoreceptors, the signal is transmitted through downstream partner in the signal transduction pathway so that the target genes related to i.e., the motility machinery, stress tolerance related transcription factors, and photosynthesis are activated. Until 2003, photoreceptor photolyase/cryptochrome family was thought to exist only in higher eukaryotes. However, Brudler et al, for the first time, identified a new class of cryptochrome (CRY-DASH) in cyanobacteria called *Synechocystis* [77]. From then on, several cryptochromes are identified in unicellular organisms. This finding supports the hypothesis that cryptochromes evolved before the divergence of prokaryotes and eukaryotes.

Cryptochromes are also candidate proteins to be the blue light photoreceptor in microorganisms. The studies investigating cryptochrome role in unicells found that those proteins not only percept light but also involve in various pathways depending on the organism itself. In a photosynthetic organism, *Prochlorococcus* ME4, it was found by genome wide gene expression analysis that the expression levels of genes related to photosynthesis are directly dependent on blue light [85]. Therefore, at least, one of the

members of photolyase/cryptochrome family in *Prochlorococcus* ME4 is thought to involve in the regulation of photosynthetic genes.

Interestingly, phylogenetic classification published in the study of Özturk et. al, revealed previously unidentified photolyase subgroup in *C.cresentus* gram negative bacteria [86]. Classified as Type III photolyase, the phylogenetic analysis indicates that they are probably the ancestors of plant cryptochromes. Functionally, Type III photolyase repair CPD lesions on dsDNA by using blue light energy in a similar way as *E.coli* CPD photolyase does. Type III photolyase whose function has not been clearly elucidated are found in the genomes of Gram negative bacteria *B.subtilis* and *B.anthara* which should be investigated whether Type III photolyase in those organisms function as a blue light photoreceptor. In another study with *Rhodobacter sphaeroides,* Cry-B served as transcription factor that regulates expression levels of photosynthetic genes depending on blue light [87]. In the same organism, stress induced transcription factors Sigma38 and ChrR gene expressions were also regulated by blue light.

In recent years, PHR or CRY that is able to carry out dual function is being discovered in unicells, frequently. In marine diatom *Phaeodactylum tricornutum*, [6-4] photolyase was reported to repress BMAL1-CLOCK mediated transcriptional activation of the circadian clock genes and meanwhile show [6-4] photoproduct repair activity [2].

Last but not the least, studying cryptochromes of simple unicellular organisms could be more effective to understand functional divergence of cryptochrome from photolyase in terms of the evolution of structure-function relationship.

2.3 Photolyase/Cryptochrome Family Structure and Photochemistry

Structure and photochemistry of photolyases have been well established over 50 years. Unfortunately, such data has not been clearly defined due to the lack of crystal and co-crystal structures of cryptochrome. In addition, the signaling partners of cryptochromes and the biological reactions they carry out in the cell have not been defined, yet. Thus, the information on structure and reaction mechanism of cryptochrome is gained mainly from photolyase studies due to the high degree of sequence identity and structural

conservation between photolyase and cryptochrome. Crystal structures of photolyases from several organisms were clearly resolved however; only *Arabidopsis* and *Drosophila* cryptochrome's crystal structures were revealed so far. In the following section, crystal structure of *E.coli* photolyase will be discussed as a representative of entire family and significant differences from other photolyases and distinctive properties of the cryptochrome will be indicated when necessary.

2.3.1 Crystal Structure

Crystal structures of CPD photolyases from bacteria, thermophilic bacteria, archea, blue - green algae and plant have been determined so far [55, 78, 88, 89]. The overall structures of these photolyases are remarkably similar. But some minor deviations are found within the subgroups. According to crystal structure of *E coli* photolyase, the protein is composed of two well-defined domains: an N-terminal α/β domain (residues 1-131) and a C-terminal α -helical domain (residues 204- 471), which are connected to one another with a long inter-domain loop (residues 132–203) that wraps around the α/β domain [25]. Moreover, there are studies that give more insight into DNA-photolyase interaction and the repair mechanism *in situ* for instance. In the study of Mees et. al, they achieved to crystallize enzyme-substrate complex of photolyase [90].
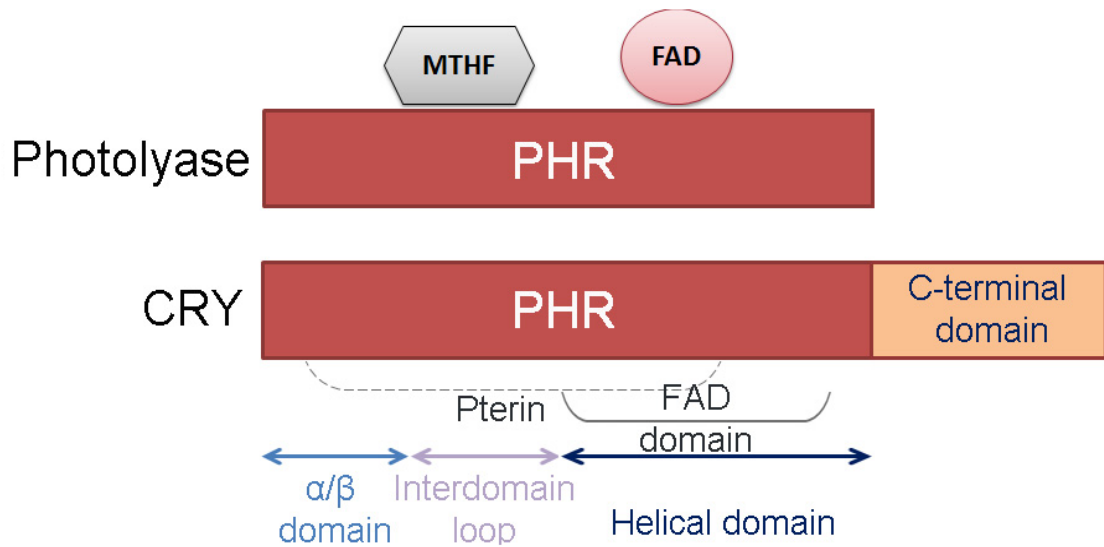
Figure 2.7 Schematic representation of photolyase and cryptochrome structures. Pterin (MTHF) and FAD binding regions are indicated with brackets and the three domains of PHR are shown below the protein. The figure is adapted from Lin et al, 2005 [17].

Figure 2.7 shows schematic representation of PHR indicating N-terminal α/β domain, C-terminal α helical domain where MTHF and FAD binds and with the interdomain loop in between. The α/β domain consists of five parallel β-sheets strands which are surrounded by five α-helices. C-terminal helical domain is consisted of 14 helices that form a flat face. FAD lingers in a U-shaped hole in the center of protein and it contacts with the surrounding 14 conserved amino acids. DNA photolyase domain in the N-terminus holds MTHF which binds to the amino acids Cys-292 and Lys-293 by a salt bridge. In deazaflavin type photolyases in *T. thermophilus* and *A. nidulans,* cleft sizes where 8-HDF binds are smaller than folate type photolyases. Cryptochrome posseses the same domains but additionally it has extensional domain at the C-terminus. The ribbon diagram of *E.coli* photolyase crystal structure where α/β and α-helical domains are seen is shown in Figure 2.8. The binding sites of MTHF and FAD reveal the distance between the centers of the two cofactors that is important for energy transfer from MTHF to FAD. In *E. coli photolyase,* it is 16,8 A and 17,7 A in the *A. nidulans* enzyme that are close enough for favorable energy transfer from MTHF to FAD during repair [26]. Besides, the proper orientation and direction of the two cofactors in the enzymes contribute to the efficiency of energy transfer, too [55]. The binding mode of photolyase has been determined by PHR-DNA co-crystal structure studies. Photolyase binds to the phosphodiester backbone of DNA weakly on the flat surface of helical domain due to positive electrostatic potential. The high affinity binding takes place when photolyase encounters a thymidine dimer. The co-crystal of *T. thermophilus* with thymine revealed the interaction topology of thymine dimer with the enzyme where thymine dimer binds to the inner cavity of protein [78]. According to base- flipping model, the thymine dimer flips out from the DNA helix into the central cavity where it comes within van der Waals contact distance of FAD molecule.
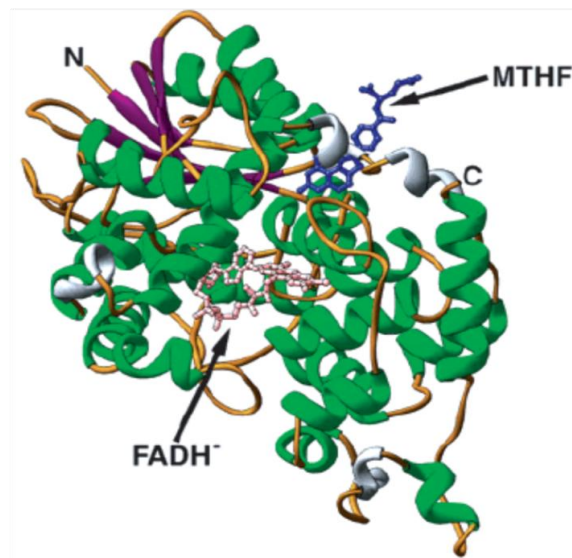
Figure 2. 8 The crystal structure of E.coli photolyase. α /β domain and C-terminal α - helical domain are connected to one another with a long inter-domain loop that wraps around the α/β domain., the distance between the centers of the two cofactors MTHF and FAD is 16,8 A that is important for energy transfer from MTHF to FAD [91].
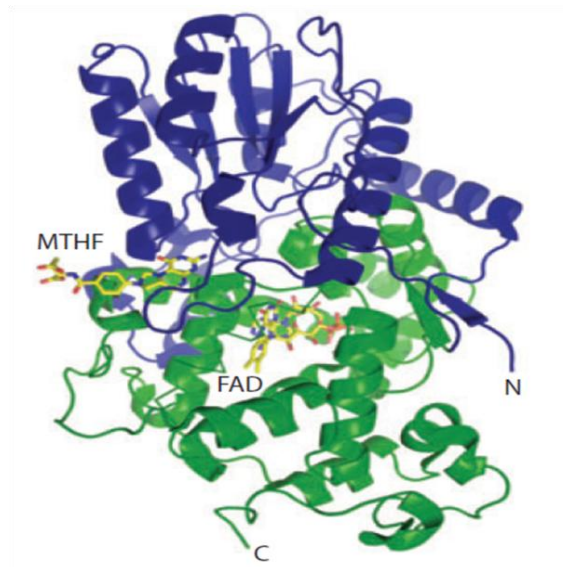
Figure 2.9 The crystal structure of Arabidopsis thaliana–CRY-DASH. The three domains of EcPhr are conserved in AtCRY-DASH. MTHF and FAD bind to apoprotein [92].

The knowledge on cryptochrome is rapidly increasing every day. Among plants, *Arabidopsis thaliana* CRY is the most characterized. The crystal structures of PHR region of *At*CRY1 with native and ATP-bound forms are available [93]. PHR domain of *At*CRY1 was achieved to crystallize with FAD cofactor bound state. Autophosphorylation of *At*CRY1 is already known [94]. In the ATP-bound crystal structure, an unconventional site where ATP most probably binds is determined. Surface features of *At*CRY1 point out the reasons under the functional differences between PHR and CRY. In Figure 2.10, the surface potential of *Ec*Phr is shown where the DNA binding groove consists of positively charged amino acids. However, on *At*CRY1 the number of positively charged amino acids near DNA binding groove is much smaller than PHR. Instead, the surface predominantly is covered by neutral and negatively charged residues. Those amino acid substitutions may account for the inability of *At*CRY1 to DNA. Another aspect of *At*CRY1 is the size of FAD binding cavity which is larger and deeper than the any of PHR member characterized to date. One more distinctive feature that may explain the lack of DNA repair activity is the two tryptophan residues in *E. coli* photolyase that are important for conserved for specific thymine-dimer binding and DNA binding. They are replaced by Leu-296 and Tyr-402 in the PHR domain of *At*CRY1.

Arabidopsis and Drosophila [6-4] photolyases' crystallographic structures have been resolved to date, too [95, 96]. Similar to CPD photolyase, At[6-4] photolyase conserves overall 3-dimensional fold. α/β and α helical domains and the two chromophores; flavin and folate exist in [6-4] PHR, too [97]. The superimposition of At[6-4] photolyase crystal structure to other CRY/PHR structures pointed out the differences in C-terminal extension, active-site channel, cofactor environment, Trp electron-transfer pathway. Also, novel functional motifs of phosphate-binding the Pro-Lys-Leu protrusion motifs and some minor residue differences in the sulphur loop of around Trp electron transfer triad were discovered [96]. Crystal structures of [6-4] photoproduct-enzyme complexes have also been available in the literature that exhibit structural binding and repair modes of [6-4] photolyase in detail [97, 98]. In Figure 2.11, the binding mode and surface

features of co-crystallized structure of *Dm*[6-4] PHR with its specific dsDNA substrate are shown. The structural and functional motifs and conserved key residues revealed by the crystal structure studies for [6-4] PHR provide a basis to establish a 3-D model of human CRYs that are not available today.

Crystal structure of *Dm*CRY has very recently become available [95]. It exhibits structural similarity to *Dm*[6-4] photolyase whose crystal structure is shown in Figure 2.11. The significant differences stand out in loop structure, antenna cofactor binding site, FAD centre and more importantly, in the C-terminal extension. The 23 amino acid C-terminal extension of from photolyase domain to 10-residue helical tail forms a short connection which stands in the active site of [6-4]PHR. Because of that, C-terminal tail acts like damaged DNA substrate of [6-4] photolyase in *Dm*CRY. This structural difference most probably results in different modes of regulation in signal transduction *Dm*CRY. Amino acid composition of DNA binding pocket shows dissimilarity with *Dm* [6-4]PHR in the number of positively charged residues (Lys-154, Lys-161, Lys-449, Arg-502, Arg-505). Additionally, position of flavin (FAD) is found to be close enough to mechanically link C-terminal conformational changes with changes in its electronic state [95]. Unconserved C-terminal is very important for controlling the activity of core domain of Type I cryptochromes. Studies carried out with C-terminal of *Dm*CRY in chimeric proteins showed that C-terminus has a role in the stability unlike the C-terminal phototransduction function of *Arabidopsis* CRY [99].
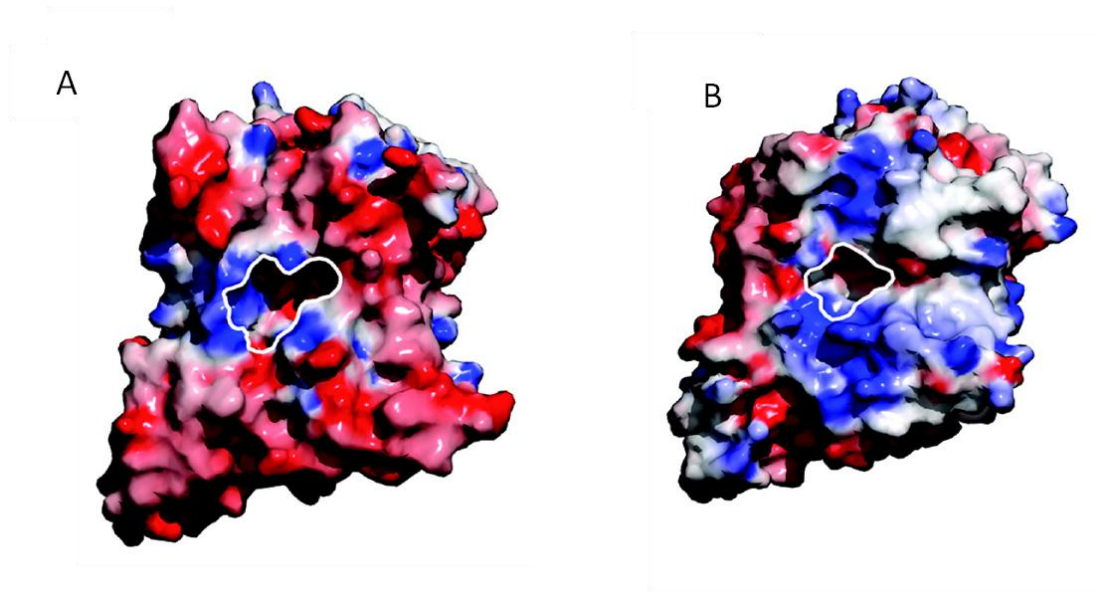
Figure 2. 10 Surface potential diagram of A) *Arabidopsis thaliana At*CRY1 and **B)** *E.coli* . Red and blue colors represent negatively and positively charged residues around DNA binding region (white line), respectively. Figure is taken from Lin et al, 2005 [17]

Crystal structure of CRY-DASH subfamily is available for *Synechocystis* and *Arabidopsis* CRY-DASH [77, 92]. Furthermore, crystal structures of *At*CRY-DASH with an in-situ-repaired CPD substrates in ssDNA and in loop structured-ds DNA in addition to CRY-DASHes in the dimeric state were revealed [100] [101]. Crystal structure of *Synechocystis* and *Arabidopsis thaliana* CRY-DASH conceded that overall three dimensional structure of DASH subfamily is remarkably similar to CPD photolyases with α/β-domain in N-terminal and a α-domain in C-terminal including FAD binding domain in U-shaped form [100]. Non-covalently bound cofactors MTHF and FAD exist in *At*CRY-DASH. As seen in CPD photolyases; the DNA binding groove consists of positively charged amino acids. However, two amino acid substitutions and the penetration of three charged side chains into the CPD-binding cavity in *At*CRY-DASH cause changes in hydrophobic environment around DNA binding pocket [92]. These minor changes are thought to cause an inability for CRY-DASH to bind dsDNA. Additionaly, one of the main structural differences of cryptochrome from photolyase is their C-terminal extension. In this respect, CRY-DASH lacks C-terminal tail of plant and animal CRYs despite their common PHR domains.

Crystallized *At*CRY-DASH with a synthetic oligonucleotide consisting of 5 thymines with a synthetic CPD analog demonstrates binding mode of *At*CRY-DASH to damaged DNA. The flipping of the CPD lesion into the active site of CRY-DASH is similar to photolyase. However, some amino acid changes at FAD binding cavity and its surrounding region result in a decrease in stability of the interactions that holds flipped out dsDNA CPD with CRY-DASH which may explain inability of CRY-DASH to bind and repair dsDNA.

Dm(6-4)PHR-dsDNA
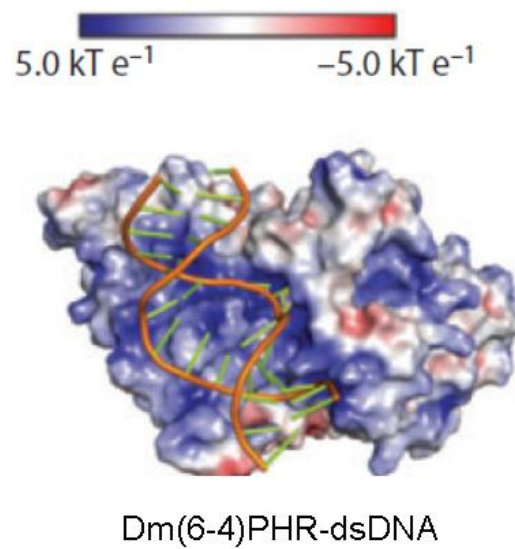
Figure 2. 11 Surface potential diagram of crystal structure of Dm[6-4] photolyase in the red and blue colors represent negatively and positively charged residues, respectively. The figure is taken from Chaves et al, 2012 [27].
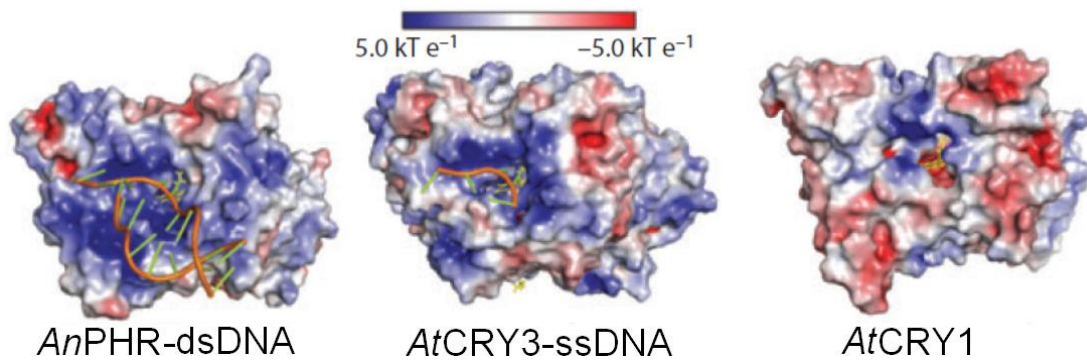
Figure 2. 12 Surface potential diagram of fungal Class I CPD PHR, plant CRY1, CRY-DASH with their substrates. Red and blue colors represent negatively and positively charged residues, respectively. Sequentially in the figure, crystal structures of *Aspergillus nidulans* PHR with dsDNA(*An*PHR-dsDNA), *Arabidopsis thaliana* CRY-DASH with ssDNA (*At*PHR-ssDNA) and *Arabidopsis thaliana* CRY1(*At*CRY1) are shown. The figure is taken from Chaves et al, 2012 [27].

2.3.2 Chromophore/Cofactors and Spectral Properties

All known photolyases contain two cofactors which noncovalently bind to the apoenzyme; flavin adenine dinucleotide (FAD) and methenyltetrhydrofolate (MTHF). At the N-terminal domain near the surface holds a light harvesting photoantenna (MTHF) or flavin derivative 8-hydroxy-7, 8-didemethyl-5-deazariboflavin (8-HDF) depending on type of organism. Recently, other than MTHF as light harvesting chromophore, FMN or FAD has been found in the photolyases of thermophilic bacteria [88, 102]. MTHF absorbs light at around 377 nm to 410 nm. Because its extinction coefficient of MTHF is high, absorption spectrum of *Ec*Phr is dominated by the absorption of MTHF around 380nm in UV/VIS spectrum. On the other hand, deazaflavin (8-HDF) absorption gives major peaks at 440nm in *T. thermophilus* and *A.nidulans* photolyases.

The catalytic cofactor FAD resides in the structural cavity at α-helical domain near C-terminus of PHR. FAD exists in three different redox states; oxidized ($FADH_{ox}$), one-electron-reduced (neutral blue radical or anionic red radical; $FADH^0$), and two-electron reduced (neutral or anionic; $FADH_2$ or $FADH^-$). Both *in vivo* and *in vitro* photoreactivation of PHR require fully reduced form of flavin $FADH_2$. Indeed, the native state of catalytic cofactor in the cell is $FADH_2$. Under physiological conditions FAD is synthesized in cell in FADox form then reduced to $FADH^o$ and then $FADH^-$ by an unknown mechanism [103]. However, during enzyme preparation, $FADH^-$ becomes oxidized to $FADH^o$ blue neutral radical or to FAD_{ox}. Thus, purified enzyme preparations contains mixture of FAD at different oxidation states. Characteristic absorption spectrum of *E.coli* PHR is shown in Figure 2.13. $FADH_2$ of purified photolyase gives absorption peak at max 380nm and $FADH^o$ FADox peak up to 420, 480, 580 and 625 nm.

Flavin contribution to absorption of photolyase is minor. Majorly, the $FADH_2$ absorption is masked by folate absorption between 360-380nm in most of PHRs. The FAD content and its redox states in a purified photolyase can be analyzed after eliminating MTHF absorption after mild denaturation of the protein by heat or alkali

treatment since MTHF is weakly bound to the protein and released during denaturation. The methenyl bridges between folate and apoprotein are broken so MTHF cannot absorb light above 300nm. Therefore, the absorption peaks only come from reduced, neutral and oxidized forms of FAD which are generated by oxidation of the molecule during purification [26].

The stoichiometry of apoenzyme: FAD is 1:1 in *Ec*Phr [86]. An *E.coli* cell contains approximately 10-20 molecules of flavin that reused in each photoreactivation. During DNA repair, electron cycles from $FADH^-$ to CPD dimer. After photorepair cycle, $FADH^-$ is restored by back electron transfer from product [25].
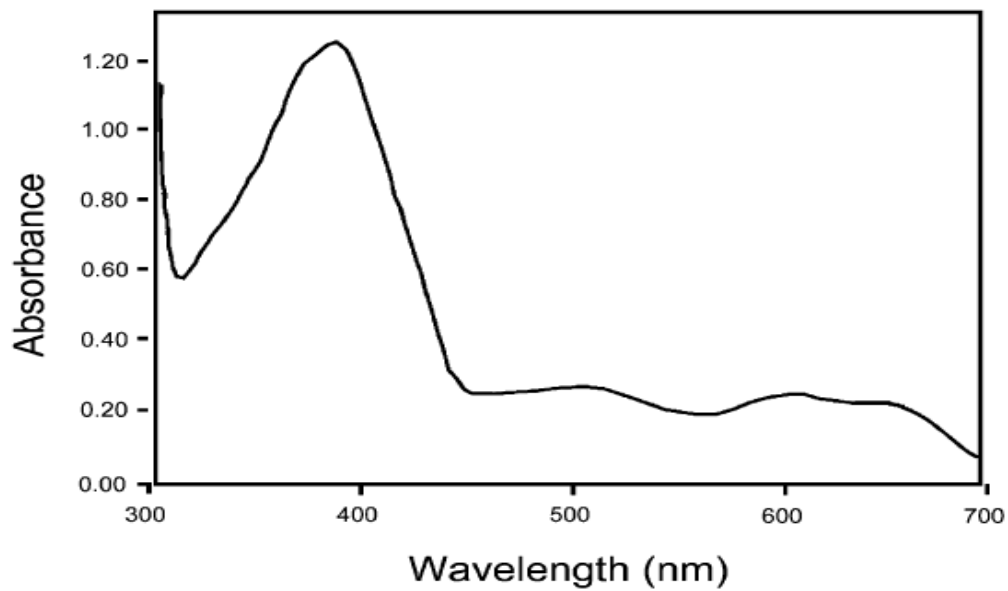
Figure 2. 13 Absorption spectrum of native E.coli photolyase. FAD radicals and MTHF absorptions are detected by UV/VIS spectroscopy between 300 and 700nm. Figure is taken from Sancar A, 2003 [25]

2.3.3 Reaction Mechanism

It has been 50 years since the first photolyase was discovered so the photochemistry of a photolyase has almost been clarified [25]. There are excellent reviews on photoreaction mechanism of photolyases [11, 25, 26]. The enzyme catalyzes the repair of lesions on DNA based on Michaelis-Menten kinetics. Basically, the reaction mechanism is initiated by light independent, structure specific DNA binding of DNA photolyase to Pyr<>Pyr dimer with a specific binding constant $K_s = 10^{-9}$. Next, DNA substrate in dimer form is flipped out and oriented into the active site of the enzyme to make ES complex. The photoactive pigment MTHF (or 8-HDF) then captures light between 300-500 nm and the excitation energy is transferred to catalytic cofactor $FADH^-$ by Forster Resonance Energy Transfer (FRET) [104]. Whole reaction takes place in 1n which is resolved by ultrafast spectroscopy [105]. Electron transfer occurs from flavin to Pyr<>Pyr dimer and breaks cyclobutane ring into two pyrimidines. Photolyase dissociates from EP complex. Then, electron cycles back to the $FADH^o$ and $FADH^-$ is regenerated. Photoreactivation by photolyase is a photon-powered cyclic electron transfer that does not results in net gain or loss electron.
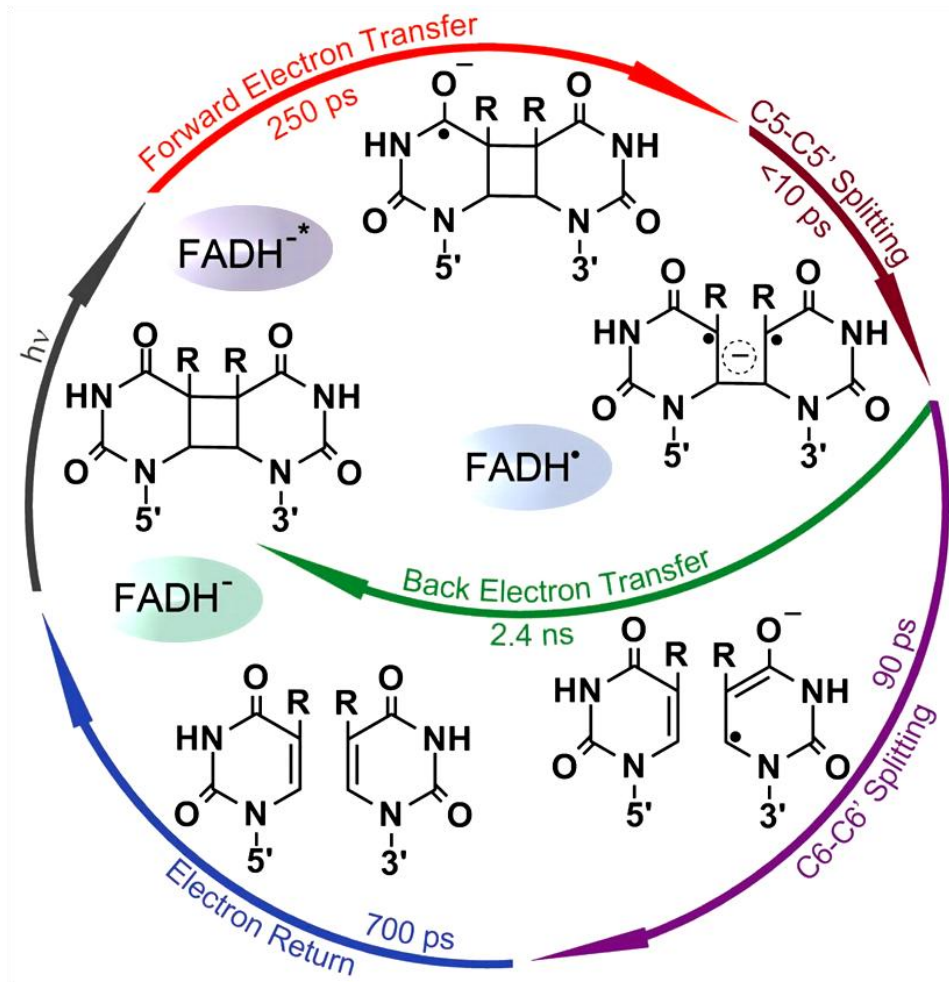
Figure 2.14. Photoreaction mechanism of *E.coli* photolyase. CPD photolyase; light is absorbed by MTHF abd energy is transferred to FAD. Electron is donated from FAD to cyclobytane ring and the damage is repaired. The figure is taken from Liu et al, 2011, [105].

Similar repair mechanism models for [6–4] photolyases are suggested as a result of photochemical and biochemical studies with *Drosophila and Xenopus* [6–4] photolyases except that [6–4] photoproduct is first converted to an oxetane intermediate that resembles cyclobutane ring [106, 107]. The photochemical reaction takes place at two steps. First, the enzyme binds with a high affinity ($K_A = 2.1 * 10^8$ M^{-1}) to single and double stranded DNA bearing [6-4] photoproduct that is converted to oxetane intermediate and then two pyrimidines are recovered photoenzymatically. Repair of Dewar isomer is also suggested through a similar photoreductive pathway except the initial conversion of DEWAR to [6–4] isomer then it is reverted in a second photoreductive step [106]. Figure 2.15 and Figure 2.16 show repair mechanisms of [6-4] and CPD PHR, respectively. Unlike CPD photolyase with a dissociation half-life 15-45 sec, [6-4] photolyase dissociates from DNA very slowly with a half-life of 5 hours [107]. As well as binding to [6-4] photoproduct, [6-4] photolyase also binds to [6-4] photoproduct's DEWAR isomer with 3 fold lower affinity ($K_A = 5.2 - 6.7 * 10^7$ M^{-1}) but it repairs DEWAR isomer at a very low efficiency [106, 107].
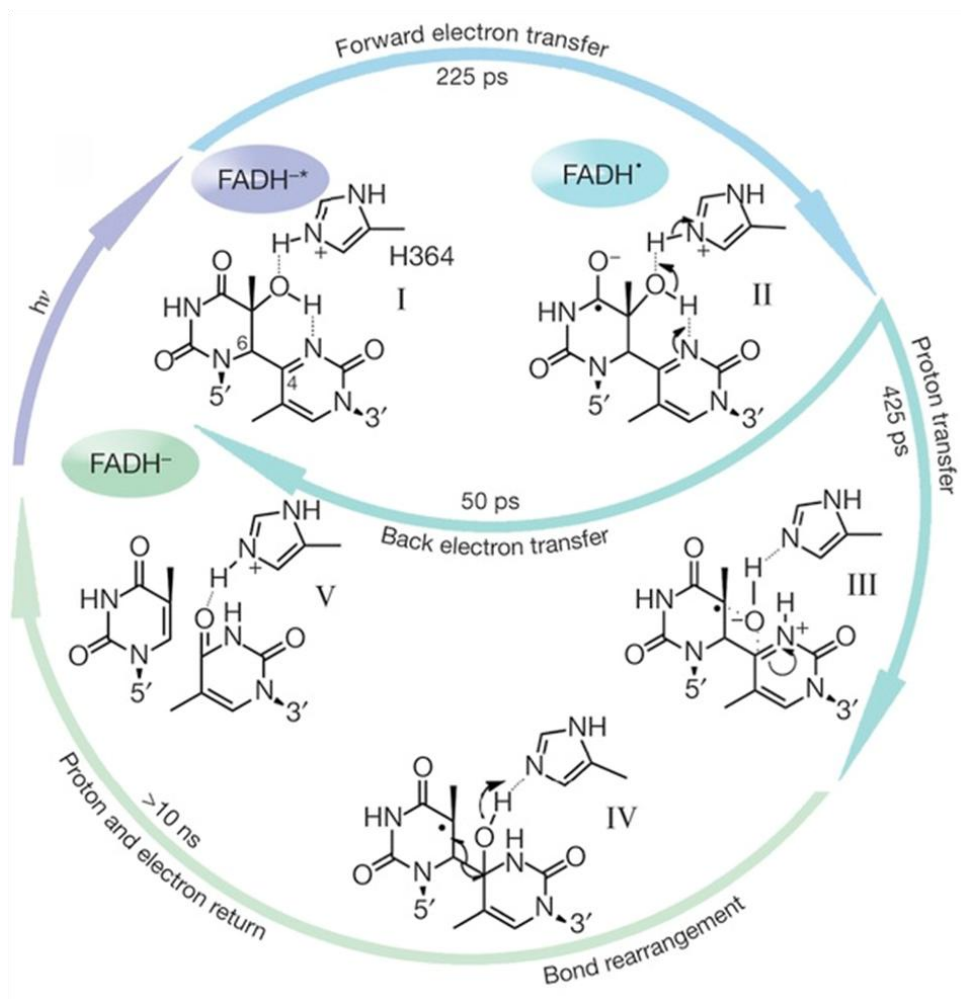
Figure 2. 15 [6-4] Photolyase photoreactivation mechanism. [6-4] photolyase binds to [6-4]PP and convert it to transient oxetane ring thermally. Then, photoreaction mechanism similar to CPD photolyase takes place for the split of pyrimidine dimer. The figure is taken from Li J. et al, 2010 [108]

Chapter 3

INVESTIGATION OF REAL-TIME PHOTOREPAIR ACTIVITY ON DNA VIA SURFACE PLASMON RESONANCE

BACKGROUND

Ultraviolet light is an electromagnetic radiation with a wavelength in the range of 10–400 nm which can cause mutagenic effects by converting a pyrimidine base on DNA to an excited state [109]. The excited base is then capable of reacting with other molecules to form covalently linked stable photoproducts [109]. CPD and pyrimidine [6-4] pyrimidone photoproducts [6–4] PPs are produced as a result of formation of stable photoproducts between adjacent pyrimidines within the same DNA strand. These four base-ring photoproducts can be lethal to cell metabolism as they may block the DNA/RNA polymerases on the same DNA strand or inhibit polymerase progression during both DNA replication or transcription [110-112]. One of the repair mechanisms to prevent DNA damage caused by the UVR from sun light at 290 nm to 320 nm is direct repair mechanism. Direct repair occurs in three steps where an enzyme called photolyase bounds to the pyrimidine dimers of DNA at dark ad repair DNA using blue light as an energy source. Cryptochromes, on the other hand, share sequence similarity to photolyases and are known to be the enzymes with no DNA repair activity. Further studies have shown that CRY regulates growth and development in plants and the circadian clock in animals [23, 68, 113]. Despite their DNA-binding capability with single-stranded DNA (ssDNA), they are introduced as photoreceptors, as they are deficient in the repair activity for CPDs in double-stranded DNA (dsDNA) [25, 70, 114]. The more recently discovered subclass of the cryptochrome/photolyase family, called Cry-DASH, is found in cyanobacteria, eubacteria, and vertebrates [76, 115]. The crystal structure of Cry-DASH is determined for *Synechocystis* Cry-DASH [77] and *Arabidopsis thaliana* Cry3 [92], and the overall protein folds are found to be similar to

class I CPD photolyases [55, 78]. The structural similarity is mostly based on an N-terminal α/β-domain and a C-terminal α-domain with the flavin adenine dinucleotides (FAD) cofactor inside a U-shaped conformation. Similar to photolyases, FAD is fully reduced to $FADH^-$ (catalytically active form) during photoactivation [93]. The surface features around the FAD-binding pocket of Cry3 and *Synechocystis* Cry-DASH have been found to be essential for DNA binding as in DNA photolyase [90]. Also, it has been shown that energy transfer from 5,10-methylenetetrahydrofolate (MTHF) to FAD in Cry-DASH, which indicates that energy transfer in Cry-DASH shares mechanistic similarities between photolyase that repairs damaged DNA and Cry-DASH that repairs ssDNA [116]. Despite their similarity at both structural and amino acid levels, Cry-DASH proteins lack C-terminal extensions which are thought to give them the signaling activity [17]. However, it was shown that DASH cryptochromes repair CPDs specifically in single-stranded DNA (ssDNA) [80], and therefore there has been emerging necessity for classification of DASH type cryptochromes as ssDNA-specific photolyases. The reason why Cry-DASH prefers single stranded substrate was revealed in crystal structure of *At*Cry3. Less hydrophobic character of binding cavity and more charged amino acid around the cavity influences DNA binding preferences [92]. It was shown that *At*Cry3 could bind and repair dsDNA if at least one hydrogen bond of the CPD lesion to the complementary strand was perturbed with a significantly distorted double helix [100]. This result evidently shows that Cry-DASH incapable of making sufficient favorable interactions with dsDNA for a favorable free energy of association. There are several assays to measure DNA repair by photolyases developed by many groups over 50 years. Photorepair activity of photolyase like proteins can be assessed by transformation assay, absorption, enzyme sensitivity assay, restriction site restoration and photophysical methods. By these assays, kinetic and equilibrium measurements of photolyase binding, repair and also quantification of the substrate are being determined regularly [117]. However, some of the assays are time consuming and not sensitive enough to detect the repair of [6-4] photoproducts. Others; such as restriction site restoration and enzyme sensitive site assays, require radioactive labeling

and personnel expertise despite their sensitivities and availability of site specific repair. The photo-physical methods need also expertise and high-tech spectroscopy to determine intermediate molecules generated during repair. So far, binding and repair kinetics of photolyase family especially for *Ec*Phr to ss and ds DNA were determined in a number of studies by biochemical assays. On the other hand, as its photorepair activity on ssDNA is relatively recent, the kinetics of Cry-DASH proteins is not widely available [79] .

In this study, we were particularly interested in determining the real time interaction of photolyase/cryptochrome family in the repair of UV-irradiated and UV undamaged ssDNA and dsDNA using SPR. I performed protein expression and purification experiments and also the preparation of single and double stranded oligomer substrates with ultraviolet-induced DNA damages.

MATERIAL AND METHODS

3.1 Surface Plasmon Resonance Spectroscopy (SPR)

Surface plasmon resonance (SPR) is an optical method to measure molecular interactions in real-time. Figure 3.1 shows working principle of SPR. When a beam of light whose angle of incidence is greater than the critical angle (θ_c), passes from material with a high refractive index (e.g. glass) into material with a low refractive index (e.g. water), the light is completely reflected (total internal reflection). If the material is coated with nobel metal such as gold then the beam of light is not fully reflected. Some of the light is lost into the metallic film [118]. The oscillation of the electrons in the valence shell of surface atoms matches with the frequency of photons of the incident light. This phenomenon is called surface plasmon resonance. The focused light provides a range of incident angles, and the reflected beam will cover the same angle range while the projection of the beam forms a band. The angle of incident light required to sustain the surface plasmon wave is called the angle of surface plasmon resonance (θ_{spr}). When SPR occurs within the spread angles, a dark line where the intensity of reflection reaches a minimum will appear in the band. SPR is very sensitive to refractive index changes at the surface so any change in refractive index of the solvent near the surface due to complex formation or dissociation is measured by SPR biosensors as a the shift in the angle of surface plasmon resonance θ_{spr}.
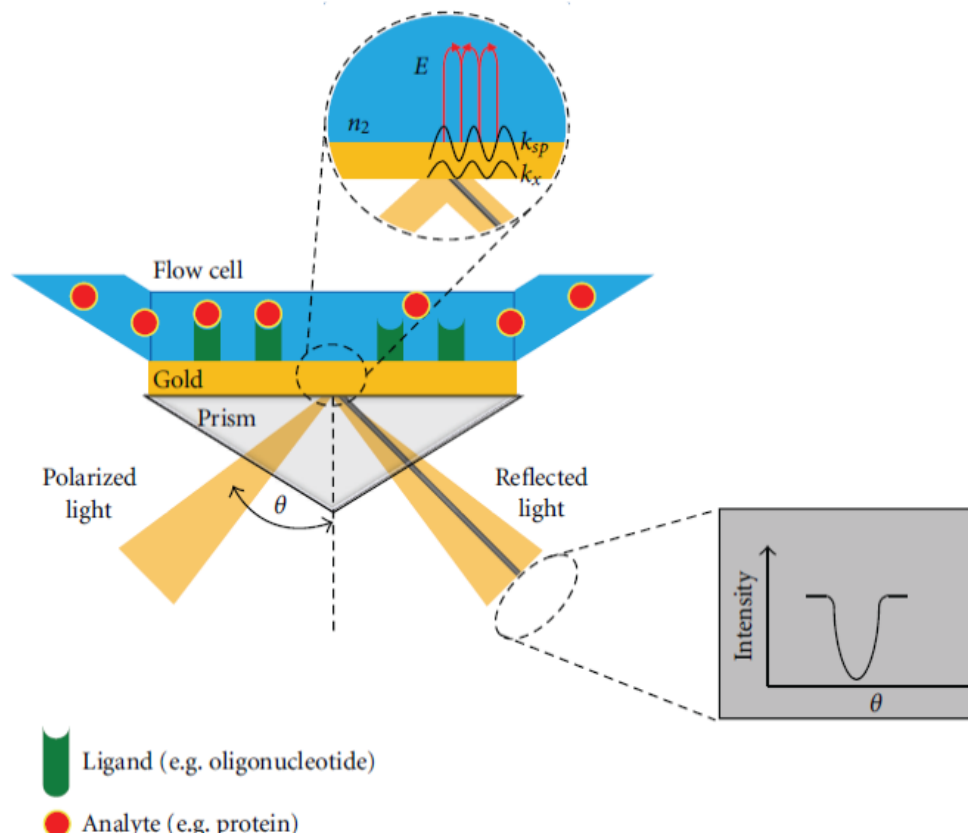
Figure 3. 1 The schematic representation of Surface Plasmon Resonance principle and analyte and ligand complex formation. Laser beam in a wide angle range is sent to film sensor. The light is reflected in the same range except for at the angle in which surface plasmon resonance occurs and reflection reaches a minimum. [118]

In order to analyze interactions between biomolecules in real time, one molecule (the analyte) such as protein, nucleic acid, antibody etc) is immobilized onto the sensor surface. Its binding partner (the ligand) is injected in aqueous solution (sample buffer) through the flow cell, continuously [119]. As the analyte binds to the ligand, refractive index of surface changes due to complex formation (Figure 3.1). The frequency of incident light photons (k_x) matches with the oscillation of the electrons at the valence shell of the surface atoms of the gold metal (k_{sp}). (Figure 3.1). The instrument uses a photo-detector array to measure very small changes in θ_{spr} due to the changes in refractive index. The result is plotted as response or resonance units (RUs) versus time (a sensogram). 1 RU is equivalent to a shift of 10^{-4} degrees. 1 RU correlates with the binding of approximately 1 pg protein/mm^2 protein to the sensor surface [118]. SPR allows for rapid qualitative and detailed quantitative analysis of both equilibrium and kinetic parameters of the protein-protein and protein-DNA interactions in real time without labeling requirements. A number of biological processes like transcription, DNA repair or recombination involve in DNA-protein interactions so several methods have been developed so far to analyze those interactions. However, mostly label–based methods are used such as the ligation of the analyte and/or ligand with reporters like enzymes fluorescent dyes, or radioisotopes. These biochemical methods sometimes result in false negative outcomes in cases where the active binding site or the conformation of the analyte is affected by labeling. High background binding is another disadvantage that leads to false positive with label based methods [120]. Alternatively, SPR is a label free method and allows the detection of real time complex formation kinetics with an a large dynamic range. In addition, SPR method is very easy to use and do not require special expertise[121]. To date, a number of protein-DNA interactions have been characterized by SPR including binding by the c-Myb DNA-binding domain to its specific DNA, non-sequence-specific binding by the HMG2 protein, and several zinc finger complexes with specific DNA. The binding constants found by SPR in these studies were found to be consistent with the ones determined by biochemical assays. DNA binding and repair activity of photolyase family proteins have been analyzed by

several different methods such as transformation, absorption, restriction site restoration, and enzyme sensitive site assays so far [25].

These assays can only give information about the kinetics of repair activity within minutes to hours with excessive required labeling steps

3.2 Apparatus and Reagents

For all experiments, two-channel SPR device SensiQ Discovery and BioCap sensor chips (neutravidin modified surface) were used (ICx Nomadics, Oklohoma City, USA). All experiments were conducted at a flow rate of 50 mL/min and at 25^0C. The buffer reagent, 1X phosphate buffer saline tablets, sodium hydroxide pellets and Tween 20 were purchased from Sigma Aldrich (Steinheim, Germany). EDTA was purchased from Applichem (Darmstadt, Germany). Dodecyl sulfate sodium salt (SDS) was bought from Merck (Hohenbrunn, GE). Synthetic oligonucleotides were purchased from The Midland Certified Reagent Co.(Midland, TX, USA). The base sequence of the 5'-Biotinylated probes (48-mers) were5'-(Biotin)-GACGCAGATCTACGAATTCGCTTAATTCGCTGCACCGGATCCCGCTAG-3'. In order to make double stranded DNA substrate, non biotinylated complementary strand was used for hybridization. Immobilization buffer was prepared from one PBS tablet in 200 mL dH2O (10 mM phosphate buffer, 2.7 mM KCl, 137 mM NaCl, pH 7.4). Tween 20 (0.005% (v/v) was also used in the running buffers as a surfactant to prevent the non-specific protein binding to sensor surface. NaOH (100 mM) and 0.1% (v/v) SDS were used as regeneration buffer and as instrument cleaning solution.

3.3 Preparation of Wild Type *Vibrio Cholerae* Photolyase (*Vc*Phr) and Wild Type *Vibrio Cholerae* Class I Cryptochrome (*Vc*CryI)

*Vc*Phr and *Vc*Cry1 were prepared using previously established method by Worthington et al. [122]. The plasmids encoding pUNC2001 (MBP-*VcPhr*), and pUNC2002 (MBP-*VcCry1*) were kindly obtained from Prof Aziz Sancar (University of North Carolina-Chapel Hill). To express proteins, *VcPhr* and *VcCry1* genes in pmalc2x bacterial

expression vector were transferred into *E.coli* UNC 523 *(phr-, uvrA-)*. The proteins were over-expressed by adding 300 mM isopropyl-1-thio-b-D-galactopyranoside (IPTG) until OD600 was reached to 0.6–0.8 the cultures were shaken to grow for another five hours at room temperature after IPTG induction. Next, the proteins were purified through affinity chromatography using amylose resin according to manufacturer's protocol (New England Biolabs, Inc.). Overexpression and purity of proteins were analyzed by Coomassie blue staining on 10% SDS-PAGE

3.4 UV irradiation and the Assessment of UV Lesions of DNA Substrate

Single stranded 48 bp oligonucleotides containing one T-T sites in the middle was suspended in sterile distilled water at final concentration of 160 µM as a stock suspension and appropriate dilutions were made in PBS buffer for SPR experiments. Stock DNA substrate was irradiated with Slyvania G8W at a fluence rate of 0.5 J/m^{2}s with total fluency of 30 J/m^2 by Slyvania G8W. The method used for UV damaged substrate was applied as described elsewhere [123]. The UV fluencies were measured using a UVX digital radiometer (Ultraviolet Products Inc.) with the appropriate sensor detecting UVR at 254 nm. The UV damage formation was assessed by the decrease in absorption of DNA substrate at 260 nm over time with a Nanodrop ND-1000 spectrophotometer Nanodrop, Wilmington, DE [124]. In order to prepare UV damaged DNA substrate, the 48 bp single strand DNA was irradiated by UVR with a flux of 0.5 j/m^2.s for 6 minutes to saturate damaged DNA with lesions, and the amount of damage was monitored by the decrease in UV absorbance due to UV lesion formation at 260 nm [124]. The total fluency of UVR was 175 J/m^2. After 100 J/m^2 UVR, most of single stranded DNA substrates were damaged and the whole DNA sample was saturated with UV lesions. Since the most commonly occurring lesions produced by UV light [109, 110, 124, 125] are CPD's, we decided to use 30 j/m^2 which was also described in previous studies [112, 122]. The ssDNA substrate prepared for this study carried mostly CPDs which were in sufficient amount for *Vc*CryI and *Vc*Phr to bind and repair in SPR experiments.

The amount and the types of damages were defined in previous studies [7, 125, 126] in which % 80 of UVR damages on DNA were mentioned to be CPDs, the second abundant lesions were defined as pyrimidine [6–4] pyrimidone photoproduct and small amount of DEWAR photoproducts. Since the most commonly occurring lesion produced by UVR are CPD's, we decided to use 30 j/m^2 which was described in previous studies [122, 127]. The ssDNA substrate prepared for this study carried mostly CPDs which were in sufficient amount for VcCry and VcPhr to bind and repair in SPR experiments. Double stranded UV damaged DNA was obtained by hybridization of UV damaged single stranded DNA with its unlabelled 48-bp complementary strand in 50 fold excess in hybridization buffer (50 mM Tris-Cl pH7.5 20 mM NaCl). Single stranded 48-bp oligos were mixed and heated at 95^{0}C for 5 minutes. Then, the mixture was slowly cooled down to room temperature overnight. This dsDNA substrate was used in appropriate dilutions for SPR assays.

3.5 Immobilization of Oligonucleotide Probes

Buffer solutions were freshly prepared from PBS tablets at room temperature just before the experiments started. All buffers were filtered through 0.45 μm filters to reduce particle load and avoid blockages in the instrument. The solution was then degassed using a vacuum pump in order to eliminate the bubbles in the flow cell which may destroy the SPR dips. The pH value of the solution was confirmed as 7.4 with MeterLabH PHM210 standard pH meter. Biotinylated DNA (14 nM) was prepared in PBS solution. Sample volume of 50 μL was used to inject over neutravidin coated surface at a flow rate of 50 μL/min. The system was allowed to equilibrate for 60 minutes.The protocol of immobilization of oligonucleotide probes was taken from Kızılel et al., (2012).

3.6 Assay Design

All protein samples were prepared freshly in 1X PBS solution at pH 7.4 and were activated in 1 mM DTT solution with exposure to blue light at 366 nm wavelength, 2

mW/cm^2 for 60 minutes. Fifty µL of each sample was injected over the DNA modified surface in the two-channel SPR device for 1 min. Bindings of the proteins to the DNA were recorded as response units. One of the channels was used as a sample channel and the other one was used as a reference in order to observe the nonspecific interaction in the channel. A control experiment was also performed for modified/unmodified-ssDNA/dsDNA in order to see the response of un-interacting couples. BSA is known as an un-interacting protein with ssDNA or dsDNA and was chosen for the control experiments. RU values are plotted after appropriate subtractions were made from a reference surface. Low RU values are measured due to the low surface analyte concentration, which is determined by the concentration of functional groups on the surface. It is also very common to observe RU values within the range of 15–20 in SPR experiments in many different studies [128-130]. Mathematical calculations and the statistical analysis of SPR results were taken from MSc. Thesis' of Enis Demir and Selimcan Azizoğlu. Details of the mathematical model and statistical analysis can also be found in the study of Kızılel et al., (2012) in PLoSOne.

RESULTS

3.1 Purification of *Vibrio cholerae* Photolyase and CRY-DASH Proteins

Genes were previously cloned into the pMal-c2x vector to express the corresponding proteins in *E. coli*, fused with maltose binding protein (MBP) to aid in solubility and purification of the recombinant proteins [121]. Both proteins were expressed at high levels, *Vc*Phr and *Vc*Cry1 were soluble and readily purified by affinity chromatography on amylose resin. Figure 3.2 shows the overexpression and purification of the three proteins by SDS-PAGE. The proteins were 95% pure after the affinity purification step and therefore appropriate for further spectroscopic and enzymatic analyses. Next, proteins were concentrated and checked for the presence of both FAD and MTHF. Figure 3.3 shows the absorption spectra of purified *Vc*Phr and *Vc*Cry1. The absorption spectrum of *Vc*Phr exhibited a major peak at 380 nm and minor peaks at 440 and 480 nm, (Figure 3.3A). This spectrum is consistent with the presence of MTHF, and a mixture of $FADH_{neutral}$ and FAD_{ox} in this protein. The near-UV absorption spectrum of VcCry1 was dominated by a peak at 380 nm and, in this preparation, minor absorption beyond 400 nm ascribable to low levels of oxidized forms of flavin (Figure 3.3B).
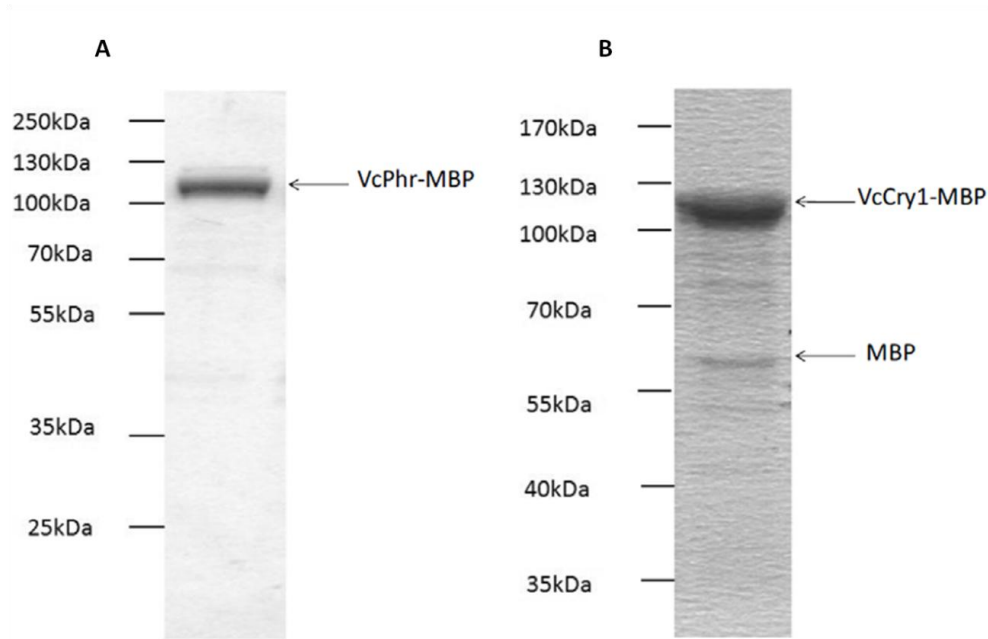
Figure 3. 2 SDS PAGE analysis of purified A; *Vc*Phr1-MBP B; *Vc*Cry1-MBP. Proteins were expressed in UNC523 photolyase deficient *E.coli* cells and purified by affinity chromatography using amylose resin. Purified *Vc*Cry1 (2 µg) of and purified *Vc*Phr (5 µg) were analyzed on %10 SDS-PAGE and stained with by Coomassie blue. Protein ladders shown in the figure were PageRuler plus prestained protein ladder (Fermentas) for *Vc*Cry1.
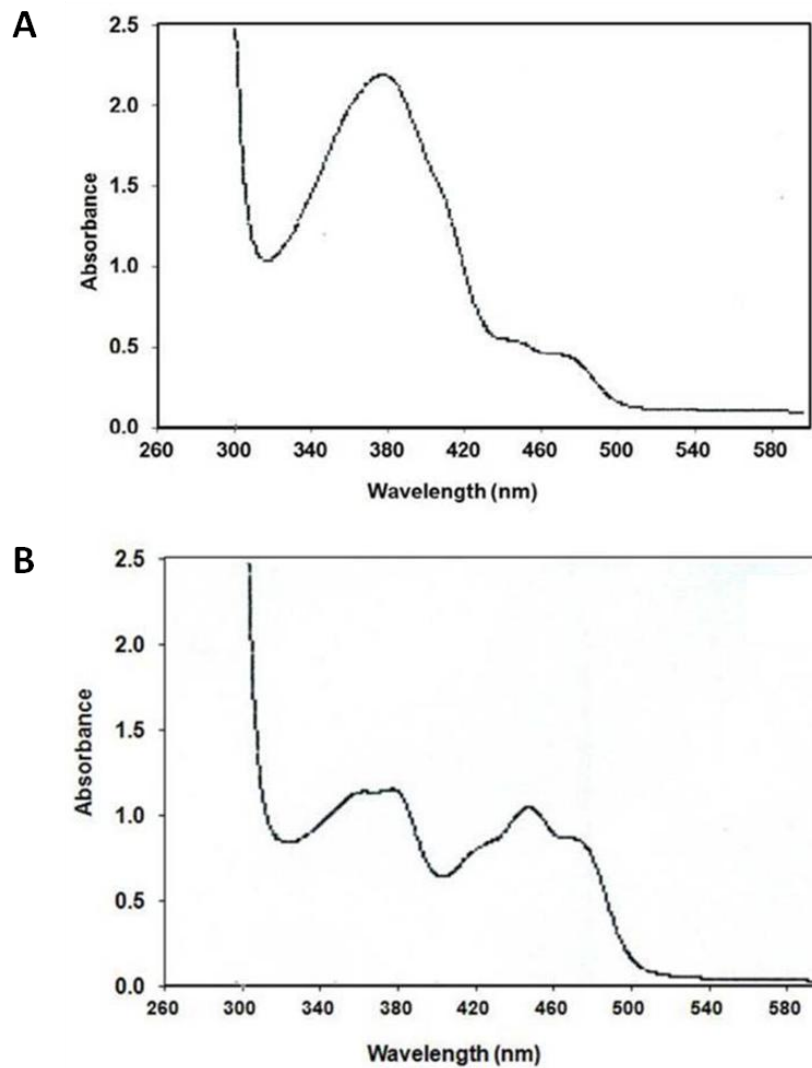
Figure 3. 3 Absorption spectra of purified proteins. Absorption spectra of purified proteins were taken between 260-600nm wavelengths. A; *Vc*Cry1-MBP. MTHF absorption at 380 nm and the minor peaks between 420-480 nm were the indication of different oxidation states of FAD in this purification. B; *Vc*Phr-MBP. The absorption peaks at 380, 420, 440 and 480 nm show reduced, oxidized, neutral radical forms of FAD existence in the purified *Vc*Phr.

3.2 Generation of Damaged DNA Substrate

The absorbance of single stranded 48-mer having T-T in the middle stock suspension at 260nm was taken before UVR. Then 200μl DNA suspension was exposed to ultraviolet light at 254nm for around 6 minutes at fluence rate of 0.5 $J/m^2.s$. During irradiation, the absorbance of DNA sample at 260nm was recorded. Due to the formation of C5-C6 bond between T-T dimers, the 260 nm absorbance of DNA decreased until UV lesions were generated in all DNA molecules in the sample Irradiation continued until the absorbance became stationary. Total fluence of UVR was calculated as 175 J/m^2 till the absorbance decline stops (Figure 3.4). After 175 J/m^2 UVR, most of single stranded DNA substrates were damaged and the whole DNA sample was saturated with UV lesions. With this absorance monitoring, the UV irradiation system was tested and it was observed that DNA could be damaged and detectable in our system. However, to become consistent with previous studies, the DNA substrate was irradiated with a total fluenceof 30 J/m^2 of UV irradiation [109, 110, 124, 125].
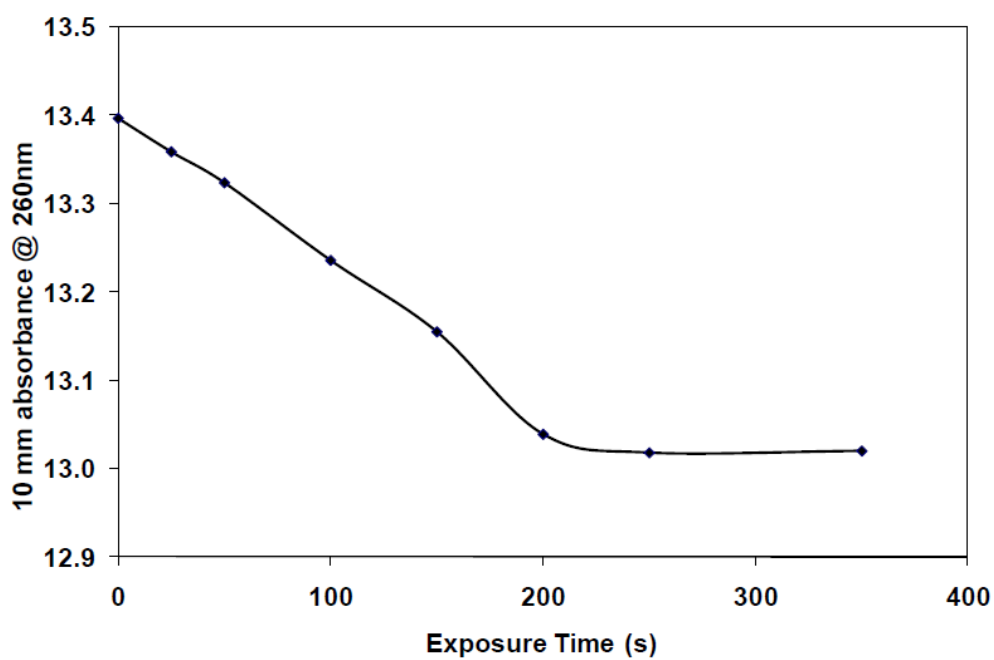
Figure 3. 4 UV_{254nm} irradiation of single strand 48-mer to saturation. ssDNA substrate was exposed to UV light at 0.5 J/m^2.s flux in quartz cuvette to saturate the number of damaged DNA molecules with UV lesions.

3.3 Characterization of DNA Interactions with *Vc*Phr

Figure 3.5A shows the binding interaction curves between immobilized undamaged ssDNA and *Vc*Phr within a photolyase concentration range of 1–40 μM. In a previous study, Sancar et.al showed that there was some insignificant binding (0.1%) between non-irradiated DNA and photolyase, and that some nonspecific binding was detected only at the highest enzyme concentration [131]. Therefore, contrary to UV-damaged DNA, the concentration of photolyase was increased from nanomolar to micromolar values in order to get a response. As the concentration of the protein increases, relatively steeper the refractive index changes (Figure 3.5A). However, this bulk index effect were recovered during ''the load mode'' immediately after the end of injection. A simple pseudo-first order binding interaction model (A+L = AL) which requires only three parameters, i.e. an association rate constant (ka), a dissociation rate constant (kd) and a maximum surface capacity (R_{max}), was fitted using Qdat analysis software. Reference surface data were subtracted from the reaction surface data in order to eliminate the refractive index change. The equilibrium dissociation constant K_D (k_d/k_a) was found within the range of 8.49–22.91 μM which is quite low, and shows only nonspecific binding between non-irradiated ssDNA and photolyase. A control experiment was also performed with bovine serum albumin (BSA) (10 μM) in order to distinguish the specific interactions from the nonspecific ones. BSA, which has no interactions with ssDNA or dsDNA,[132] was injected over the modified gold surface and the interactions were examined. BSA showed slightly higher interaction with surface bound DNA compared to the response unit observed with 10 μM *Vc*Phr. This result clearly showed nonspecific interaction of tested protein, i.e other components of the sample might be adhering to the sensor surface without a suitable selection of the ligand and that these cannot be attributed to the specific interaction of protein with the surface bound DNA. Low and nonspecific binding was also observed when *Vc*Phr was injected over undamaged dsDNA bound surfaces (Figure 3.5B). Compared to unmodified ssDNA, a relatively slower increase in nonspecific binding was observed

during injection. However, similar binding intensities (in terms of response units) of *Vc*Phr-dsDNA and *Vc*Phr-ssDNA were observed at the end of the injection phase (15–25 RU). Maximum binding responses in the case of 40 µM *Vc*Phr injections were observed as 22 and 24 RU with dsDNA (Figure 3.5B) and ssDNA (Figure3.5A), respectively. This indicates that the protein has low interaction with unmodified DNA regardless of its form. The SPR analysis showed lower equilibrium dissociation constant, and it was within the range of 8.46–41.30 µM. This is most probably due to the lower affinity of *Vc*Phr to the unmodified dsDNA. It takes longer time to remove the protein from the surface and that the form of the DNA has a slight affect on the dissociation rate.
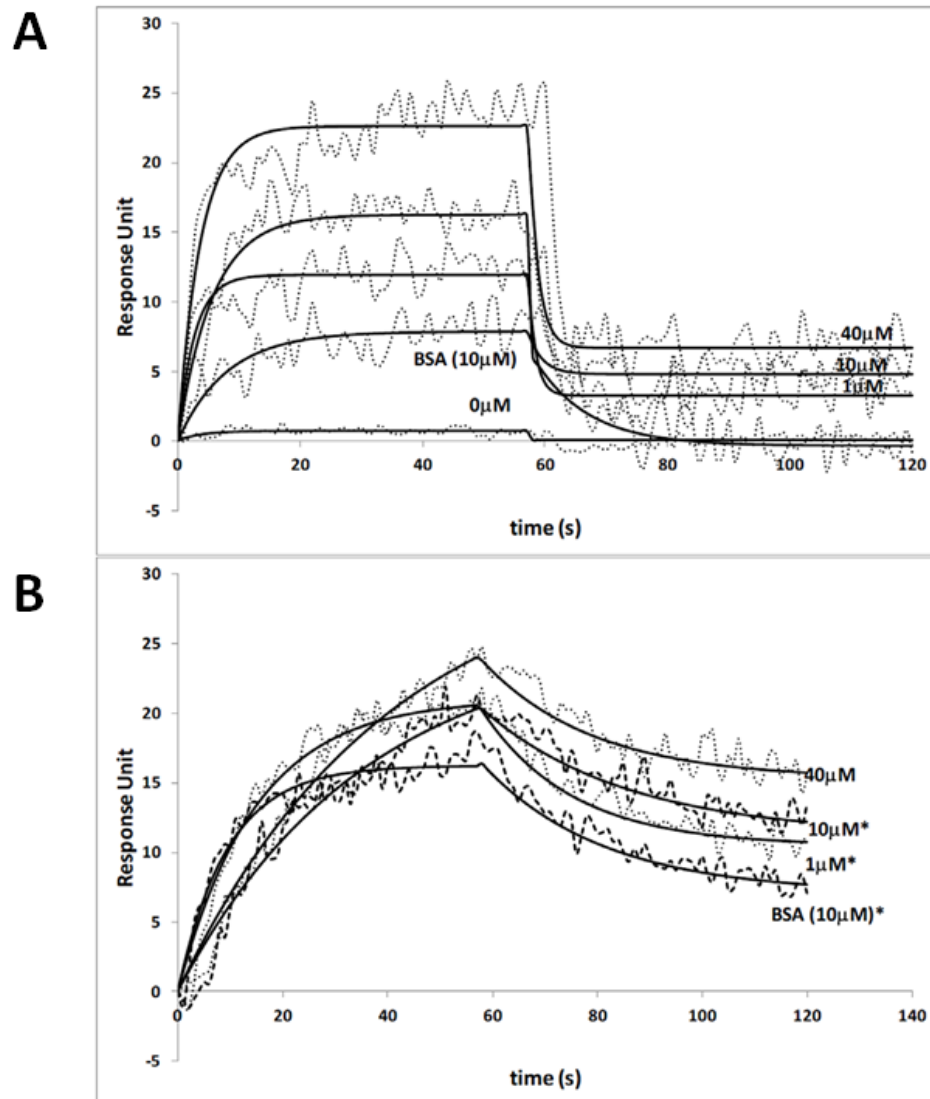
Figure 3. 5 (A) Interactions of VcPhr and undamaged ssDNA at various protein concentrations. Injection concentrations of 0, 1, 10 and 40 μM were used for VcPhr, while for BSA 10 μM injection concentration was used. (B) Interactions of VcPhr and undamaged dsDNA at various protein concentrations. Injection concentrations of 1, 10 and 40 μM were used for VcPhr, while for BSA 10 mM injection concentration was used. Data are mean 61.4 RU for 3 independent experiments. Response units are statistically significant with p<0.05 unless denoted with*, * = statistically not different. The figure was taken from Kızılel et al., 2012.

Next we were interested in exploring the affinity of the both proteins towards their true substrates by SPR. Figure 3.6 A shows the real-time interaction of UV-damaged ssDNA with VcPhr (10 nM in 1X PBS). The numbers on the figure denote injection sequences of VcPhr over UV-damaged DNA bound surface. It is established in the literature that photolyase binds to UV-damaged DNA with high affinity [133]. Photolyase binds to pyrimidine dimers in DNA and accumulation of binding of VcPhr to pyrimidine dimers on the surface increases the refractive index. The immediate increase in response unit right after the beginning of the injection mode could be occurring due to the start of the repair mechanism. As the repair mechanism completes, the photolyase starts to dissociate from the repaired DNA which results in lower refractive index. In this experiment, we have performed 6 consecutive injections of VcPhr onto UV-damaged DNA bound surface. Injections 1–3 showed a decreasing trend in response units even during injection mode, which could be attributed to the continuation of the repair mechanism. The intensity of interaction between the protein (VcPHR) and pyrimidine dimers decreases as the availability of damaged DNA decreases, i.e. as the UV damaged DNA is repaired during a specific injection, lower response units are observed at the subsequent injection. Injection 6 shows the low number of damaged DNA on the surface in the beginning of the experiment. It also shows the completion of the repair in in the middle of the injection with a very low response. Injection 6 further confirms that there is no available damage DNA on the surface. In Figure 3.6A**,** the decrease of the response units during association phase is faster in earlier injections compared to the decreases observed in following injections. This is most probably due to the fast repair of UV damaged DNA during earlier injections which results in fast dissociation in earlier injections. The equilibrium dissociation constant varies within the range of 10^{-8}–10^{-9} M [134]. Our data analysis shows that the K_D value varies between 0.8–1.8 nM which is similar to the previously measured biochemical equilibrium dissociation constant of 0.5 nM between VcPHR and UV damaged-ssDNA (Table 1). [134]
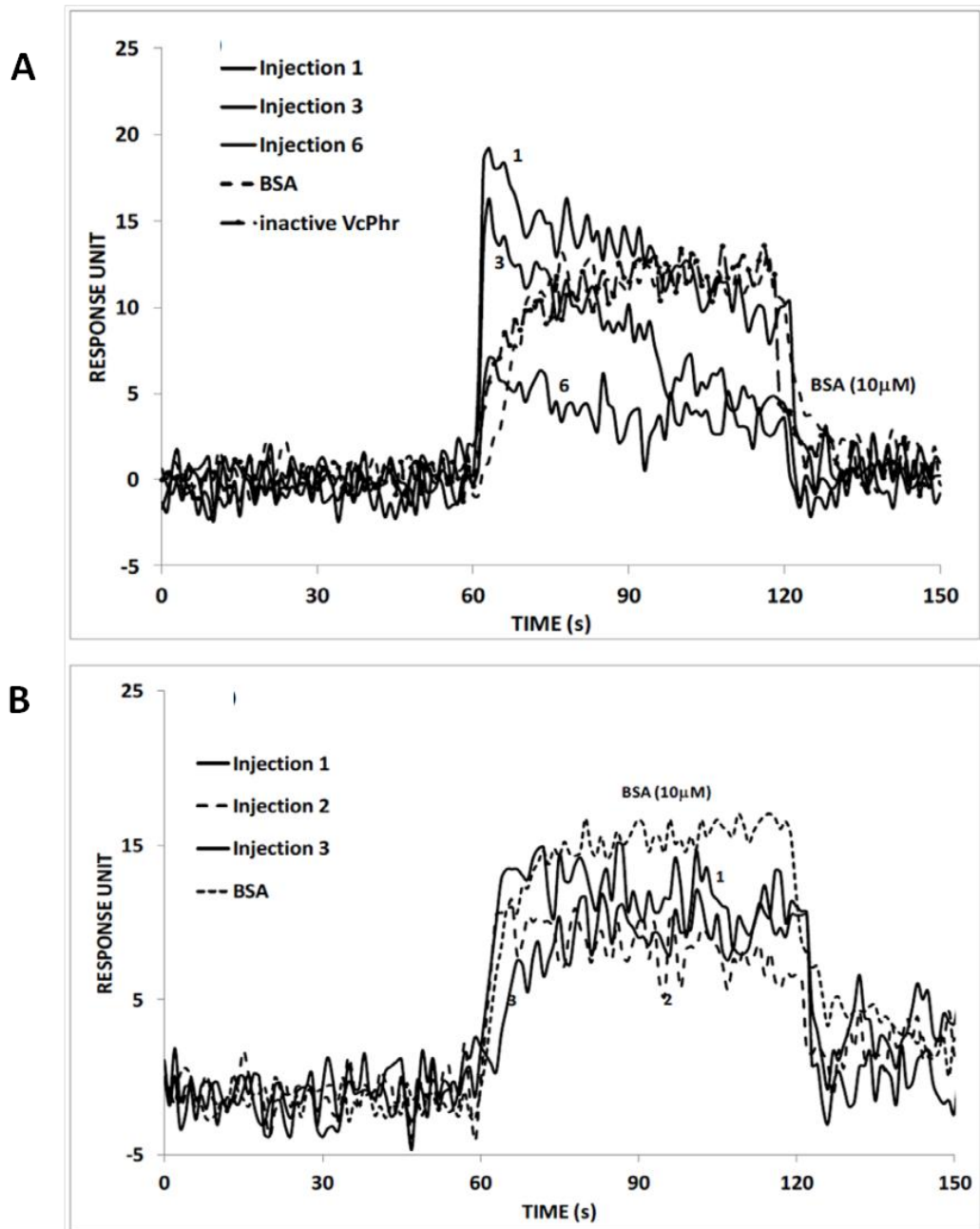
Figure 3. 6 (A) Sequential injection of *Vc*Phr on UV-damaged ssDNA, and injection of inactive *Vc*Phr on UV-damaged ssDNA. (Injection concentration of 1 μM was used for inactive *Vc*Phr) (B) UV-damaged dsDNA bound surfaces where the concentration of *Vc*PHR was kept constant at 10 nM for all injections. Data are mean ±SEM for 3 independent experiments (p<0.0002). *The figure was taken from Kızılel et al., 2012.

Table 3. 1 Comparison of binding constants obtained from this study and the ones obtained from biochemical assays in the literature

Protein	SPR K_d	Biochemical Assay
*Vc*Phr/UV damaged ssDNA	0.8–1.8 (±0.3) nM	0.5 nM [27]
*Vc*Phr/Undamaged ssDNA	8.49–22.91 (±1.4) µM	NA
*Vc*Phr/UVdamaged dsDNA	18.53–26.08 (±0.5) nM	0.79 nm [45] 4.76 nM [28]
*Vc*Phr/Undamaged dsDNA	8.46–41.30 (±0.6) µM	NA
Cry-DASH/UV damaged ssDNA	29–140 (±7.5) nM	NA
Cry-DASH/Undamaged ssDNA	106.4–128.6 (±12.2) µM	NA
Cry-DASH/UV damaged dsDNA	11.6–27.3 (±15.3) µM	NA
Cry-DASH/Undamaged dsDNA	33.8–80.2 (±10.7) µM	NA

*The table was taken from Kızılel et al., 2012.

In previous studies, it is demonstrated that photolyase had preference for single-stranded over double-stranded substrates [135, 136]. We also studied the interactions between UV-damaged dsDNA and *Vc*Phr (10 nM), and the response curve of the interaction with SPR is shown in Figure 3.6B. A sudden increase followed by a decrease in the response unit was observed with the start of first injection. Contrary to modified ssDNA, decrease in the response unit was slower when the surface is modified with dsDNA. This may be due to the lower accessibility of the pyrimidine dimers in dsDNA compared to ssDNA. The consecutive injections showed that the repair

mechanism continued during the first and the second injections. However, third injection showed a slight increasing trend in response unit which may be an indication of completion of the repair mechanism.

The calculated equilibrium dissociation constant found via SPR is within the range of 18.53–26.08 nM and about one order of magnitude higher than the value calculated from the interactions between ssDNA and the *Vc*Phr. The results clearly show that *Vc*Phr bind their substrate with a high affinity, and carry out the desired reaction rapidly. In order to validate further that specific interactions between UV-damaged ssDNA and *Vc*Phr could be attributed to the DNA repair activity, we investigated the interaction of inactive *Vc*Phr with UV-damaged ssDNA. For this experiment, *Vc*Phr was prepared as inactive by dissolving in PBS only, where the protein was not exposed to DTT and blue light. Figure 3.6A also demonstrates the real-time interaction of UV-damaged ssDNA with *Vc*Phr (1 µM in 1X PBS). Injection of high concentration of *Vc*Phr (1 µM) onto ssDNA bound surface resulted in low and mostly nonspecific binding. An interesting finding that was obtained in this experiment was the lack of dissociation of the protein from the surface, and hence decreases in response unit during the injection mode. When the active form of the protein was used, the dissociation of the protein from the surface, and decrease in response unit was observed even during injection mode (Figure 3.6A). The lack of decreasing trend in the response during the injection mode in Figure 3.6A may suggest that the inactive protein, which is incapable of DNA repair, cannot repair UV damaged and surface bound DNA, and hence may be interacting with surface bound DNA in a nonspecific manner.

3.4 Characterization of DNA Interactions with CRY-DASH

Interaction of Cry-DASH was also studied and quantified between ssDNA and dsDNA with SPR (Figure 3.7). Even though high concentrations of Cry-DASH were used for injections over undamaged ssDNA bound surface, the interactions between the protein and undamaged ssDNA were observed as nonspecific. Injection of high concentration

of Cry-DASH onto ssDNA bound surface resulted in very low and mostly nonspecific bindings, where similar responses have been obtained in control experiments done with BSA (Figure 3.7A). Low affinity for ssDNA also resulted in lower equilibrium dissociation constant, which was calculated within the range of 106.4–128.6 μM. Nonspecific bindings were also observed when high concentrations of Cry-DASH were injected onto dsDNA bound surface (Figure 3.7B). Even at high concentrations, both BSA and CRY-DASH injections resulted in low intensities in response units. Selby and Sancar observed that CRY-DASH repair CPDs specifically in ssDNA [124]. They were able to observe an apparent binding of Arabidopsis thaliana cryptochrome 3 and *Xenopus laevis* XlCry-DASH to the dimer in ssDNA. In this study, we investigated the interaction of the CRY-DASH with UV-damaged ssDNA bound surfaces by injecting protein samples over UVdamaged ssDNA bound surface. We performed subsequent five to six separate injections of CRY-DASH onto UV-damaged ssDNA bound surface, where Cry-DASH concentration was kept constant at 10 nM. Despite low concentration of the protein injected, a sudden increase in response curve was observed, while the intensity of the response gradually decreased even during the continuation of the protein injection (Figure 3.8A). Cry-DASH and UV-damaged ssDNA demonstrated similar interaction profile compared to the one observed with *Vc*Phr and UV-damaged ssDNA. The decreasing trend in response may indicate a repair mechanism on UV-damaged ssDNA by Cry-DASH. Even though subsequent injections did not show significant response changes, the decrease in responses continued by only a few response units. This could be due to the completion of the repair process, where further injections of protein did not result in binding of protein with ssDNA, most probably due to the depletion of damaged sites on surface bound DNA. It is critical to see a decrease in the response curve with the first injection as this decrease in profile shows the dissociation of injected protein from the surface even during injection mode. This could be attributed to real time repair of UV-damaged ssDNA with Cry-DASH. The equilibrium dissociation constant was calculated within the range of 29–140 nM. The equilibrium dissociation constant calculated here is within the nano-molar range, and may be

explained by the presence of significant binding interactions between Cry-DASH and UV-damaged ssDNA due to the repair of lesions in DNA structure. Contrary to the interactions observed with UVdamaged ssDNA and Cry-DASH, we did not observe significant binding interactions between UV-damaged dsDNA and Cry-DASH (Figure 3.8B). At higher concentrations of Cry-DASH (40 and 100 μM), Cry-DASH demonstrated nonspecific interactions with UV-damaged dsDNA, as the trends and magnitude in response units were similar to the binding observed with 40 μM BSA injection (Figure 3.8B). This could be explained with the absence in repair activity and hence lower affinity of Cry-DASH to UV-damaged dsDNA compared to its affinity to UV-damaged ssDNA. Similar result was also observed by Huang et al., where the authors proposed that the free energy of association for Cry-DASH and the CPD lesion is less favorable than the alternative stacking and pairing interactions of the CPD within the dsDNA [92]. As a result, our findings demonstrate that Cry-DASH proteins are unable to stabilize CPD lesions ''flipped out'' from double strand DNA.
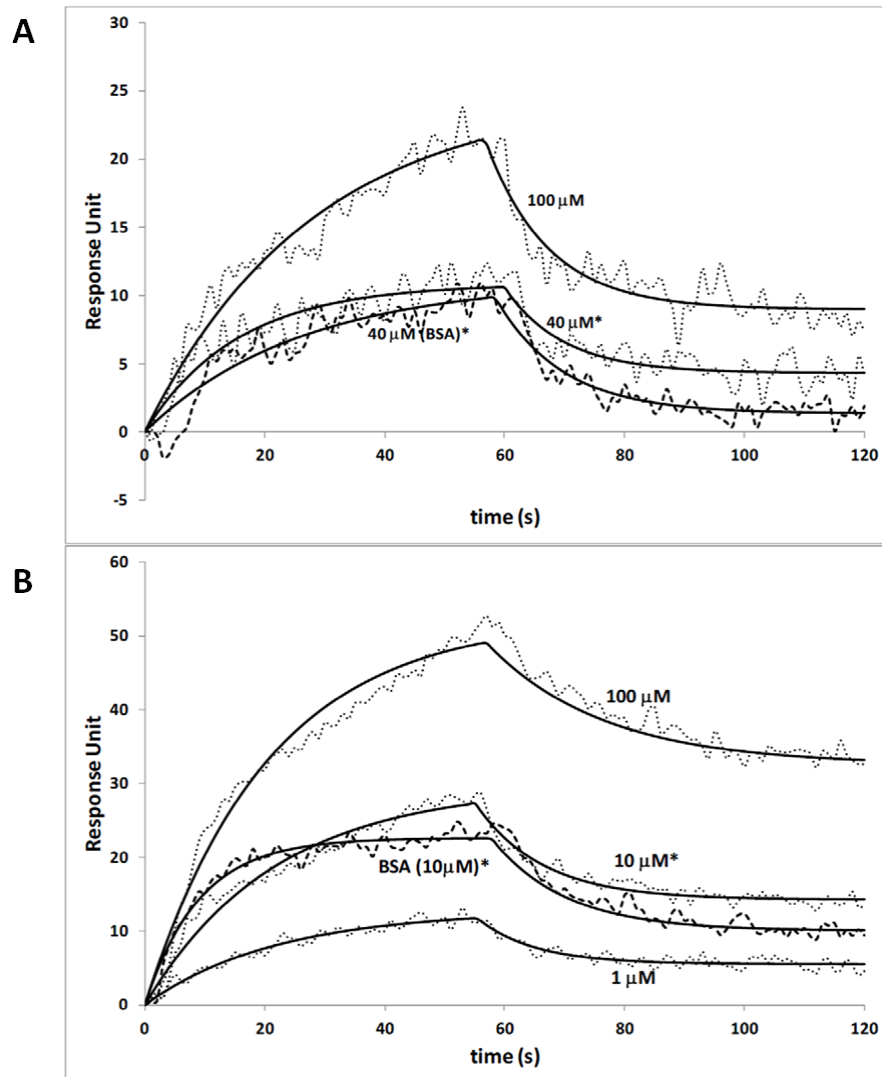
Figure 3. 7 (A) Interaction of **Cry**-DASH **with** undamaged ssDNA at various protein concentrations. Injection concentrations of 40, and 100 μM were used for **Cry**-DASH, while for BSA 40 μM injection concentration was used. (B) Interactions of **Cry**-DASH and undamaged dsDNA at various protein concentrations. Injection concentrations of 1, 10, and 100 μM were used for CRY-DASH, while for BSA 10 μM injection **c**oncentration was used. Data are mean ± SEM for 3 independent experiments (p<0**,**0001). *The figure was taken from Kızılel et al., 2012.
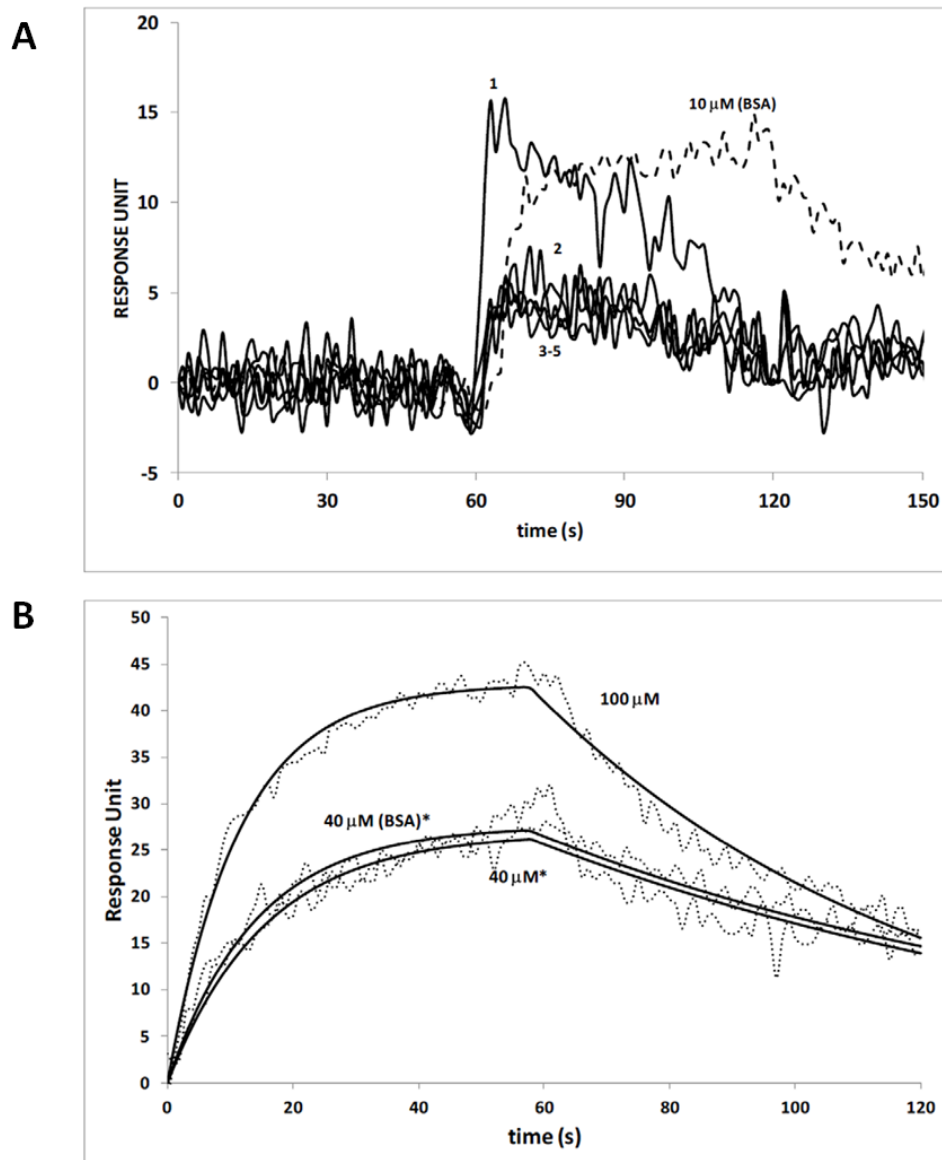
Figure 3. 8 Sequential injection of Cry-DASH on (A) UV-damaged ssDNA, and (B) UV-damaged dsDNA bound surfaces where the concentration of Cry-DASH was kept constant at 10nM for all injections. Data are mean ±SEM for 3 independent experiments ($p<0.0002$). *The figure was taken from Kızılel et al., 2012.

Chapter 4

PURIFICATION AND CHARACTERISATION OF

PHOTOLYASE/ CRYPTOCHROME FAMILY FROM

Cyanidioschyzon merolae

BACKGROUND

Photolyases/cryptochrome is flavoprotein family which is widely distributed within the three kingdoms, eubacteria, archaea and eukaryotes [76]. Photolyases use near UV/blue light photon energy to repair Pyr<>Pyr dimers and [6-4] photoproducts on double stranded DNA caused by UV whereas cryptochromes have diverse functions among unicellular and higher organisms despite the high structural similarity to photolyases. Instead of the repair function, cryptochromes are involved in the entrainment of biological clock through the reception of blue light, regulation of plant flowering, development or constitute a central part of the clock itself. Furthermore, they function as light-coupled magnetoreceptors in insects and possibly in migratory birds. Despite the functional characterization studies, there is little knowledge about their response to light and the photoreaction mechanism. Indeed, there are some photochemistry studies to date conducted with purified cryptochromes isolated from diverse sources, especially from higher eukaryotes such as *Arabidopsis, Drosophila, zebrafish, monarch butterfly* [64, 137-140]. Comparatively, photochemical behavior of mice and human cryptochromes could not even be investigated since it is very difficult to purify those proteins with their FAD cofactors from either their natural sources or heterologous

hosts [141]. For a comprehensive understanding about the action mechanism of cryptochrome, biochemical and genetic analyses require a well characterized protein in terms of identified substrate and a defined physiological function.

Unicellular microorganisms; bacteria, algae, fungi and protozoa are used as model organisms for genetic and biochemical studies since they have compact and structurally basic genome. Moreover, there is rapidly growing knowledge on the genome sequences of those unicellular microorganisms so genetic and biochemical manipulations such as generation of knock out mutant, site directed mutagenesis, identification of possible protein-protein or protein-DNA interactions can be carried out straightforward.

Cryptochromes have been evolutionarily conserved throughout the kingdoms, from archaea and fungi to humans. Several studies have indicated that aquatic organisms, particularly cryptogams such as ferns, mosses, and algae, contain several members of the cryptochrome and photolyase gene family. Recently, it has been shown that *Chlamydomonas reinhardtii* [142] and *Ostreococcus tauri* [3] contain these photoreceptors. However, there have been few studies on the roles of CRYs in unicellular photosynthetic organisms. Because light is an important environmental cue, one would expect that the CRYs and other blue-light photoreceptors are important for the ability of aquatic organisms to regulate their metabolism and behavior under light conditions. Moreover, some of the members of photolyase/cryprochrome family in lower eukaryotes have been shown to have dual functions like DNA repair and a role in gene regulation. Thus, the investigation of photolyase/cryptochrome family in simple/ unicellular organisms holds a potential to discover a novel function belonging to this family. Presumably, the examination of photolyases and cryptochromes of such primitive organisms may also shed light on the evolutionary history of the functional divergence of photolyase and cryptochromes due to the possibility of the existence of transient forms.

Cyanidioschyzon merolae is a primitive unicellular, photosynthetic microorganism that inhabits sulfate-rich hot springs. The genome of *C. merolae* has been completely sequenced [143, 144].This organism has been suggested as a good model system for the

exploration of cell structure and composition as well as organelle biogenesis and division. With its unique genome and cellular features, this primitive organism may help us evaluate the hypotheses that concern the origin of eukaryotic cells such as the primary endosymbiosis between cyanobacteria and eukaryotic hosts and the secondary endosymbiosis between red algae and their hosts.
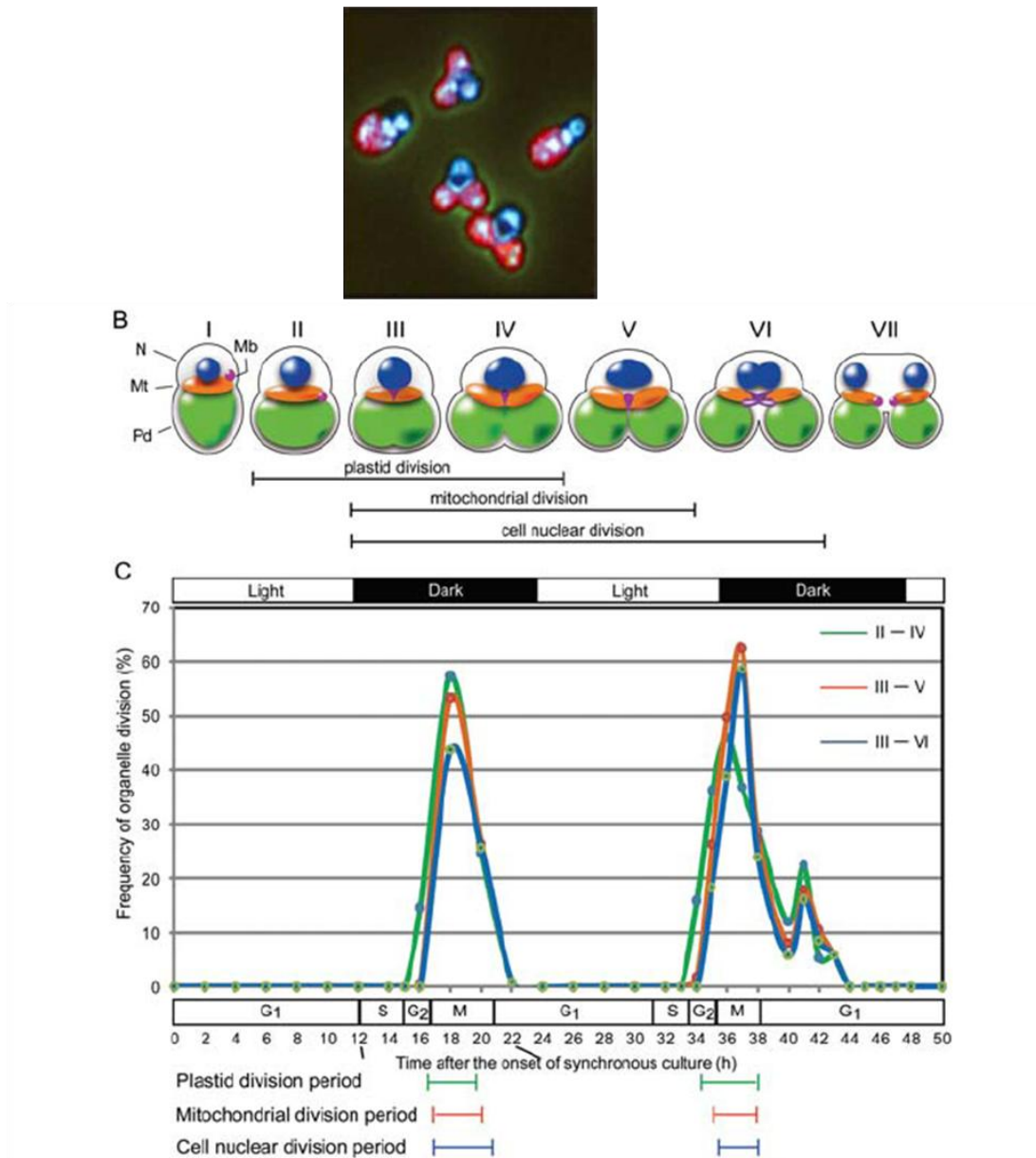
Figure 4. 1 Light/dark synchronized divisions of *C.merolae* plastids; chloroplast mitochondria, and nucleus. All of these organelles are undergo division only at dark period and in a sequence. The figure is taken from Fujiwara et al, 2009 [145].

In the genome of unicellular red algae *Cyanidioschyzon merolae,* seven putative photolyase/cryptochrome homolog genes with unknown function were identified. Interestingly, the genome sequence also revealed that there are no other photoreceptor genes that are homologous to the phototropins, BLUF proteins or phytochromes. Besides, *C. merolae* possesses a single nucleus, a single mitochondrion, and a single chloroplast [146]. Figure 4.1 shows the graphic that the division of Cm' plastid, mitochondria and nucleus are synchronized with light/dark periods. All of these organelles are undergo division only at dark period. Conclusively, in these red algae, photolyase/ cryptochrome family most probably is the only photoreceptor that plays a role in blue light photoreception, photosynthesis, gene regulation, and cell cycle.

The goal of this work is to investigate the involvement of photolyase and cyptochrome in from blue light reception to physiological responses of the red algae at all steps. For this, first photolyase and cryptochrome coding genes were isolated and overexpressed by heterologous expression. Then, proteins were purified at sufficient amounts for spectroscopic and biochemical analyses. The ancestral lineage of *C. merolae's* photolyases and cryptochromes were examined by phylogenetic classification.

MATERIAL AND METHODS

4.1 Phylogenetic Classification

Protein alignments and phylogenetic analyses were performed by MEGA 4.0 software (www.megasoftware.net) as previously described [86] [147]. The phylogeny was tested by neighbour-joining methods using 1000 bootstrap replicates to test the reliability of the inferred tree. The unrooted tree is drawn to scale with branch lengths in the same units as those of the evolutionary distances used to infer the phylogenetic tree.

4.2 Plasmids and Bacterial Strains

The PCR products of *Cm*PHR gene family were subcloned into the pGEM-T-easy vector (Promega Corp., Madison, WI). The *Escherichia coli* DH5α (F−endA1 glnV44 thi-1 recA1 relA1 gyrA96 deoR nupG φ80dlacZΔM15 Δ(lacZYA-argF)U169, hsdR17(rK-mK-),λ −) strain was used for genetic manipulations. The amplified genes were cloned into the pMal-c2x bacterial expression vector. This expression vector provides the *malE* gene sequence of *E. coli*, which encodes the Maltose Binding Protein (MBP) as the fusion protein in the N-terminus of CmPHR-like proteins. The plasmid constructs were named pMalc2x-*Cm*PHR1, pMalc2x-*Cm*PHR2, pMalc2x-*Cm*PHR3, pMalc2x-*Cm*PHR4, pMalc2x-*Cm*PHR5, pMalc2x-*Cm*PHR6 and pMalc2x-*Cm*PHR7. All pMALc2X constructs were subjected to full sequencing to make sure that there is no mutation within the coding region of *Cm*PHR genes during PCR amplification. The *Cm*PHR homologous genes were expressed in the *E. coli* UNC523 (*uvrA−, phr−*) host strain that was kindly provided by Prof. Dr. Aziz Sancar (Dept. of Biochemistry and Biophysics, UNC School of Medicine, NC, USA). The bacterial cultures were grown at 37°C in LB medium that contained 100μg/ml ampicilin. For luciferase reporter assays and subcellular localization experiments in mammalian expression system, all constructs were cloned into pGFP-N (Clontech Lab. Inc) mammalian expression vector which encodes Green Fluorescent Protein (GFP) at

the C-terminal of *Cm*PHR genes. The glycerol stocks were maintained at $-80\ ^{0}$C in LB medium that contained 15% (v/v) glycerol.

4.3 Genomic DNA Isolation from *C. merolae*

The red algae *Cyanidioschyzon merolae* cells grown at 42^{0}C with gentle shaking in 100 ml Allen's medium (10^{-5}M $(NH)_4H_2SO_4$, 2.10^{-6}M K_2HPO_4, 10^{-6}M $MgSO_4$, 5.10^{-7}M $CaCl_2$, trace metal solution; 7.16×10^{-8} M Fe-Na-EDTA $3H_20$, 4.67×10^{-8} M H_3BO, 3 9.04×10^{-9} M $MnCl_2\ 4H_2O$, 1.05×10^{-9}M $(NH_4)_6Mo_7O_{24}\ 4H_2O$, 7.65×10^{-10} M $ZnSO_4\ 7H_2O$, 3.16×10^{-10} M $CuSO_4\ 5H_2O$, 1.97×10^{-10} M NH_4VO_3) under constant white light for 1 month. Cells were collected by centrifuge at 5000rpm 5 minutes. 0,12g fresh algae were weighed. Then cells were frozen with liquid nitrogen and grounded with pestle and mortal. 700µl SDS extraction buffer (0.1 M Tris-Cl pH 8.0, 0.005 M EDTA, 0.5M NaCl, 1.6% SDS, 0.2% PVPP, 2% β-mercaptoethanol) was added onto cell to disrupt cell membrane and incubated at 37^{0}C one hour. Equal volume of 5M KOAc pH 7.5 ice cold was added onto cell lysate and incubated 20 min. Cell debris and undisrupted cells were collected by centrifuge at maximum for 15 minutes. Phenol:chloroform:isoamylalcohol extraction was carried out for protein elimination. Then, total DNA of *C. merolae* was precipitated with equal volume of absolute EtOH. 70% EtOH was added on to DNA pellet to wash remaining salts. The pellet was dried under vacuum. Total DNA was resuspended in 50µl 1X TE pH.8.0 buffer.

4.4 PCR Amplification and Cloning of *Cm*PHR/CRY Family Genes into Bacterial Expression Vector pMalc2-x

The probable photolyase/cryptochrome family genes were amplified from the genomic DNA of the *C. merolae* that was kindly gifted by the Matsuzaki's group. Seven *phr*-like gene-coding sequences were amplified by polymerase chain reaction (PCR) with gene-specific primers using a purified *C. merolae* genomic DNA template. Table 3.2 lists the primers to amplify *Cm*PHR (1-7) from genomic template for the cloning of bacterial expression vector.

*Cm*PHR1 was amplified with primers that flank BamH1 restriction sites are added to the end of the primers. *Cm*PHR2 was amplified with forward and reverse primers that flank HindIII and BamH1 sequences, respectively. *Cm*PHR3 primers have EcorI and HindIII sequences recognized in their forward and reverse primers, respectively. *Cm*PHR4 was amplified by the primers with BamHI and EcoRI restriction sites *Cm*PHR5 was amplified with forward and reverse primers that flank EcoR1 and HindIII sequences. *Cm*PHR6 was amplified with EcoRI and HindIII restriction sites. *Cm*PHR7 primers have restriction of BamH1 and HindIII. Except for *Cm*PHR4 and *Cm*PHR3, PCR amplifications were performed under these conditions with Taq polymerase (NEB, England) for 30 cycles of the following program: 94^0C for 30s, 55^0C for 30s and 72^0C for 90s. Open reading frame of *Cm*PHR3 amplified in two steps as shown in Figure 4.2. First fragment included 2500bp and the second fragment consisted of 1200bp. First, fragments were amplified with sequence specific primers. PCR products were straightly subcloned into pGEM-Teasy vector. Then, fragment II was cut out from subcloning vector with SalI and HindIII restriction enzymes. Digested fragment was isolated from agarose gel by Qiagen gel extraction kit. Next, subclone having fragmentI was digested with EcoRI and SalI enzymes. At a common restriction site at 3'end of fragmentI and 5' end of fragmentII were subjected to ligation with T4 DNA ligase (Fermentas). Full length *Cm*PHR3 was amplified with forward and reverse primers specific to 5' and 3' ends. Full length *Cm*PHR3 was cloned into EcoRI and HindIII restriction sites of pMALc2-x. *Cm*PHR4 was amplified in the presence of 6% ethylene glycol using 30 cycles for amplification at the following modified program; 94^0C for 30s, 50^0C for 30s, and 72^0C for 120s. PCR products were purified with Qiagen PCR purification kit (Qiagen). Then, all PCR samples and the vector subjected to restriction digestion. Digested vector DNA and PCR products were run on 1% agarose gel for an hour and then corresponding DNA bands were cut out of the gel and extracted from agarose gel by Qiagen Gel extraction kit. Isolated vector DNA and genes were cloned by ligation.

Table 4. 1 Sequence of CmPHR /CRY specific primers for pMALc2-x vector cloning

*Cm*PHR1	Fwd	GAATTCGGATCCATGTGGGTCATCTTGACCATGG
	Rev	TCTAGAGGATCCTCATGACGACGATGACGATGACGATG
*Cm*PHR2	Fwd	ATTTCAGAATTCATGTACGTTGTGTTGCCTGCACAC
	Rev	CAAGCTTGCTCACGACTCGTGATGCACCGC
*Cm*PHR3	Fwd	ATTTCAGAATTCATGTCGTCGTCGAGACGACCTTCGG
FragmentI	Rev	GGTACCTGGATCAACCGCCGCGTT
FragmentII	Fwd	ACAAATCCTGACTTTATGCGCGCG
	Rev	CAAGCTTGCTCAGGGCGCGGCACGCTGTAGCGC
*Cm*PHR4	Fwd	GAATTCATGCACCATTGTGTCACAGTGAACGGC
	Rev	CAAGCTTGCTCAGGCAGCAGCTTGAGCGTCACTTTT
*Cm*PHR5	Fwd	ATTTCAGAATTCATGAGTTGGGGACTGGTCTGG
	Rev	CAAGCTTGCTCACCGCTTCTG GGATCGAAGGTA
*Cm*PHR6	Fwd	GAATTCGGATC-CATGGTTCTGGGCTTTGCTTTTG
	Rev	CAAGCTTGCTCAGCTCGCCTGGGGCGCTGCAGC
*Cm*PHR7	Fwd	TTCGGATCCATGCCCGCGTATCCTCCT
	Rev	CAAGCTTGCTCATCTGCGCTTGTCGTC

Ligation reaction was performed for an hour at room temperature in 10μl volume including 5 μl T4 DNA ligase buffer (2X), 1 μl pMALc2-x plasmid (50ng/ μl), 1 μl T4 DNA ligase (3 Weiss Unit/ μl) ve 3 μl PCR (50 ng) product. 10μl ligation product was chemically transformed to 100μl competent *E.coli* DH5α (2 minutes incubation on ice following 90 sec at 42^{0}C incubation). Then, 900μl LB was added on to bacteria and incubated at 37°C with shaking 1 hour. Following incubation, grown cells were spread on to LB-amp (100 μg/ml) and incubated overnight at 37°C for selection of

transformants. Colonies resistant to ampicilin were selected from the plate and grown in 2ml LB-amp (100 µg/ml) liquid media overnight at 37°C. Grown cultures were subjected to alkaline lysis mini–prep plasmid DNA isolation process. 1.5 ml grown culture was centrifuged at 14,000 rpm to obtain cell pellet. Supernatant was discarded. 150 µl GET buffer (50 mM glucose, 10 mM EDTA and 25 mM Tris-HCl pH8.0) was added on to cell pellet for resuspension. Then, 150µl lysis buffer (0.2N NaOH, %1 SDS) was added on to cell suspension to disrupt cell membrane and chromosomal DNA structure. At final, 200µl 3M KOAc pH4.8 buffer was added to form chromosomal DNA and protein aggregate. Samples were centrifuged at max. (14000rpm) 15 min. to separate precipitate. Supernatant having plasmid DNA was taken into a new eppendorf tube and 2 volumes absolute EtOH was added to precipitate nucleic acids. Samples were centrifuged at max. (14000rpm) 25 min. to obtain plasmid DNA pellet. Pellet then was washed with 70% EtOH. Supernatant was discarded and DNA pellet was dried at vacuum drier. Each plasmid DNA sample was resuspended in 50 µl TE (10 mM Tris-HCl pH.7.4 and 1 mM EDTA) buffer. In order to select plasmid construct bearing PCR gene product, 10µl plasmid DNA samples were subjected to restriction digestion with corresponding enzymes. Samples were loaded on 1% agarose gel and run for 20 minutes at 90V. Agarose gel was visualized by Bio-Rad gel documentation system.
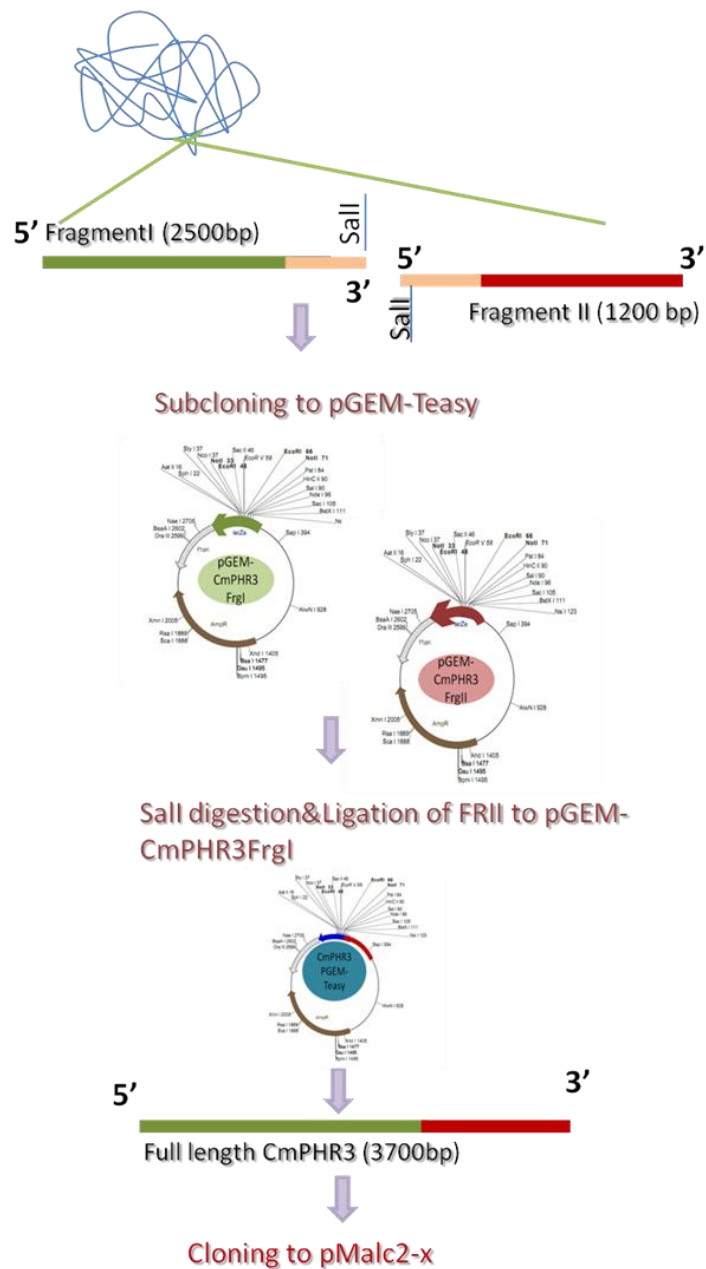
Figure 4.2 Schematic representation of the amplification and cloning strategy of CmPHR3 gene. 3700nt long CmPHR3 gene was amplified from *C.merolae* genome as two fragments (FRI-2500nt and FRII-1200nt). Fragments were subcloned into pGEMT-easy vector. Overlap region of the two fragments holds single restriction site of Sal1. FRI and FRII were digested with SalI and FRII was ligated into linearized FRI-

pGEMT-easy construct. Full length CmPHR3 gene was finally constructed in pGEMT-easy vector. CmPHR3 full length was amplified by PCR from CmPHR3-pGEMT-easy construct with five prime and three prime specific primers. Full length gene was cloned into pMALc2-x bacterial expression vector.

4.5 Protein Expression and Purification

The plasmid pMalc2-x constructs were chemically transferred to the *E. coli* UNC523 strain. The proteins were expressed at 37°C in 2 L of LB-amp (100μg/ml) medium until the OD.600 of 0,6–0,8 was reached. Isopropyl-1-thio-d-galactopyranoside (IPTG) was added to the medium to reach a final concentration of 0.3 mM. Then, the cultures continued growing at 23°C for 5 h. *Cm*PHR3, *Cm*PHR4, *Cm*PHR7 were also induced at 16^{0}C for 16–18 h to increase its solubility. To purify the proteins, the cells were harvested by centrifugation at 5000× rpm for 10 min. The pelleted cells were resuspended in MBP buffer (20 mM Tris–HCl, pH 7.4; 150 mM NaCl; 1 mM EDTA; and 10μM β-mercaptoethanol). The cells were sonicated 10 times for 10s each on ice for lysis, and the cell debris was removed by centrifugation at 14,000 rpm for 1 h. The MBP-tagged proteins were purified on amylose resin by affinity chromatography according to the manufacturer's protocol (NEB, England). Briefly, soluble fraction of cell lysate was passed through amylose containing chromatography column under air pressure. Column was washed twice with 0.5 M NaCl containing MBP buffer. MBP tagged CmPHR proteins were eluted with 15mM maltose in MBP buffer at 2X column volume. The eluates were identified by SDS-PAGE followed by Coomassie blue staining and western blotting using anti-MBP antibodies. The eluates were dialyzed against a storage buffer that contained 50 mM Tris–HCl, pH 7.5; 100 mM NaCl; 1mM EDTA; 5μM dithiothreitol (DTT); and 50% (v/v) glycerol. The purified proteins were stored at −20°C in storage buffer.

4.6 Spectroscopic Analysis

The native photolyase-like proteins absorb wavelengths between 360–550 nm. The protein-bound form of FAD has absorption maximum at 380nm for its reduced form (FADH⁻) and absorbencies belong to blue neutral radical or FAD_{ox} can be seen at 420, 480, 580 and 625nm, respectively. During purification, the oxidation of FAD cannot be avoided, so most of the purified protein contains oxidized or neutral FAD. Folate class of photolyases absorbs at 380nm and dominates the spectrum in the visible range so that FADH⁻ absorption cannot be detected clearly in native protein spectra.

In order to measure flavin and folate contents of CmPHR proteins, both spectra from native and denatured proteins were taken. The absorption spectra of the native proteins were measured with a Shimadzu UV-1601 spectrophotometer. To determine the stoichiometric ratio of the apoprotein to the cofactors, the holoproteins were heated at 95^0C for 5 min in a buffer that contained 50 mM Tris–HCl, pH 7.5, 50 mM NaCl; 5 mM EDTA, 1mM dithiothreitol and 0,8% SDS. The precipitated protein was then removed by centrifugation, and the absorption spectra of cofactors were measured. When the proteins were denatured, MTHF was released from the enzymes. The 5–10 methenyl bridge responsible for the 380nm absorption peak was broken at neutral pH to generate 10-formyltetrahydrofolate, which does not absorb wavelengths above 300 nm and hence does not contribute to the near-UV absorption spectrum of the cofactors [148]. The molar extinction coefficient of methenyltetrahydrofolate (MTHF) at 370–380 nm is 24,495 $M^{-1} cm^{-1}$, and the molar extinction coefficient of FADox at 450nm is 11,300 $M^{-1} cm^{-1}$. The concentrations of the apoenzymes were calculated from their absorption values at 280 nm using their theoretical extinction coefficients ($\varepsilon 280$ for CmPHR1= 109780 $cm^{-1} M^{-1}$, CmPHR2 = 147820 $cm^{-1} M^{-1}$, CmPHR3=176700 $cm^{-1} M^{-1}$ CmPHR4= 152290 $cm^{-1} M^{-1}$, CmPHR5 = 126280$cm^{-1} M^{-1}$ and CmPHR6=49850$cm^{-1} M^{-1}$, CmPHR7=177730 $cm^{-1} M^{-1}$).

4. 7 Radioactive DNA Substrate Preparation

Single stranded 48-bp deoxyribooligonucleotides containing cyclobutane pyrimidine dimer (CPD) or [6-4] photoproduct in the middle were kindly gifted by Prof. Sancar's Lab (UNC, Chapel Hill, NC, USA).

48-bp single strand was consisted of three oligonucleotides; right and left arms were 18 nucleotides long and middle oligo was 12 nucleotides long. The single stranded oligo was radiolabeled at the 5' end of CPD or [6-4] UV lesion containing middle oligo with ^{32}P ATP by T4 polynucleotide kinase (NEB). 100 pmoles of middle oligo nucleotide labelled with ^{32}ATP in 70 mM Tris-HCl pH7.6, 10 mM $MgCl_2$, 5 mM dithiothreitol with T4 polynucleotide kinase (40 U) at 25°C for 4 hours. 100pmoles of right and left arms and 100pmoles of the complementary oligonucleotide also were labeled with cold ATP at the 5' end in the same reaction conditions given above. Hot and cold reactions were mixed and DNA's were precipitated with 2X volume absolute EtOH. DNA pellet was washed three times with 70% EtOH. Then, pellet was dried under vacuum. Oligonucleotide pellet was dissolved in 20µl 1x annealing buffer (20mM Tris-Cl pH7.4, 50mM NaCl, 2mM $MgCl_2$). Annealing mixture was heated at 95^0C 5 min. then slowly cooled down to room temperature for stochiometric annealing to occur.

After annealing, oligonucleotides were ligated with 2U T4 DNA ligase (Fermentas) in 1xT4 DNA ligation buffer in 40µl overnight at 16^0C. Ligation products were EtOH precipitated. [6-4] PP containing radiolabelled substrate was subjected to CPD repair with *E.coli* PHR to eliminate residual CPD containing oligonucleotides. 1µM purified *Ec*Phr was incubated with [6-4] PP ligation product in photoreactivation buffer (50 mM Tris–HCl, pH 7.5; 100 mM NaCl; 1 mM EDTA; and 10mM DTT) in 100µl reaction volume under blue light (364nm) for 1 hour at room temperature . To prevent UVR under 300nm, reaction took place under glass layer. In parallel, CPD ligation product was treated with 1µM Xl[6-4] PHR at the same conditions. After photoreactivation, oligonucleotides were subjected to 1:1(v/v) phenol:choloroform extraction and finally, DNA was precipitated with absolute EtOH (1:2.5 v/v). Then the pellet dissolved in restriction digestion buffer NEB2 (NEB). CPD and [6-4]

photoproduct containing oligonucleotides were subjected to restriction digestion to eliminate impurities that are oligos without any UV lesion. The middle oligo at the UV lesion site contains MseI restriction site so if any impurity remains in prepared DNA substrates , MseI cuts 48bp oligo into two pieces. Ligation products for CPD and [6-4] DNA substrates were precipitated with equal volume of absolute EtOH. The DNA pellets were dissolved in 1x NEB2 buffer and digested with 10U Mse1 enzyme in 100µl volume for 16 hours at 370C. Restriction digestion reaction dried under vacuum and pellet dissolved in 1xformamide loading buffer. At 950 C, samples were heated for 5 minutes and loaded on to 8% sequencing gel. The gel runs 2 hours at 20mA. Corresponding bands were excised from the gel and the gel was dissolved in 1ml gel extraction buffer (0.3M NaOAc pH 5.2, 10mM EDTA, 0.5% SDS) overnight. DNA was subjected to EtOH precipitation. The resulting DNA pellet was dissolved in 50µl 1XTE buffer (10mM Tris-Cl pH8.0, 1mM EDTA).

4.8 *In vitro* Photolyase Repair Assay

The radiolabeled 48-bp DNA substrates that contained CPD or ([6-4]) damages within MseI restriction sites (TTAA) were prepared as described above according to given protocol [86] . The substrates were prepared as single stranded. To obtain double-stranded substrates, the appropriate complementary strands were added at 100-times the concentration of the single-stranded substrate to a final concentration of 10 µM in hybridization buffer (50 mM NaCl, 10 mM Tris–HCl, 10 mM $MgCl_2$ and 1 mM DTT). Each hybridization reaction was   heated at 95^0C for 5 min and   slowly cooled to room temperature. The assay is based on the restoration of the MseI restriction site on the substrates due to the photorepair of the UV damage   by the   appropriate DNA photolyases. For   each reaction, 0.3 nM substrate in 20 µL photoreactivation buffer (50 mM Tris–HCl, pH 7.5; 100 mM NaCl; 1 mM EDTA; and 10mM DTT) was   incubated   with 1 µM of   the appropriate enzyme in the dark at room temperature for 30 min and   was then exposed to 366nm light from two black light lamps (F15J8-BLB,General

Electric) filtered through a glass plate to remove wavelengths less than 300 nm. Irradiation was performed at a rate of 0.2 mW cm^{-2} for 90 min. Following photoreactivation, the DNA was extracted with phenol, precipitated with ethanol, and resuspended in 40 µL of buffer that contained 10 mM Tris–HCl, pH 7.9; 50 mM NaCl; 10 mM MgCl$_2$, and 1 mM DTT. Forty units of MseI were added to the sample, and digestion was performed at 37^{0}C overnight. Products were analyzed on 8% polyacrylamide sequencing gels.

4. 9 Photolyase Complementation Assay

To identify the photoreactivating function, the members of the *C. merolae* photolyase/cryptochrome family that had already been cloned into the pMal-c2x vector were transformed into E. coli UNC523 strain. The cells were grown for 16 h at 37^{0}C to a concentration of 2–5 × 10^{-9} cells ml^{-1}. The cultures were washed with phosphate-buffered saline (PBS) and resuspended in PBS buffer of the same volume as the original culture. Then the cells were exposed to UV radiation (General Electric germicidal lamp GT5, emitting mainly at 254 nm) at fluences of 10 J/m^{-2}, 20 J/m^{-2} and 40J/m$^-$2 with a fluence rate of 1 J/m^{-2} s^{-1}. The photoreactivation was performed under blue light at 366nm (Sylvania F15T8/BLB black light, emitting mainly 366 nm) with a fluence rate of 2 J m^{-2} s^{-1} for 90 min with shaking. The UV and black light fluencies were measured using a UVX digital radiometer (Ultraviolet Products Inc.). The plates were covered with a plastic Petri dish cover and a 1-cm-wide window glass to eliminate wavelengths below 300 nm. Following the UV and photoreactivation treatments, the appropriate dilutions were made, and the cells were spread on LB plates that contained 100 µg/ml ampicillin. The plates were incubated in the dark at 37^{0}C for 16 h. Then the colonies were counted and the numbers of surviving colonies relative to the non-irradiated controls were calculated.

4.10 Electromobility Shift Assay (EMSA)

48-nt radiolabelled unmodified ssDNA was also used for DNA binding of purified CmPHR proteins for electromobility shift assay (EMSA). The DNA binding ability of CmPHR proteins both to single stranded and double stranded DNA was evaluated. To prepare double stranded substrate, 10nM radiolabelled single stranded DNA was mixed with an unlabeled 48-mer complementary strand at 500nM before annealing. Then, mixture was heated at 95^0 C for 5 min. and cool down very slowly to hybridize. The purified proteins at 100, 250 and 500nM were incubated with radiolabeled ss or ds DNA in 20μl binding buffer 15mM Tris-Cl(pH 7.5), 20mM NaCl, 5mM DTT, 0.5nM radiolabelled DNA substrate at 30 ^{0}C for 30 min [124]. DNA-protein complexes were analyzed by separating products with nondenaturing 5% polyacrylamide gels in a buffer of 25 mM Tris, 25 mM borate, and 0.6 mM EDTA, pH 8.3. Gels were run in the dark at 4°C.

4. 11 Luciferase Reporter Gene Assay

CmPHR family was investigated for transcriptional repression activity. For this, CmPHR genes were cloned into pEGFP-N1 vector by regular cloning protocols [149]. Mammalian two hybrid system was used to determine protein-protein interactions and dual luciferase reporter assay system was used for measuring the luminescent signal resulted from the activation of luciferase reporter gene up on protein-protein interaction. mBmal1 gene and mClock genes were cloned previously into pCMV-SPORT6 mammalian expression vector. Luciferase reporter gene was under the control of mPER2 promoter in pGL3 reporter vector. Mouse circadian rhythm transactivator proteins mBMAL1 and mCLOCK forms a heterodimer and bind to mPER2 promoter. So, the transcription of luciferase gene becomes activated. On the other hand, mCryptochrome acts as a transcriptional repressor by forming a complex with mBmal1: mClock heterodimer. The presence of repressor protein like cryptochrome in the system causes a decrease in luciferase expression since it interferes with BMAL1-CLOCK-DNA interaction. Hence, the potential repressor activities of Cm Phr/Cry proteins were

analyzed by comparing the decrease in luminesence. In order to investigate the transcriptional repressor activities, *Cm*PHR 1-7 were cloned into multiple cloning site of pEGFP-N1 vector (Clontech Lab. Inc)

4. 11.1 Primer Design and PCR Amplification

Gene specific primers with flanking restriction sequences were designed to amplify CmPHR genes for cloning them to the appropriate restriction sites in the multiple cloning site of pEGFP-N1 vector. PCR reactions were set up in 50µl total volume including 1X Taq polymerase buffer, 6mM from each primer, 200µm dNTP, 0.5U Taq polymerase (Fermentas), and 50ng plasmid DNA template. PCR conditions were set up as follows; 1 cycle 95^0 C 4 min, 95^0C 30sec, 55^0C 30sec, 72^0C 1.5min for CmPHR1, CmPHR5, CmPHR6 and 72^0C 2 min. for CmPHR2, CmPHR 4, 72^0C 4 min. for CmPHR3, CmPHR7 for 30 cycles. PCR products were purified with Qiagen PCR purification kit (Qiagen). Then, all PCR samples and the vector subjected to restriction digestion.

4. 11.2 Cloning of *Cm* PHR/CRY Genes into pEGFP-N1 Vector

Digested vector DNA and PCR products were run on 1% agarose gel for an hour and then corresponding DNA bands were cut out of the gel and extracted from agarose gel by Qiagen Gel extraction kit. Isolated vector DNA and genes were cloned by ligation. Ligation reaction was performed for an hour at room temperature in10µl volume including 5 µl T4 DNA ligase buffer (2X), 1 µl pEGFP-N1 plasmid (50ng/ µl), 1 µl T4 DNA ligase (3 Weiss Unit/ µl) ve 3 µl PCR (50 ng) product. 10µl ligation product was chemically transformed to 100µl competent *E.coli* DH5α (2 minutes incubation on ice following 90 sec at 42^oC incubation). Then, 900µl LB was added on to bacteria and incubated at 37 ^{o}C with shaking 1 hour. Following incubation, grown cells were spread on to LB-Kan (50µg/ml) and incubated overnight at 37 ^{o}C for selection of transformants. Colonies resistant to ampicilin were selected from the plate and grown in 2ml LB-Kan (50µg/ml) liquid media overnight at 37 ^{o}C. Grown cultures were

Table 4. 2 Sequence of Cm PHR/CRY specific primers for pEGFP-N1 vector cloning

*Cm*PHR1	Fwd	ATCTCGAGACCATGTGGGTCATCTTGACC
	Rev	TGGATCCCGTGACGACGATGACGATGACG
*Cm*PHR2	Fwd	CTCAAGCTTACCATGTACGTTGTGTTGCCTG
	Rev	TGGATCCCGCGACTCGTGATGCACCGC
*Cm*PHR3	Fwd	CTCAAGCTTACCTGTCGTCGTCGAGACGACCT
	Rev	CAGAAT TCGGGGCGCGGCACGCTGTAG
*Cm*PHR4	Fwd	CTCAAGCTTACCATGCACCATTGTGTCACAG
	Rev	CAGAATTCGGGCAGCAGCTTGAGCGTCACTTTTGC
*Cm*PHR5	Fwd	ATCTCGAGACCATGAGTTGGGGACTG
	Rev	CGAAGCTTCCGCTTCTGGGATCGAAG
*Cm*PHR6	Fwd	CTCAAGCTTACCATGGTTCTGGGCTTTGC
	Rev	TGGATCCCGGCTCGCCTGGGGCGCTGC
*Cm*PHR7	Fwd	CTCAAGCTTACCATGCCCGCGTATCCTCCT
	Rev	TGGATCCCGTCTGCGCTTGTCGTCGCTCGC

subjected to alkaline lysis mini–prep plasmid DNA isolation process. 1.5 ml grown culture was centrifuged at 14,000 rpm to obtain cell pellet. Supernatant was discarded. 150 µl GET buffer (50 mM glucose, 10 mM EDTA and 25 mM Tris-HCl pH8.0) was added on to cell pellet for resuspension. Then, 150µl lysis buffer (0.2N NaOH, %1 SDS) was added on to cell suspension to disrupt cell membrane and chromosomal DNA structure. At final, 200µl 3M KOAc pH4.8 buffer was added to form chromosomal DNA and protein aggregate. Samples were centrifuged at max. (14000rpm) 15 min. to separate precipitate. Supernatant having plasmid DNA was taken into a new eppendorf tube and 2 volumes absolute EtOH was added to precipitate nucleic acids. Samples were centrifuged at max. (14000rpm) 25 min. to obtain plasmid DNA pellet. Pellet then was washed with 70% EtOH. Supernatant was discarded and DNA pellet was dried at vacuum drier. Each plasmid DNA sample was resuspended in 50 µl TE (10 mM Tris-HCl pH.7.4 and 1 mM EDTA) buffer. In order to select plasmid construct bearing PCR gene product, 10µl plasmid DNA samples were subjected to restriction digestion. Samples were loaded on 1% agarose gel and run for 20 minutes at 90V. Agarose gel was visualized by Bio-Rad gel documentation system.

4. 11.3 Transfection and Luciferase Reporter Assay

In the assay, the mBmal1-pCMVSPORT6 and mClock-pCMVSPORT6 and *Cm*PHR (1-7)-pEGFP-N1 constructs were transfected along with mPer1-Luc reporter vector into mammalian HEK293T cells by TurboFect (Fermentas, USA) transfection reagent in 96-well Opti-Plate plates by reverse transfection method. In total, 300 ng plasmids DNAs were diluted into 50µl DMEM (GIBCO). 0.9µl TurboFect transfection reagent was added into the mixture. DNA and tranfection reagent were incubated for 20min. at room temperature.After incubation, 4.104 HEK293t cells in 2X growth medium (DMEM with 20%FBS, 200µg/ml Pen-Strep, 8mM L-glutamine) were added onto tranfection mixture in 96-well plates. 16 hrs hours after transfection, 100µl/well BriteLite (Perkin Elmer) solution was added on to 100µl sample. After shaking the plate 10 seconds, relative luminescence was measured by luminometer.

RESULTS

4.1 Evolutionary Analysis

The genome analysis of *C. merolae* [22, 30] was carried out by performing a BLAST search with the E. coli photolyase amino acid sequence using web site (http://merolae.biol.s.u-tokyo.ac.jp/) [150]. Seven probable members of the photolyase/cryptochrome gene family were detected within the *C. merolae* genome, none of which contained introns. We also searched for the presence of both phytochromes and phototropins and found no homologous that were consistent with previous reports [22]. A phylogenetic tree was constructed using the neighbor-joining method with a bootstrap value of 1000 replicates using MEGA 4 software (Fig.1). The reference protein sequences were selected according to the previously published methods [21, 28, and 29] and were retrieved from the National Center for Biotechnology Information Entrez Protein Database. The amino acid sequences of the Photolyase/Cryptochrome family were retrieved from the *C. merolae* Genome Project web site (http://merolae.biol.s.u-tokyo.ac.jp/) with the following accession numbers: CmPHR1 (CMER:CM0348C), CmPHR2 (CMER:CMJ130C), CmPHR3 (CMER:CMM076C), CmPHR4 (CMER:CMH274C), CmPHR5 (CMER:CMA044C), CmPHR6 (CMER:CMD121C), and CmPHR7 (CMER:CMQ453C).

According to our phylogenetic analysis, *C.merolae* contains seven sequences that are homologous to the photolyase/cryptochrome family, thus we named these genes *Cm*PHR. It is interesting to find a family with seven homologous genes in such primitive eukaryotic organism because of its simple and compact genomic structure and organization [22, 25]. Of the seven members of this gene family, three (CmPHR2, CmPHR5 and CmPHR6) fall within the clade of cryptochrome DASH, three (CmPHR3, CmPHR4 and CmPHR7) group with plant cryptochromes, and one (CmPHR1) is a homolog of ([6-4]) photolyase. It was surprising to see a primitive microorganism possess 3 CRY-DASHes. In our analysis, one of the members (CmPHR4) was also classified as plant cryptochrome even though it has a low bootstrap value so it is not

possible to exclude the fact that CmPHR4 could be separate clade or a photolyase. We characterized the 3 CRY-DASHs at the biochemical level to determine whether these three genes repair DNA or have a photoreceptor function. In addition, it was interesting to find that such a primitive eukaryote possess a gene that is homologous to [6-4] photolyase, so we selected CmPHR1 for further characterization to determine whether it is indeed a [6-4] photolyase
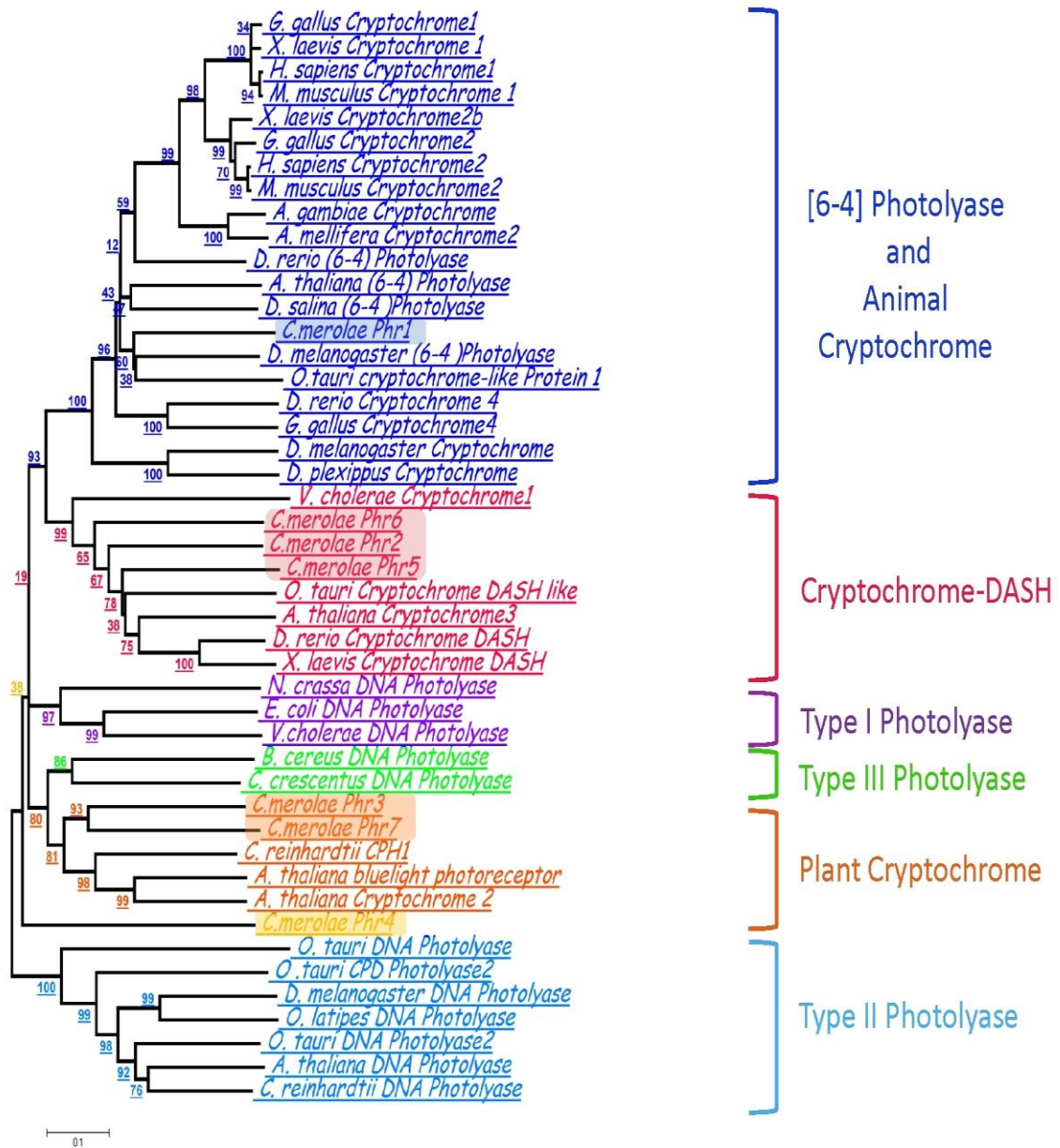
Figure 4.3 Phylogeny of the photolyase/cryptochrome family identified from *Cyanidioschyzon'merolae*. The unrooted phylogenetic tree of the photolyase/cryptochrome family members was inferred using the neighbor-joining method. The optimal tree with the sum of branch length= 10.04 is shown. **B**ootstraps of 1000 replicates are expressed in percentage. The black arrow indicate *C. merolae* PHR family member.

4.2 Genomic DNA Isolation

Total DNA of *C. merolae* cell was isolated from one month old culture growing under constant light with shaking. 16mbp long nuclear genome along with plastid genomes were observed as a single band longer than 10,000 bp. Figure 4.4 shows isolated total DNA of *C. merolae* as a single entity without breaking and degradation. Quality of isolated total DNA was good enough to be used as template DNA to amplify photolyase homologous genes of *C.merolae* PCR.
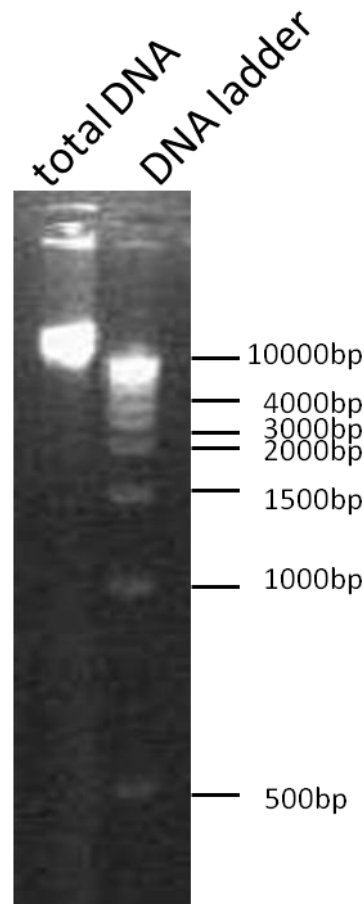
Figure 4. 4 Total DNA isolation from red algae lane 1; The band indicates the isolated total DNA run on 1% agarose gel, lane 2; 1kb DNA ladder (Fermentas)

4.3 Amplification of *Cm* PHR/CRY like Genes

BLAST analysis of *C.merolae* genome revealed seven photolyase homologous genes. We named the homolog genes from *Cm*PHR1 to *Cm*PHR7. Except for *Cm*PHR3, all genes were amplified at a single step PCR. On the other hand, *Cm*PHR3 was amplified at two steps. At first step, *Cm*PHR3 gene was amplified as two fragments. Figure 4.5 shows PCR products of *Cm*PHR3 fragment I (FRI) and fragment II (FRII-1200bp). Figure 4.5 shows amplified fragments I at 2500bp and FRII at 1200bp. At the second step, full length *Cm*PHR3 was amplified from the ligated fragments in the subclone vector pGEM-TEasy.

Amplified products of *Cm*PHR1 (1557bp), *Cm*PHR2 (2007bp), *Cm*PHR3 (3675bp), *Cm*PHR4 (2175bp), *Cm*PHR5 (1794bp), *Cm*PHR6 (1314bp), *Cm*PHR7 (3144bp) genes were run on 1% agarose gel shown in Figure 4.6. Amplification of related genes with specific primers by PCR yielded products whose sizes corresponded to targeted gene lengths in the genome.
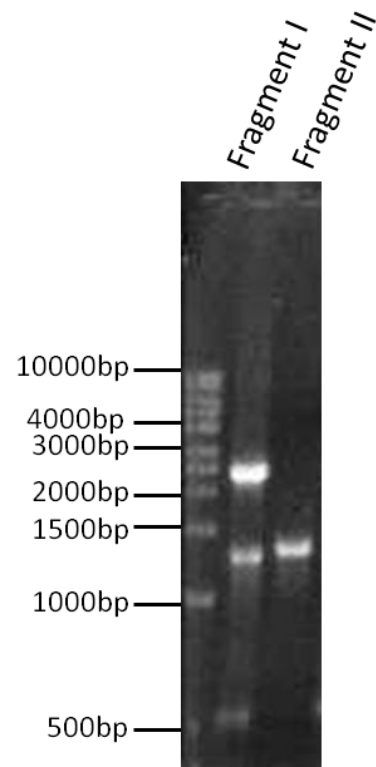
Figure 4. 5 Amplified fragments of CmPHR3. Fragment I, the major band was seen at 2500nt band and fragment II (1200bp) amplified and run above 1000nt band.
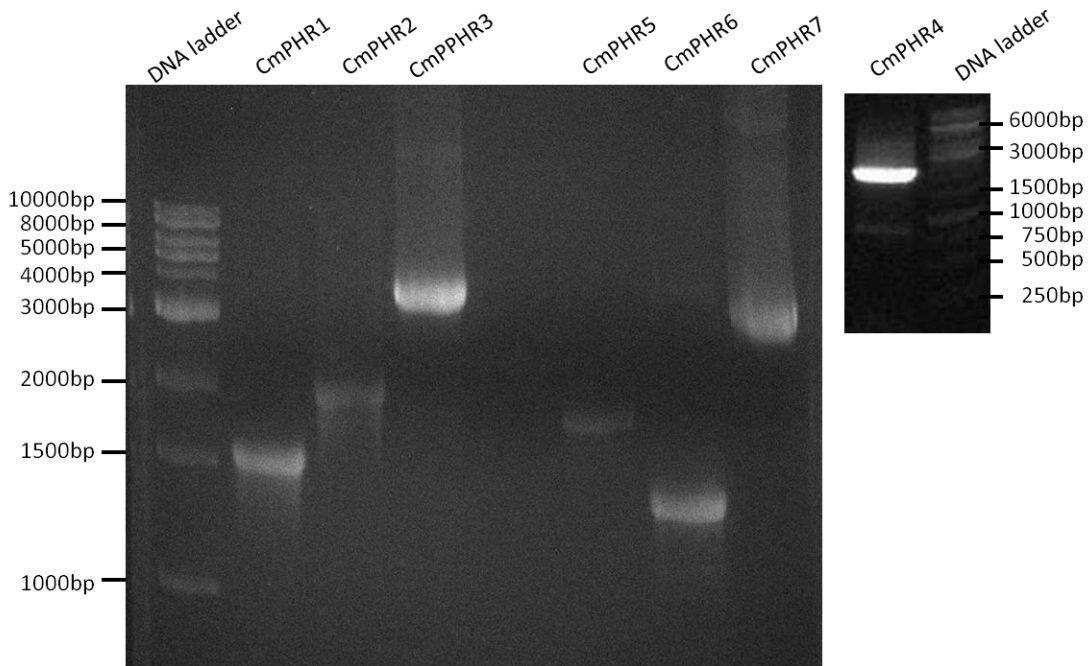
Figure 4. 6 The amplification of CmPHR genes from the genome of C. merolae with gene specific primers by polymerase chain reaction (PCR). PCR products subjected to agarose (1%) gel electrophoresis at 120V for 15 min.

4.4 Cloning of *Cm*PHR/CRY like Genes into Bacterial Expression Vector

The amplified *Cm*PHR genes were cloned in to bacterial expression vector pMalc-2x. For this, amplified genes were purified with PCR purification kit. Both PCR product and the vector were subjected to restriction digestion with selected restriction enzymes. Digested vector and PCR products were then run on agarose gel and subjected to gel extraction. Gel purified gene and vector samples were ligated and transformed into *E.coli*. Selection of transformants was performed on LB-amp (100μg/ml) agar plates. For each gene, 10 colonies were selected and grown in liquid LB-amp(100μg/ml). Plasmid DNA's were isolated from grown cultures and digested with restriction enzymes to check insert presence and size in the plasmids. Colonies having the right insert were grown and stored in the presence of %20 glycerol at -20^0C. Figure 4.7 shows the results of restriction digestion of prepared constructs isolated from selected transformant. The expression vector pMalc-2x and the inserts were indicated by arrows on agarose gel pictures. *Cm*PHR (1-7) gene sizes from digestion were consistent with PCR amplified products from the genome so those colonies were selected as positive transformants and they were used for protein expression experiments in UNC523 strain of *E.coli.*
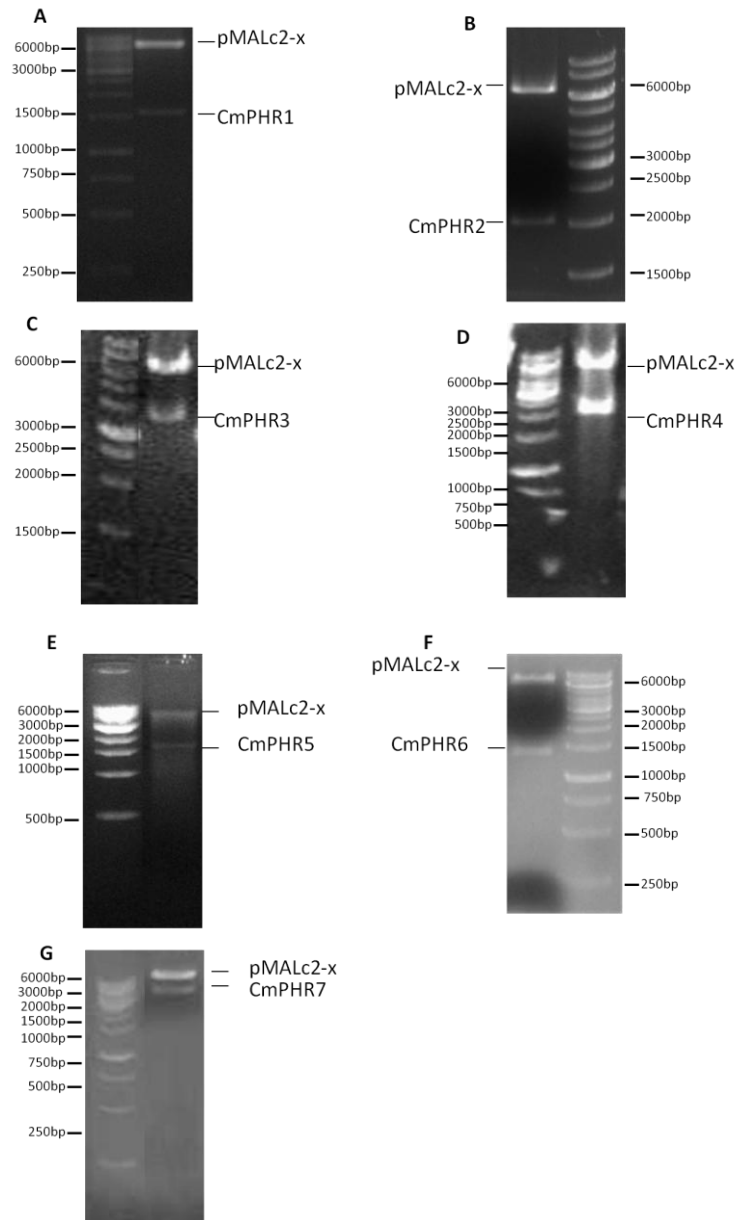
Figure 4. 7 Insert analysis of prepared pMALc2-X constructs by restriction digestion. Plasmids were digested to check inserted DNA (CmPHR genes) with appropriate restriction enzymes. A) CmPHR1-pMalc2-x, B) CmPHR2-pMalc2-x, C)CmPHR3-pMalc2-x, D)CmPHR4-pMalc2-x, E)CmPHR5-pMalc2-x, F)CmPHR6-pMalc2-x, G)CmPHR7-pMalc2-x

4.5 Recombinant Expression and Purification of Cm PHR/CRY Family Proteins

The members of the photolyase/cryptochrome family of *C. merolae* were cloned into the pMal-c2x vector so that they were fused with MBP to aid their solubility. The cloned plasmids were expressed in *E. coli* UNC523 (phr::kan;uvrA::Tn10). The resulting proteins were soluble and readily purified by affinity chromatography using amylose resin. All of the proteins except CmPHR4 were expressed at high levels at room temperature. However, CmPHR4 was insoluble when cells were grown at greater than 20 °C. Therefore, preparative-scale quantities could be obtained only when the cells were grown at 12∘C, a temperature at which most CmPHR4 was soluble. Figure 4. 8 show the overexpression and purification of the five proteins analyzed using 10% SDS-PAGE with Coomassie blue staining. SDS-PAGE analysis revealed that this particular batch of purified proteins also contain a single MBP at 40 kDa. The extra bands seen on the gel were most likely the result of incomplete translation and partial degradation of the proteins. This was confirmed by a western blot analysis (data not shown). The molecular weights of the CmPHR proteins fused with MBP (40 kDa) were estimated to be the following: CmPHR1 (97kDa), CmPHR2 (113,5 kDa), CmPHR3(173kDa), CmPHR4 (112 kDa), CmPHR5 (108 kDa), and CmPHR6 (88 kDa) CmPHR7(157,7kDa).When compared with the molecular weight (MW) marker (Figure 4.8), the apparent molecular weights of the purified recombinant proteins are in agreement with their theoretical molecular weights calculated from their predicted amino acid sequences .CmPHR3 and CmPHR7 (plant CRYs) were overexpressed at 16^{0}C and room temperature to increase their solubility. Since those proteins are at high molecular weight to express in bacterial expression system, the expression temperature was reduced to support proper folding of the proteins. The overexpressions were checked by Western blotting as shown in Figure 4.9 at both temperatures, both proteins were soluble (data not shown).
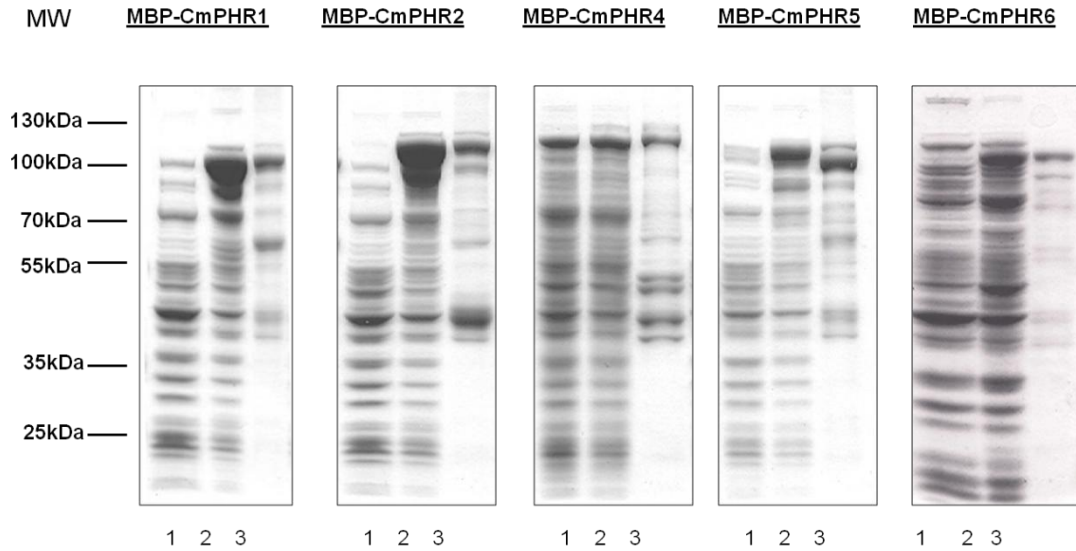
Figure 4.8 Expression and purification of CmPHR proteins. Overexpressions and purifications of MBP-CmPHR1 (97KDa), MBP-CmPHR2 (113.5KDa), MBP-CmPHR4(149KDa), MBP-CmPHR5(108KDa), MBPCmPHR6(88KDa), Lane 1-2 contained approximately 20μg of total protein; Lane 3 contained 5-10μg of purified protein. CmPHR-like genes were overexpressed in E.coli UNC523 (phr-,uvrA-) and purified through affinity chromatography as MBP-fusion proteins. The overexpression and purity of the proteins were analyzed by Coomassie Blue staining of a 10% acrylamide SDS-PAGE gel. Lanes 1-3 represent the samples from E.coli UNC523 expressing the CmPHR like proteins before induction (Lane 1), after induction(Lane 2) with 300μm IPTG, and the affinity purified proteins (Lane 3).
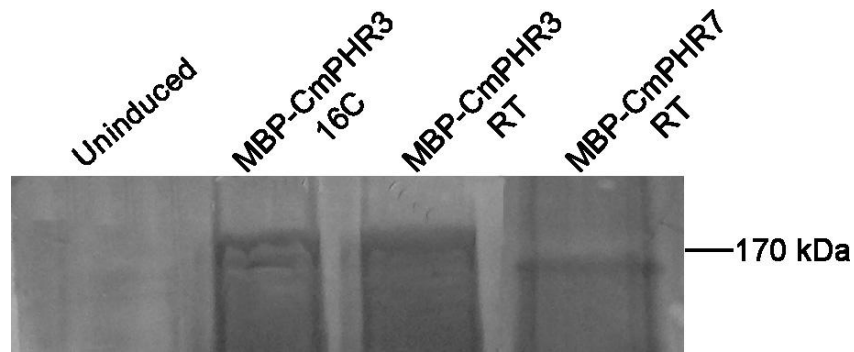
Figure 4.9 MBP-CmPHR3 (173KD and MBP-CmPHR7 (113KDa) were overexpressed in E.coli UNC523 to increase their solubility at 160 C and room temperature. The protein expressions were analyzed by Western Blot by using anti-MBP antibody. Colorimetric antibody detection was carried out by NBT/BCIP. Overexpression was compared with cell lysate of an uninduced culture.

4.6 Spectroscopic Analysis and Cofactor Content

All members of the photolyase/cryptochrome family characterized to date contain FAD as an essential cofactor. In addition, these proteins contain a second chromophore, which is methenyltetrahydrofolate (MTHF) in the majority of organisms and is 5-deazariboflavin in a limited number of species [25, 113] The typical spectroscopic characteristics of the members of the photolyase/cryptochrome family that contain folate exhibit major peaks at 380–420nm that are mainly absorbed by MTHF and reduced FADH− in the native protein[25]. Minor peaks at 440, 480, and 580nm that correspond to the oxidized and neutral states of FAD are also seen in the spectrum. Figure 4.10 (A–E) shows the absorption spectra of purified MBP-CmPHR1, MBP-CmPHR2, MBP-CmPHR4, MBP-CmPHR5 and MBP-CmPHR6, respectively. Major peaks seen in each spectrum correspond to absorption of purified proteins at 280nm and the insets were placed to show specific absorption peaks corresponding to FAD and MTHF. The highest absorption peak was exhibited by MBP-CmPHR5 at 380nm which corresponds to the presence of reduced FAD and folate absorption (Fig. 4.10D inset). Its shoulder at 420nm and the minor peak at 450nm indicate the existence of MTHF and the different redox states of FAD (Fig. 4.10D inset). The absorption spectrum of MBP-CmPHR5 indicated that it contains MTHF and a mixture of FAD_{ox} and $FADH^{o}$ blue neutral radical with peaks at 420 and 480nm. Then, to determine whether all MBP-CmPHR proteins exhibit flavin peaks, the proteins were concentrated 50–100-fold and their absorption spectra were measured. As can be seen in the inset of Fig. 4.10A, B, and E, MBP-CmPHR1, MBP-CmPHR2, and MBP-CmPHR5 contain FAD at a concentration of less than 0.2%. In each case, there was a peak at 420nm that indicates the presences of FAD_{ox}. However, there was no detectable FAD in the MBP-CmPHR4 as indicated by the absorption spectrum in the inset of Figure. 4.10C. To calculate the stoichiometries of the two cofactors relative to the apoenzyme, the MBP-CmPHR5 protein was heat-denatured at a neutral pH, and following the removal of the denatured protein by centrifugation, the absorption spectra was measured for MBPCmPHR5. Due to the removal of the methenyl bridges of MTHF to the protein, the absorption above

300nm resulted from the flavin cofactor. The stoichiometry of the cofactor was calculated from the absorption spectrum of FAD at 440nm by taking the ratio of the FAD absorbance at 450nm (with an extinction coefficient of $11.3M^{-1}$) to the holoenzyme absorbance at 280 nm. The stoichiometric ratio could be estimated only for CmPHR5-MBP from the absorption spectra shown in Figure 4.10 because the other four proteins did not exhibit significant absorption peaks in the spectrum for both native and denatured proteins (data not shown). The stoichiometric values of the MTHF: FAD: apoprotein ratio of CmPHR5 was approximately 0.3:0.1:1. It should be considered that the cofactor composition has been found to depend on the growth and purification conditions. However, we did not see a significant difference or enhancement, especially in the FAD content of the remaining four proteins, even when the growth conditions were changed to 16^{0}C overnight.
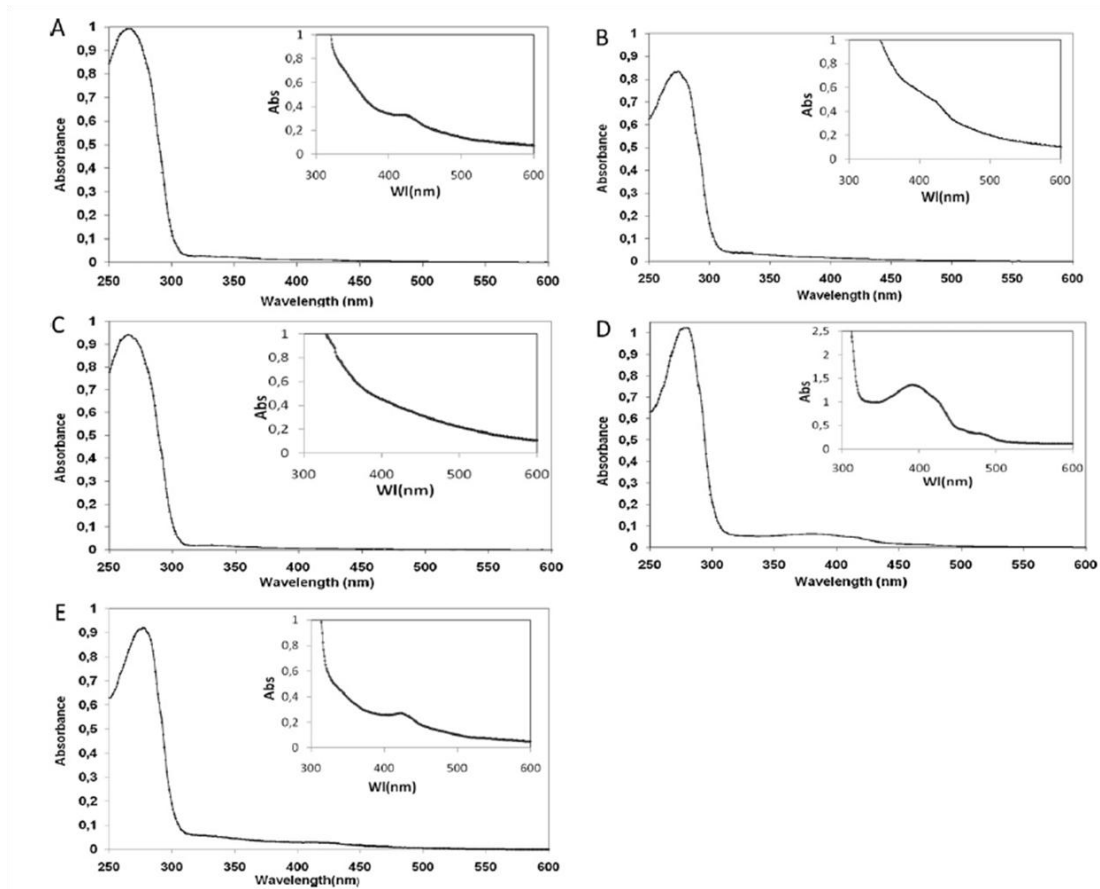
Figure 4. 10 Absorption spectra of purified CmPHR family members **between** 280**nm an** 600nm. The insets show an expanded scale of the absorption spectra from 300 to 600 nm. The absorption spectra are (A) CmPHR1, (B) CmPHR2, (C) CmPHR4, (D) CmPHR5, and (E) CmPHR6. CmPHR1, CmPHR2, and CmPHR4 contain less than 2% flavin absorbance in 420–480-nm region, which is indicative of the presence of some FAD_{ox}. CmPHR5 has maximum absorption peaks at 380, 420, and 450 nm, which indicate the protein-bound MTHF and the oxidized and semiquinone states of the FAD cofactor, respectively. Note that the oxidized flavin peaks at 420nm and the absorbance peaks between 480 and 60nm indicate the existence of flavin neutral radicals.

4.7 Radiolabelled DNA Substrate for *in vitro* Repair Assays

Single stranded 46bp oligonucleotides was labeled with phosphorus 32 isotope (^{32}P) at the 5' end of middle arm oligo where an restriction site exist . To do an *in vitro* DNA repair assay to asses [6-4] photolyase and CPD photolyase activities of CmPHR proteins, two separate radiolabelled DNA substrates holding either CPD or [6-4] UV lesions at their MseI restriction sites were prepared. For the control and DNA binding experiments with EMSA, unmodified single stranded oligonucleotide was also radiolabelled with ^{32}P at the 5' end. Figure 4.11 shows radiolabelling procedure was given in a schematic. Stars indicates hot (red) and cold (blue) ATP. Only middle arm 5 end was labeled radioactively and other arms 5ends were labeled with non radioactive ATP to efficiently ligate right and left arms. Through polynucleotide kinase reaction, oligonucleotides were phosphorylated and then the the strand consisted of 3 oligonnucleotides was completed by the ligation of 3 oligonucleotides. Next, ligated strand was hybridized with its complementary strand. At this step, oligonucleotide having [6-4] photolesion were subjected to photorepair by CPD photolyase to repair residual CPD lesions that may come during its synthesis. Also, CPD containing substrate was treated with [6-4] photolyase in the same way. Double stranded and photorepaired CPD and [6-4] containing substrates were then subjected to restriction digestion with Mse I enzyme to remove and cut the molecules without any UV damages into two pieces. Oligonucleotides having UV damages and unmodified DNA substrate were run on urea containing sequencing gel to separate single stranded, nonlabelled, and digested DNA fragments. The DNA band of interest from the gel (shown by an arrow in Figure 4.12) were cut and eluted from the gel. The concentrations of radiolabelled substrates were determined by scintillation counter. The yield of CPD,
 [6-4] and unmodified substrates were determined as 26nM, 30nM and 52nM at final, respectively.
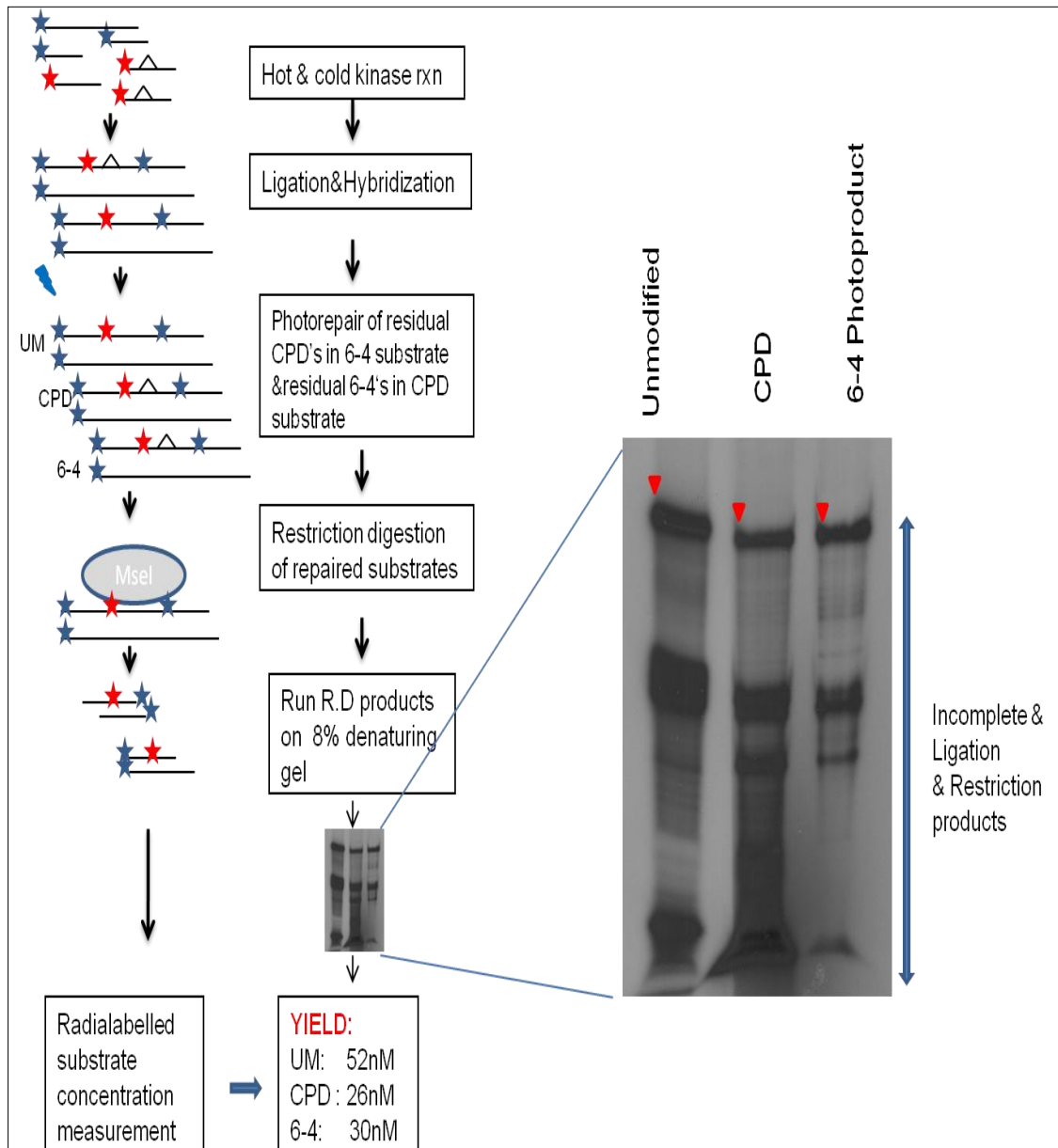
Figure 4. 11 Schematic representation of radiolabelled DNA substrate preparation for *in vitro* photolyase repair assay and EMSA. *In vitro* photolyase assay with CmPHR/CRY family

4.8 Photolyase Repair Assay

Photolyase reaction mechanism is based on a photon-powered cyclic electron transfer that does not result in a net gain or loss of an electron. Therefore the existence of cofactors at sub-stochiometric amounts does not affect the enzyme activity[106]. In our study, we purified recombinant MBP-CmPHRs of *C.merolae* with less than 0.2% flavin except for MBP-CmPHR5. By such a sensitive radioactive assay, we expect to identify DNA repair activities of CmPHRs even though they might have very little repair activities even with the small amount of chromophore/cofactor content of CmPHRs. Radiolabelled 48-bp-long single-stranded (ssDNA) or double-stranded (dsDNA) DNA that contained the -TTAA- MseI restriction site were used for the photolyase repair assay. In the substrates, the MseI restriction sites contain either a [6-4] PP or a CPD dimer. Figure 4 shows the DNA repair of the CmPHRs using either ssDNA or dsDNA substrates of [6-4]PP. Among the tested CmPHRs, only CmPHR1 exhibited a repair activity of both [6-4] -ssDNA (Figure 4.12A lane 2) and [6-4]-dsDNA (Figure 4.12B, lane 2) as evidenced by the 24-bp product of the MseI-digestion. The activity was comparable to the *Xenopus leavis* [6-4] photolyase that was used as a control (Figure 4.12A and B, lane 12). As shown in Figure 4.12, when the samples were incubated with the radiolabelled [6-4] -damaged DNA, there was no DNA repair (as evidenced by the 48-bp-products) compared with samples exposed to the blue light (Figure 4.12A-B, lanes 1 and 2; lanes 11 and 12). There are residual activities are observed for other samples during the assay (Figure 4.12A, lanes 4, 6). This possibly due to the substrate contains the undamaged DNA, which is not separated from damaged ones during the substrate preparation.
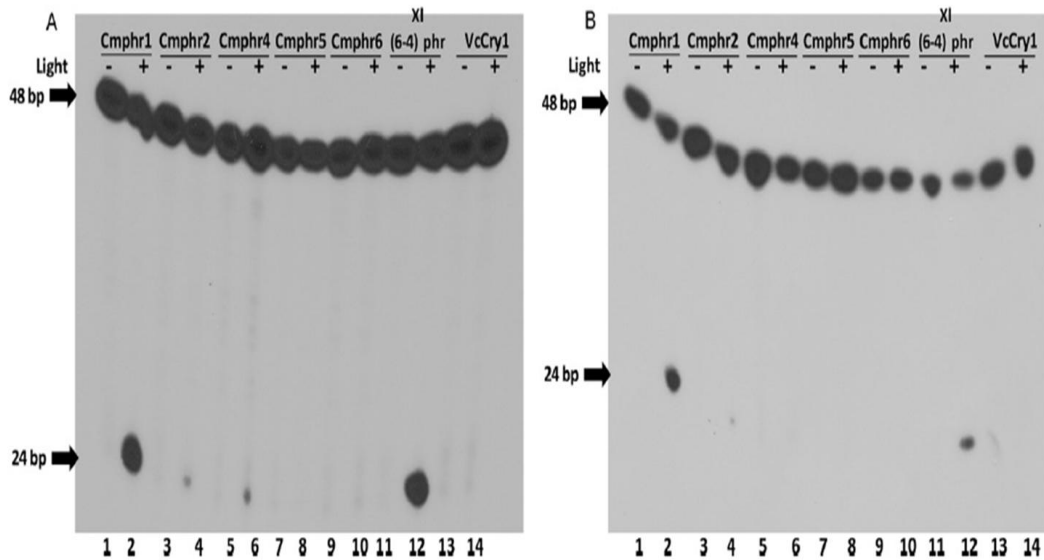
Figure 4. 12 *In vitro* photolyase assay of CmPHR family with ss and ds DNA having [6-4] photoproduct. The CmPHR proteins were analyzed for their repair activites of [6-4] photoproduct in A) ssDNA and B) dsDNA substrates. Radiolabelled 48bp nt-long ssDNA and dsDNA oligomers (0.3mM) that contained [6-4]PP were incubated with the appropriate enzymes in the dark and under 200μW/s.cm2 photoreactivating light. All purified enzymes were used at 1μM for photoreactivation except that *Xenopus leavis* [6-4] photolyase was used at 300nM. The repair activities of the CmPHR proteins were assessed by restriction enzyme analysis. The restriction products were separated on an 8% sequencing gel. The gels were visualized by autoradiography.

Then we performed similar experiments using the CPD damaged DNA in both dsDNA and ssDNA substrates. For the repair activity, 1μmol of each enzyme, along with the appropriate controls, was incubated with either ssDNA or dsDNA substrates for 90 min in the dark or under blue light for photoreactivation. Following deproteinization by phenol: chloroform extraction, the radiolabelled DNA substrates were digested overnight with the MseI endonuclease. The repair activities were assessed by detecting the 24-bp product after the MseI digestion.CmPHR2 and CmPHR5 showed CPD repair activity only on ssDNA (Figure4.13, lanes 4 and 8). These proteins did not display any repair activity on CPD lesions on dsDNA. These results are consistent with the previously published data that showed that Cry-DASH (*Vc*Cry1) repairs only CPD lesions on ssDNA, which was used as a positive control in this experiment (Figure 4.13A, lane 14). If these two proteins are indeed Cry-DASH, one would expect that they would not repair CDP lesions on dsDNA. Therefore, we performed the same experiments in the presence of CPD-damaged dsDNA. MBP-CmPHR2 and MBP-CmPHR5 had no repair activity when CPD-damaged dsDNA was used as a substrate (Figure 4.13B, lanes 4 and 8). The absence of digested dsDNA fragments of 24 bp indicated the absence of repair activity in the samples that were incubated either under dark or blue-light conditions (Figure 4.13B, lanes 3, 4, 7, 8, 13, and 14). In this work, *Vibrio cholerae* photolyase was used as a positive control because it is able to repair CDP lesions on dsDNA (Figure 4.13A and B, lane 12). *Vc*Cry1 (classified as Cry-DASH), repairs ssDNA, was used as a negative control to show CRY-DASH cannot repair dsDNA (Figure 4.13 A and B, lane 14). All of these results suggest that CmPHR2 and CmPHR5 indeed belong to the DASH family. Interestingly, CmPHR6, which is classified as member of the DASH family in the phylogenetic tree, did not display any repair activity using any of the substrates. Therefore, we conclude that a Cry-DASH from *C.merolae* acts as a cryptochrome that may function in photoreception to regulate different physiological variables in this organism. From an evolutionary point of view, it is possible that this Cry-DASH is a transient form between the DNA repair function

and the CRY function. Finally, we also identified a [6-4] photolyase from this primitive eukaryote.
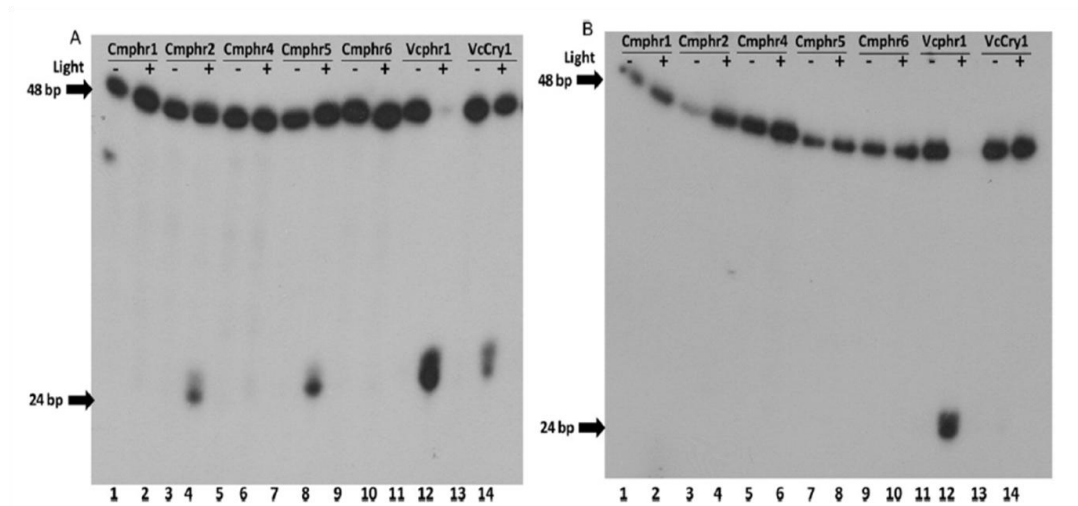
Figure 4. 13 *In vitro* CPD photolyase assay of CmPHR like proteins. CmPHR-like proteins were analyzed for their repair acitivites of a CPD (T< >T) PP in A) ssDNA and B) dsDNA substrates. Radiolabelled 48 nt long ssDNA and dsDNA oligomers (0.3nM) that contained the CPD PPs were incubated with the appropriate enzymes both in the dark and under $200\mu W/s.m^2$ photoreactivating light. All purified enzymes were used at 1μM for photoreactivation except that *V.cholerae* photolyase was used at 300nM. The repair activities of the CmPHR proteins were assessed by restriction enzyme analysis. The restriction products were separated on an 8% PAGE sequencing gel. The gels were visualized by autoradiography.

4.9 CPD Photolyase Activity of Cm PHR/CRY Family Proteins

Contribution of the CmPHRs to biological photoreactivation was evaluated by performing a more sensitive assay that confirmed in vivo photoreactivation of CmPHRs. To this end, the *E. coli* strain UNC523, which had been transformed with plasmids expressing MBP, MBP-CmPHR1, MBP-CmPHR2, MBPCmPHR4, MBP-CmPHR5 and MBP-CmPHR6 at high levels, was first exposed to 254-nm light and then to photoreactivating light. For each construct, a single colony selected from ampicillincontaining LB-agar plates (100μg/ml) was grown in liquid LB-Amp (100μg/ml). The survival rates of *E. coli* strain UNC523 (*uvrA⁻,phr⁻*) cells bearing pMalc2x-CmPHR-like gene constructs after UV and a subsequent blue-light irradiation and photoreactivation are shown in Figure 4.14. In each experiment, pMALc2x-*Vc*Phr used as a positive control and empty plasmid (pMALc2x) plasmid was used as a negative control. Cells that contain pMALc2x-*Vc*Phr plasmid result in 500–100 fold survivors whereas cells that contain empty plasmid result in only 5–15 fold survivors upon exposure to the blue-light (Figure 4.14A–E), which is consistent previously published results [106, 122]. Photolyase complementation assay indicated that the CmPHR1 plasmid constructs did not rescue of irradiated photolyase deficient *E. coli* UNC523 cells (approximately 20-fold) when compared to the positive control (Figure 4.14A) upon exposure cells to the blue-light. There was only 40% repair in the cells that contains CmPHR1 genes (data not shown). Since only 20% of UV-induced damage is [6-4] PPs, it is not expected that CmPHR1 will complement *Phr* gene in E. coli UNC523 (Figure 4.14A). Although both CmPHR2 and CmPHR5 did not complement *Phr* gene in *E. coli* UNC523 as much as cells carrying pMALc2x-*Vc*Phr, they contributed to photoreactivation up to 100-fold compared with cells carrying empty plasmid vector (Figure 4.14B and D). To see whether other Cry-DASH behaves similarly we decided to carry out a similar experiment with a Cry-DASH (*Vc*Cry1) from *V. cholerae*. The result indicated that *Vc*Cry1 also partially complemented *Phr* gene in *E. coli* UNC523 (data not shown). Therefore we conclude that CmPHR2 and CmPHR5 are most likely to have similar properties with *Vc*Cry1 in terms of DNA binding and

repair, which was reported to cause photoreactivation *in vivo* at a rate of less than 0.3% [124]. *In vivo* photorepair mediated by these two proteins may result from the actual repair of dimers in dsDNA, or from repair in regions of the supercoiled genomic DNA which transiently assume single-stranded character in the vicinity of the damage [124, 151] It is worth to note that cells carrying CmPHR4, CmPHR5 and especially CmPHR6 more resistance to the UV killing compared with the cells carrying pMalc2x-*Vc*Phr and pMalc2x (Figure 4.14C–E) in the dark. This intriguing observation is may be due to "dark function" of photolyase or CRYs, as has been observed in *E. coli*, *V. cholerae*, and *Saccharomyces cerevisiae*, and is the result of the stimulation of nucleotide excision repair by photolyase bound to UV photoproducts [122] [152].
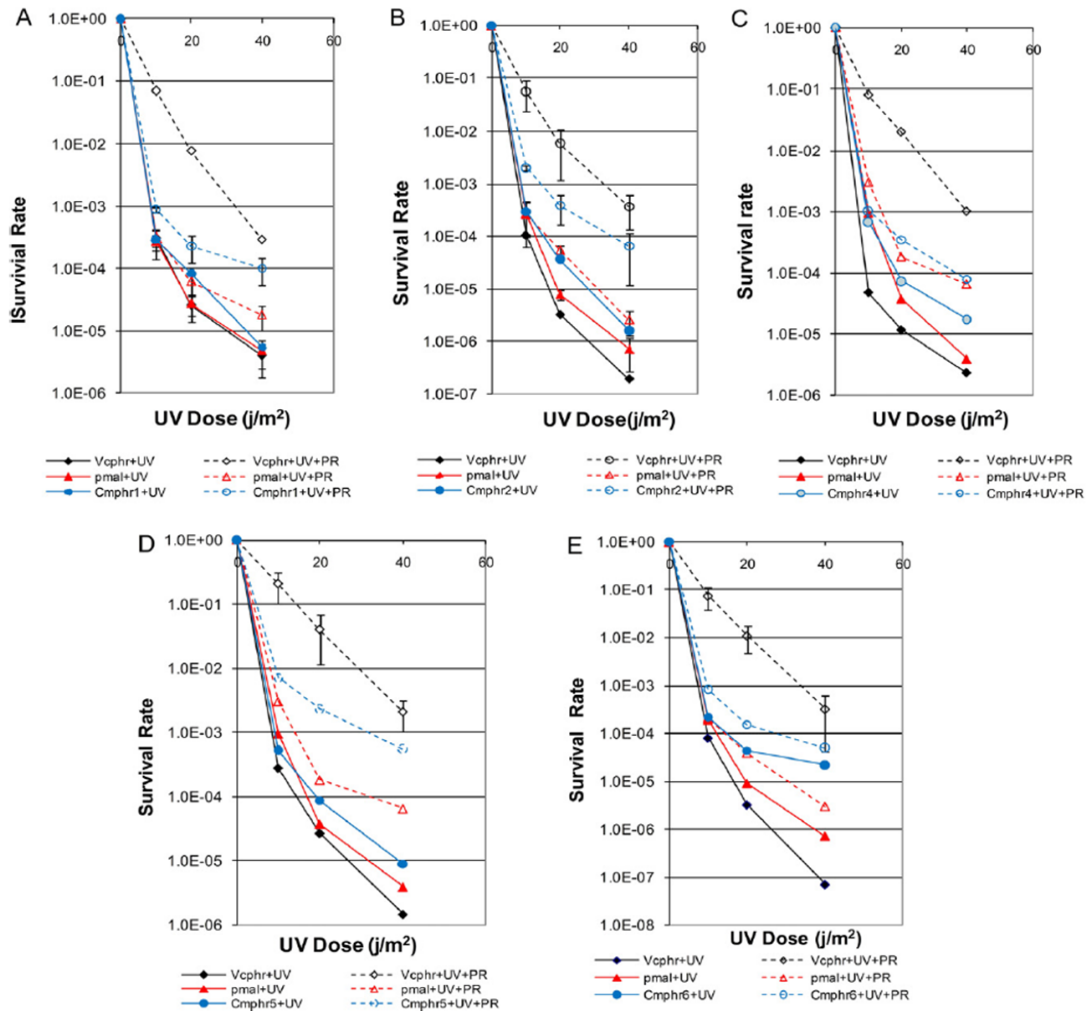
Figure 4. 14 Photolyase complementation assay, *E.coli* UNC523(*phr⁻,uvrA⁻*) cells carrying the appropriate constructs were irradiated by UV-C(254nm) at a fluence rate of 1 J/m^2.s with fluencies of 10, 20, 40 J/m^2. The effects of the photoreactivation on the survival of UV irradiated *E.coli* UNC523 cells that carried the pMALc2-x vector triangle-red), pMalc2-x-*VcPhr* (diamond-black), pMalc2-x-*Cm*PHR(square-blue), constructs were evaluated. Closed and open markers indicate the survival rate of without blue light irradiation and with blue light irradiation, respectively. The survival of *E.coli* UNC523 cells carrying A) pMalc2-x*Cm*PHR1, B) pMalc2-x*Cm*PHR2, C)

pMalc2-x*Cm*PHR4, D) pMalc2-x*Cm*PHR5, E) pMalc2-x*Cm*PHR6, constructs were evaluated by counting cell numbers on the plates. Each experiment was performed on duplicate plates and repeated three times. Note that the photoreactivation percentages were approximately 30-40% similar to the control photoreactivation of the pMalc2-x control plasmid.

4.10 DNA Binding

Electrophoretic mobility shift assays were conducted to examine the binding of CmPHR enzymes to the CPD, unmodified and [6-4] in ss and dsDNA. The results shown in Figure 4.15 A and B display the binding abilities of CmPHRs to dsDNA and to ssDNA, respectively.

For both assays conducted with ss and ds DNA substrates, *Vc*Phr enzyme was used as control due to its higher affinity to ss and ds CPD over unmodified substrate. CmPHR1, CmPHR4, CmPHR5 and CmPHR6 bound neither ds unmodified (dsUM) nor dsCPD substrate even at relatively high concentrations. Considering repair activities and DNA binding abilities of these enzymes, CmPHR1 was conclusively found to bind and repair [6-4] photoproducts, specifically. Besides, the proteins without any repair properties, CmPHR4 and CmPHR6, were unable to bind dsDNA. CmPHR5, a member of CRY-DASH subgroup, showed neither affinity to unmodified nor CPD on double stranded DNA. Its specificity was apparently high for ssDNA regardless of the presence of UV lesion. On the other hand, another member of CRY-DASHs of *C. merolae,* CmPHR2, did bind to dsDNA. However, the binding was not structure specific. Among the CRY-DASH enzymes that have been characterized to date, this was the first study showing its ability to bind dsDNA (Figure 4.15A) [124].

Figure 4.15B exhibits EMSA results of ssDNA-CmPHR complexes detected by autoradiography. Among CmPHRs, as it was expected, only CmPHR2 and CmPHR5 (Cry-DASHs) could bind to ssDNA robustly. Although their DNA binding parallels with their ability to repair CPD in ssDNA, CmPHR2 and CmPHR5 do not have a higher preference to CPDs in ssDNA over unmodified ssDNA whereas *Vc*Phr does. Other CmPHR proteins, CmPHR1, CmPHR4 and CmPHR6 displayed negligible binding to CPD and unmodified ssDNA.

A
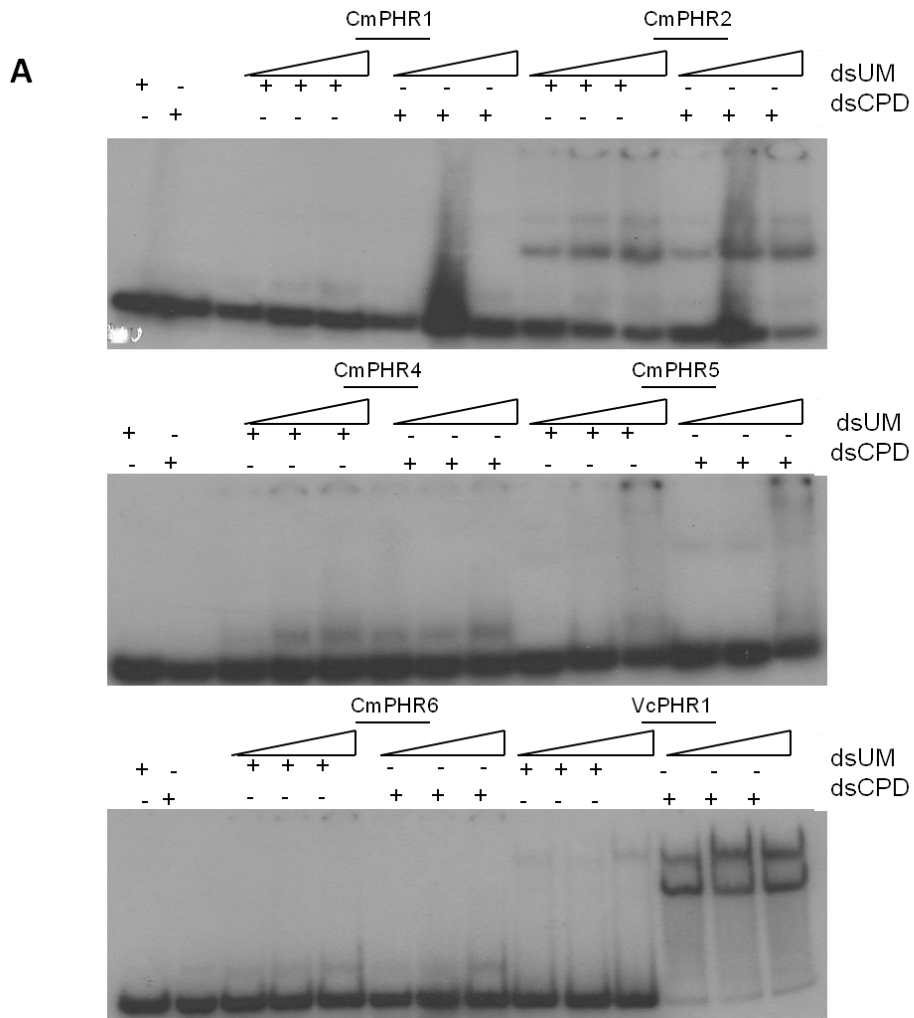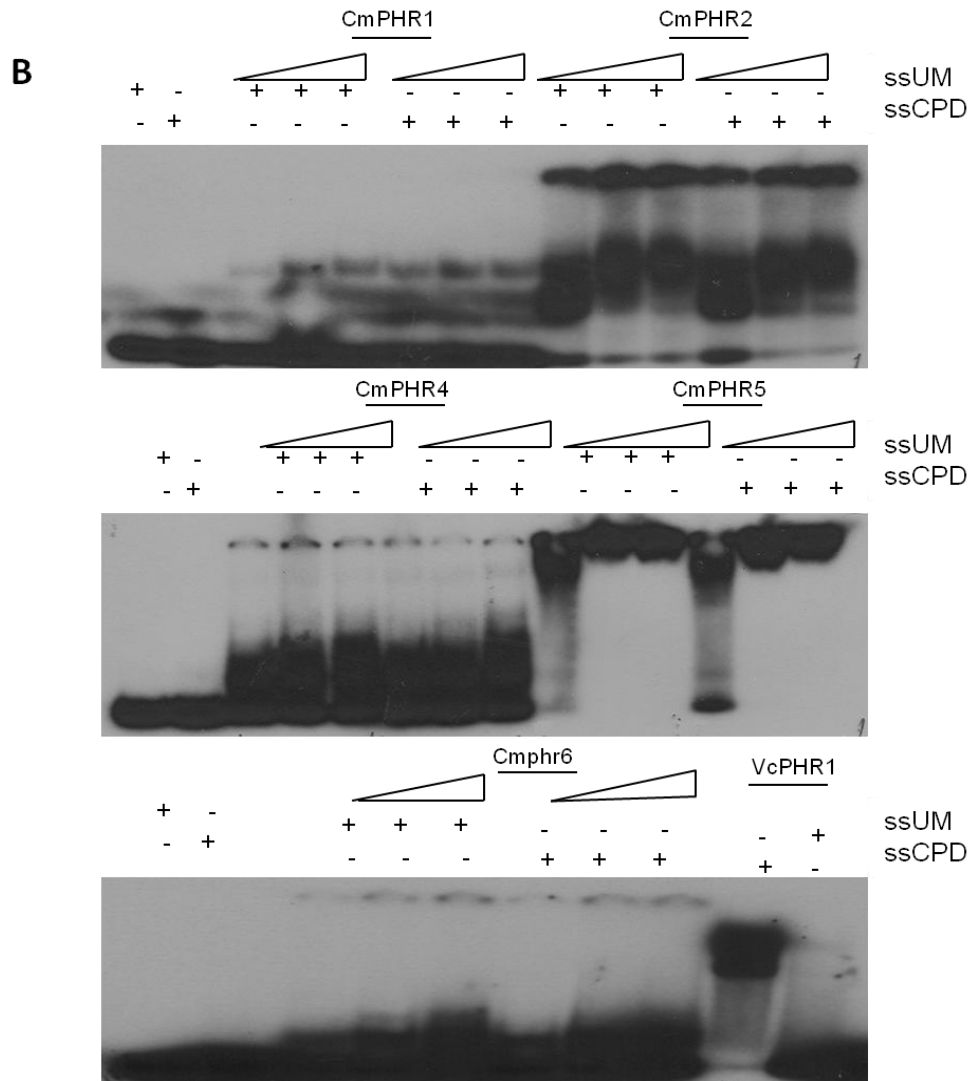
Figure 4. 15 DNA binding properties of CmPHR proteins by electroctromobility shift assay (EMSA). CmPHR1 as [6-4] PHR do not bind any of the ss- and ds-substrates holding CPD lesions. The binding of DASH type cryptochromes of C. merolae (CmPHR2, CmPHR5, CmPHR6) are in consistency with their ssDNA repair activity except CmPHR6. CmPHR6 is incapable to bind ss and ds DNA independent of the existence   UV   lesion.

4.11 Repression of Transcriptional Activation of BMAL-CLOCK by CmPHR Family Proteins

Transcriptional repression activities of CmPHRs on mPer1 promoter were tested on by luciferase assay. The activation of luciferase gene under the control of mPer1 promoter by mBmal1-mClock heterodimers was repressed by CmPHR2 at around %30 (Figure 4.16). Although the repression level of CmPHR2 seems much less than the repression level of mCRY2, it is statistically significant with t-test analysis. However, further assays are needed to verify that repression activity. Those preliminary results may indicate that this result can be attributed to the ability of Cry-DASH proteins to perform dual functions in the cell. However, the physiological aspects should be tested *in vivo* conditions.
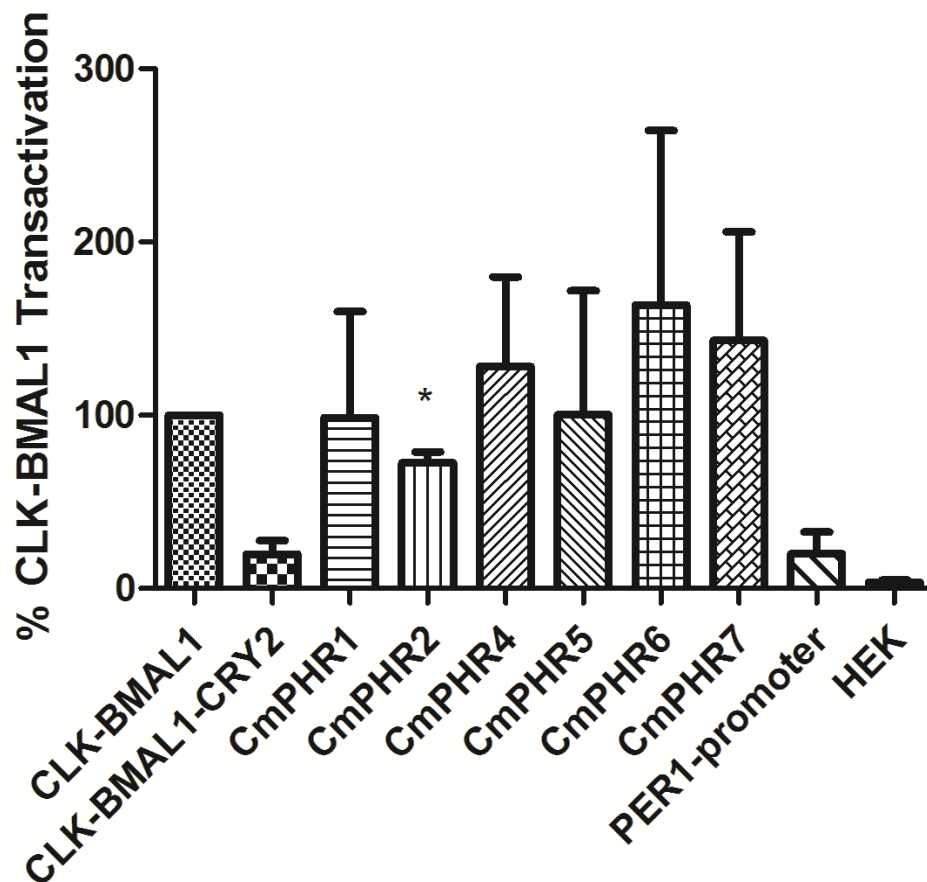
Figure 4. 16 Transcriptional repressor activity of CmPHR family in HEK293T cells. Inhibition of Clock: BMAL1-mediated transcription of luciferase gene from the mPER1 promoter were tested by mammalian mCRY2 (control) and Cyanidioschyzon merolae CmPHR's. Values are mean±S.E.M of three independent experiments, ($p<0.05$). Activation of luciferase gene by Clock: BMAL1 was taken as %100. Repression values are calculated as % value.

Chapter 5
CONCLUSION

The photolyase/cryptochrome is a large and diversified gene family that encodes blue-light photoreceptor found throughout the biological kingdom, from archaebacteria to mammals. There are 3 major categories of proteins represented by this family. 1) The cyclobutane pyrimidine dimer (CPD) photolyases, 2) the [6-4] photolyases, and 3) the cryptochromes (CRY). Photolyases are enzymes that utilize light energy for repair of UV-damaged DNA, either of [6-4] photoproducts or of cyclobutane pyrimidine dimers. Cryptochromes, in contrast, function as signaling molecules that regulate diverse biological responses such as entrainment of circadian rhythms in plants and animals. Photolyases are found in almost all species of prokaryotes and eukaryotes and are also found to be encoded in certain viral DNAs. Cryptochromes are far less widespread, being present in higher plants and most animals but in only a handful of other eukaryotes and prokaryotes. Structurally, photolyases and cryptochromes are very similar, share similar photoactive domains, and they bind similar photoactive pigments, leading to the suggestion that photolyases are ancestors to cryptochromes. The accepted definition of a cryptochrome is therefore a protein with similarity to photolyase that has lost or reduced DNA repair activity and has gained a novel role in signaling. Photolyases are monomeric proteins of 450−550 amino acids with two noncovalently bound chromophore/cofactors. One of the cofactors is always FAD, and the second is either methenyltetrahydrofolate (MTHF) or 8-hydroxy-7,8-didemethyl-5-deazariboflavin (8-HDF). Accordingly, the enzymes have been classified into folate class and deazaflavin class photolyases. The "second chromophore" (MTHF or 8-HDF) is not necessary for catalysis and has no effect on specific enzyme-substrate binding. Cryptochromes are seemed to evolve from photolyases by gene duplication events but their function appears to differentiate through evolution. Although photolyases are studied in detail and their reaction mechanism are deciphered, cryptochromes are

recently being studied and currently great efforts have been made towards understanding the role of the CRY in various organisms. Indeed, functional differentiation of photolyase from functioning as DNA repair enzyme to blue light photoreceptor regulating growth and development in photosynthetic eukaryotes and the circadian rhythms is still needed to be explored [153]. Moreover, in the recent years cryptochromes having dual or triple functions have been open to debate. In some algae and fungi, Phr/Cry members have been shown to mediate blue light perception and/or involve in the circadian clock and also are able to repair DNA damages [1] [2],[3]. Discussion is that in lower organisms the observation of residual DNA repair activity in cryptochromes could/might be logical from an evolutionary point of view. Aforementioned, the role of the CRY is ill-defined especially in unicellular organisms.

In the first part of my thesis, the repair kinetics of a DASH cryptochrome and a CPD photolyase of gram negative aquatic bacteria were investigated. RNA and DNA binding capability of *Vc*Cry-DASH is revealed in the study of Worthington et al. [122] that lead to the discovery of ssDNA repair activities of DASH type cryptochromes including *Vc*Cry1 in 2006 [124]. Although, CRY-DASH can be characterized by biochemical assays, literature lacks the quantitative data on binding and repair kinetics. Here, interactions and the activity of the photolyase/cryptochrome family group with ss/ds DNA were quantitatively observed with SPR. The interactions between UV-undamaged-DNA and *Vc*Phr resulted in typical SPR response curves, i.e an increase in the injection mode and a decrease in the load mode. However, the responses observed between UV-damaged-DNA and *Vc*Phr clearly indicated the immediate binding of repair proteins to the target DNA bound to the surface. Decreases in response units observed during injection mode may be explained by the release of proteins just after the completion of the repair of pyrimidine dimers from DNA lesion. The lack of decrease during injection mode for the case of inactive *Vc*Phr injection on ss UV damaged DNA further suggests that repair protein *Vc*Phr specifically interacts with UV damaged-DNA. Low concentrations of proteins were sufficient to observe the interactions of *Vc*Cry-DASH or *Vc*Phr with UV-damaged ssDNA, where nonspecific

interactions were present between UV-damaged dsDNA and Cry-DASH or UV damaged ssDNA and *Vc*Phr. Decrease in binding response profile was observed when *Vc*Cry-DASH was injected onto UV-damaged ssDNA bounds surface. The proteins were able to bind with UV-damaged ssDNA immediately after the start of injection mode, which was an indication of specific interactions between proteins and DNA, and high tendency to repair the pyrimidine dimers. The release of proteins from DNA bound surface was probably due to the completion of proteins' task of repairing lesions. Unlike the specific interactions observed with UV-damaged ssDNA and Cry-DASH, we did not observe specific interactions between *Vc*Cry-DASH and UV-damaged dsDNA, which confirms the previous findings about the interactions of this protein and UV-damaged dsDNA.

These results clearly depict the effective use of SPR in order to see the real time response of the interacting molecules, i.e protein and modified-DNA in this study. The technique requires only small amounts of the samples to be tested. The binding parameters were determined by the analysis of the association and dissociation phases. The strength of association and the tendency of dissociation during the injection mode most probably represent the real time repair mechanism. Our result supports the separate biochemical assay findings in the literature, where SPR was used here to quantify and demonstrate the interactions of UV damaged/undamaged ss/dsDNA with CPD photolyase and DASH cryptochrome.

Accordingly, we utilized the advantage of real time response of surface plasmon resonance spectroscopy not only for the characterization of DNA-protein interactions quantitatively but also for monitoring the binding and repair kinetics. To our knowledge, this is the first time that the affinities of *Vc*Cry-DASH to ssDNA and dsDNA containing CPD lesion were determined through a novel, non-biochemical technique. Strikingly, while the equilibrium binding constant (K_d) of *Vc*Cry-DASH to damaged dsDNA is in micromolar range, its affinity to ss damaged DNA increases and reaches to nanomolar levels. Moreoever, the comparison of binding interactions with

the active *Vc*Phr and inactive *Vc*Phr and UV damaged ssDNA further suggest that it might be possible to monitor repair activities of these proteins using SPR in real time.

I believe by SPR method, real time monitoring of DNA repair contributed to the field in a way that classification of a new member of PHR/CRY superfamily can be made easily, without the need of exhausting biochemical assays.

In this dissertation, to address functional diversity of cryptochromes; new gene members of CRY family were identified in primitive red algae (*C.merolae*) at biochemical level.

Firstly, we started with searching the genome of red algae called *Cyanidioschyzon merolae* that is one of the most primitive of eukaryotic photosynthetic organism. The basic local alignment search (BLAST) against *E.coli* photolyase amino acid sequence revealed seven candidate genes encoding photolyase /cryptochrome proteins within this genome. We also searched the whole genome for other photoreceptor coding genes but none of the known genes coding for the red (phytochrome) or blue light receptors (LOV domain, BLUF domain, phototropism) exist. This feature made the red algae more attractive for blue light photoreception studies. We performed phylogenetic classification of seven photolyase homolog's by neighbor-joining method with a bootstrap value of 1000 replicates using MEGA4 software. One of the *C.merolae* PHR/CRY family members (CmPHR1) was found to be evolutionarily close to [6-4] photolyase. Three of them (CmPHR2, CmPHR5, CmPHR6) were classified in Cry-DASH subfamily while other three (CmPHR3, CmPHR4, CmPHR7) fall within the clade of plant cryptochromes. To characterize this gene family, we have cloned all the members of *Cm*PHR family genes and expressed them in a photolyase deficient strain of *E.coli* called UNC523. Five of CmPHR proteins were purified and functionally characterized and the two of them were cloned and expressed recombinantly for further characterization assays. Spectroscopic analyses showed that all CmPHRs except plant CmPHRs (CmPHR3 and CmPHR7) contain FAD cofactor in substochiometric amounts. CmPHR5 retained the highest FAD content and the MTHF photoantenna.

The flavin of CmPHR5 was obtained at three redox states due to oxidation of flavin during purification processes.

We defined two functional Cry-DASHes (CmPHR2, CmPHR5) as a result of biochemical and complementation assays.

Surprisingly in this work, a CRY-DASH (CmPHR6), having FAD without repair ability of either CPD or the [6-4] damage in both ss- and dsDNA, was identified for the first time as a member of DASH family. Since CRY–DASH are considered to be intermediate form between photolyase and cryptochromes [33, 34]. Therefore, we concluded that CmPHR6 functionally may be an evolutionarily transient form of cryptochrome.

Another contribution of this study is the discovery of a new [6-4] photolyase in a primitive eukaryotic organism. From an evolutionary point of view, it shows that even lower organisms possess not only CPD photolyase but also the [6-4] photolyase to repair their genome from the UV-induced damages in a direct and efficient way. It provides organisms to gain advantageous over other organism to preserve its genome not only intact but also from deleterious mutations.

CmPHR4 can form a separate clade by itself in evolutionary classification. CmPHR4 is assumed to be a cryptochrome since it did not complement photolyase gene *in vivo* and also it is classified in a distinct clade in the phylogenetic tree between plant cryptochromes and Type II photolyases that are mostly found in plants. Other two cryptochromes (CmPHR3 and CmPHR7) have been under investigation for blue light photoreceptive function. Blue light regulated transcriptional expression analyses of those proteins are being determined.

In summary, *C. merolae* contains multiple blue-light photoreceptors, including CRY-DASH, [6-4] photolyase, CRYs. The presence of those photoreceptors help this organism repair the UV-induced damages in their genome efficiently and adopt its behavior to aquatic environment to cope with light stress and so increase its survival fitness in a given habitat.

Lastly, in my Ph.D, I investigated and characterized seven members of PHR/CRY family in a unicellular organism called, *Cyanidioschyzon merolae*. To my knowledge, it is the first time that cryptochrome DASHes of one of the most primitive eukaryotic organism that have been published so far were identified. Interestingly, I found one cryptochrome-DASH without single strand DNA repair function that proves how functional heterogeneity exists within the same cryptochrome subfamily. The light dependent replication of *C.merolae* cells may also imply that Cm CRY-DASHes can also play role in cell and plastid division processes since cryptochrome family is the only blue light photoreceptor protein in the red algae. Such functions should be investigated at proper experimental conditions with *C.merolae* mutants.

BIBLIOGRAPHY

1. Bayram, O., et al., *More than a repair enzyme: Aspergillus nidulans photolyase-like CryA is a regulator of sexual development.* Mol Biol Cell, 2008. **19**(8): p. 3254-62.

2. Coesel, S., et al., *Diatom PtCPF1 is a new cryptochrome/photolyase family member with DNA repair and transcription regulation activity.* EMBO Rep, 2009. **10**(6): p. 655-61.

3. Heijde, M., et al., *Characterization of two members of the cryptochrome/photolyase family from Ostreococcus tauri provides insights into the origin and evolution of cryptochromes.* Plant Cell Environ, 2010. **33**(10): p. 1614-26.

4. Ulijasz, A.T., et al., *Cyanochromes are blue/green light photoreversible photoreceptors defined by a stable double cysteine linkage to a phycoviolobilin-type chromophore.* J Biol Chem, 2009. **284**(43): p. 29757-72.

5. Zoltowski, B.D. and K.H. Gardner, *Tripping the light fantastic: blue-light photoreceptors as examples of environmentally modulated protein-protein interactions.* Biochemistry, 2011. **50**(1): p. 4-16.

6. Schiffmann, R., et al., *Mucolipidosis IV*, in *GeneReviews*, R.A. Pagon, et al., Editors. 1993: Seattle (WA).

7. Svoboda, D.L., et al., *DNA repair by eukaryotic nucleotide excision nuclease. Removal of thymine dimer and psoralen monoadduct by HeLa cell-free extract and of thymine dimer by Xenopus laevis oocytes.* J Biol Chem, 1993. **268**(3): p. 1931-6.

8. Rupert, C.S., S.H. Goodgal, and R.M. Herriott, *Photoreactivation in vitro of ultraviolet-inactivated Hemophilus influenzae transforming factor.* J Gen Physiol, 1958. **41**(3): p. 451-71.

9. Setlow, R.B., W.L. Carrier, and F.J. Bollum, *Pyrimidine dimers in UV-irradiated poly dI:dC.* Proc Natl Acad Sci U S A, 1965. **53**(5): p. 1111-8.

10. Todo, T., et al., *A new photoreactivating enzyme that specifically repairs ultraviolet light-induced (6-4)photoproducts.* Nature, 1993. **361**(6410): p. 371-4.

11. Essen, L.O., *Photolyases and cryptochromes: common mechanisms of DNA repair and light-driven signaling?* Curr Opin Struct Biol, 2006. **16**(1): p. 51-9.

12. Hitomi, K., et al., *Eukaryotic class II cyclobutane pyrimidine dimer photolyase structure reveals basis for improved ultraviolet tolerance in plants.* J Biol Chem, 2012. **287**(15): p. 12060-9.

13. Okafuji, A., et al., *Light-induced activation of class II cyclobutane pyrimidine dimer photolyases.* DNA Repair (Amst), 2010. **9**(5): p. 495-505.

14. Oberpichler, I., et al., *A photolyase-like protein from Agrobacterium tumefaciens with an iron-sulfur cluster.* PLoS One, 2011. **6**(10): p. e26775.

15.   Sancar, A., K.A. Franklin, and G.B. Sancar, *Escherichia coli DNA photolyase stimulates uvrABC excision nuclease in vitro.* Proc Natl Acad Sci U S A, 1984. **81**(23): p. 7397-401.

16.   Hitomi, K., et al., *Role of two histidines in the (6-4) photolyase reaction.* J Biol Chem, 2001. **276**(13): p. 10103-9.

17.   Lin, C. and T. Todo, *The cryptochromes.* Genome Biol, 2005. **6**(5): p. 220.

18.   Nakajima, S., et al., *Cloning and characterization of a gene (UVR3) required for photorepair of 6-4 photoproducts in Arabidopsis thaliana.* Nucleic Acids Res, 1998. **26**(2): p. 638-44.

19.   Todo, T., et al., *Flavin adenine dinucleotide as a chromophore of the Xenopus (6-4)photolyase.* Nucleic Acids Res, 1997. **25**(4): p. 764-8.

20.   Yi, Y., et al., *Cloning and sequence analysis of the gene encoding (6-4)photolyase from Dunaliella salina.* Biotechnol Lett, 2006. **28**(5): p. 309-14.

21.   Todo, T., *Functional diversity of the DNA photolyase/blue light receptor family.* Mutat Res, 1999. **434**(2): p. 89-97.

22.   Briggs, W.R. and E. Huala, *Blue-light photoreceptors in higher plants.* Annu Rev Cell Dev Biol, 1999. **15**: p. 33-62.

23.   Cashmore, A.R., et al., *Cryptochromes: blue light receptors for plants and animals.* Science, 1999. **284**(5415): p. 760-5.

24.   Ahmad, M. and A.R. Cashmore, *HY4 gene of A. thaliana encodes a protein with characteristics of a blue-light photoreceptor.* Nature, 1993. **366**(6451): p. 162-6.

25.   Sancar, A., *Structure and function of DNA photolyase and cryptochrome blue-light photoreceptors.* Chem Rev, 2003. **103**(6): p. 2203-37.

26.   Thompson, C.L. and A. Sancar, *Photolyase/cryptochrome blue-light photoreceptors use photon energy to repair DNA and reset the circadian clock.* Oncogene, 2002. **21**(58): p. 9043-56.

27.   Chaves, I., et al., *The cryptochromes: blue light photoreceptors in plants and animals.* Annu Rev Plant Biol, 2011. **62**: p. 335-64.

28.   Somers, D.E., P.F. Devlin, and S.A. Kay, *Phytochromes and cryptochromes in the entrainment of the Arabidopsis circadian clock.* Science, 1998. **282**(5393): p. 1488-90.

29.   Devlin, P.F. and S.A. Kay, *Cryptochromes are required for phytochrome signaling to the circadian clock but not for rhythmicity.* Plant Cell, 2000. **12**(12): p. 2499-2510.

30.   Thresher, R.J., et al., *Role of mouse cryptochrome blue-light photoreceptor in circadian photoresponses.* Science, 1998. **282**(5393): p. 1490-4.

31.   Takahashi, J.S., et al., *The genetics of mammalian circadian order and disorder: implications for physiology and disease.* Nat Rev Genet, 2008. **9**(10): p. 764-75.

32.   Albrecht, U., *Timing to perfection: the biology of central and peripheral circadian clocks.* Neuron, 2012. **74**(2): p. 246-60.

33.   Carneiro, C., et al., *Fatigue in psoriasis with arthritis.* Skinmed, 2011. **9**(1): p. 34-7.

34.   Liedvogel, M. and H. Mouritsen, *Cryptochromes--a potential magnetoreceptor: what do we know and what do we want to know?* J R Soc Interface, 2010. **7 Suppl 2**: p. S147-62.

35.   Solov'yov, I.A. and K. Schulten, *Magnetoreception through cryptochrome may involve superoxide.* Biophys J, 2009. **96**(12): p. 4804-13.

36.   Ritz, T., S. Adem, and K. Schulten, *A model for photoreceptor-based magnetoreception in birds.* Biophys J, 2000. **78**(2): p. 707-18.

37.   Ahmad, M., et al., *Magnetic intensity affects cryptochrome-dependent responses in Arabidopsis thaliana.* Planta, 2007. **225**(3): p. 615-24.

38.   Foley, L.E., R.J. Gegear, and S.M. Reppert, *Human cryptochrome exhibits light-dependent magnetosensitivity.* Nat Commun, 2011. **2**: p. 356.

39.   Yuan, Q., et al., *Insect cryptochromes: gene duplication and loss define diverse ways to construct insect circadian clocks.* Mol Biol Evol, 2007. **24**(4): p. 948-55.

40.   Geyfman, M. and B. Andersen, *How the skin can tell time.* J Invest Dermatol, 2009. **129**(5): p. 1063-6.

41.   Lin, C. and D. Shalitin, *Cryptochrome structure and signal transduction.* Annu Rev Plant Biol, 2003. **54**: p. 469-96.

42.   Lin, C., et al., *Enhancement of blue-light sensitivity of Arabidopsis seedlings by a blue light receptor cryptochrome 2.* Proc Natl Acad Sci U S A, 1998. **95**(5): p. 2686-90.

43.   Guo, H., et al., *Regulation of flowering time by Arabidopsis photoreceptors.* Science, 1998. **279**(5355): p. 1360-3.

44.   Shalitin, D., et al., *Regulation of Arabidopsis cryptochrome 2 by blue-light-dependent phosphorylation.* Nature, 2002. **417**(6890): p. 763-7.

45.   Ninu, L., et al., *Cryptochrome 1 controls tomato development in response to blue light.* Plant J, 1999. **18**(5): p. 551-556.

46.   Hirose, F., et al., *Involvement of rice cryptochromes in de-etiolation responses and flowering.* Plant Cell Physiol, 2006. **47**(7): p. 915-25.

47.   Platten, J.D., et al., *Cryptochrome 1 contributes to blue-light sensing in pea.* Plant Physiol, 2005. **139**(3): p. 1472-82.

48.   Ahmad, M. and A.R. Cashmore, *Seeing blue: the discovery of cryptochrome.* Plant Mol Biol, 1996. **30**(5): p. 851-61.

49.   Yanovsky, M.J., M.A. Mazzella, and J.J. Casal, *A quadruple photoreceptor mutant still keeps track of time.* Curr Biol, 2000. **10**(16): p. 1013-5.

50.   Jiao, Y., et al., *A genome-wide analysis of blue-light regulation of Arabidopsis transcription factor gene expression during seedling development.* Plant Physiol, 2003. **133**(4): p. 1480-93.

51.   Kleine, T., et al., *Genome-wide gene expression analysis reveals a critical role for CRYPTOCHROME1 in the response of Arabidopsis to high irradiance.* Plant Physiol, 2007. **144**(3): p. 1391-406.

52. Yang, H.Q., R.H. Tang, and A.R. Cashmore, *The signaling mechanism of Arabidopsis CRY1 involves direct interaction with COP1.* Plant Cell, 2001. **13**(12): p. 2573-87.

53. Zuo, Z., et al., *Blue light-dependent interaction of CRY2 with SPA1 regulates COP1 activity and floral initiation in Arabidopsis.* Curr Biol, 2011. **21**(10): p. 841-7.

54. Mas, P., et al., *Functional interaction of phytochrome B and cryptochrome 2.* Nature, 2000. **408**(6809): p. 207-11.

55. Park, H.W., et al., *Crystal structure of DNA photolyase from Escherichia coli.* Science, 1995. **268**(5219): p. 1866-72.

56. Kobayashi, Y., et al., *Molecular analysis of zebrafish photolyase/cryptochrome family: two types of cryptochromes present in zebrafish.* Genes Cells, 2000. **5**(9): p. 725-38.

57. Zhu, H. and C.B. Green, *Three cryptochromes are rhythmically expressed in Xenopus laevis retinal photoreceptors.* Mol Vis, 2001. **7**: p. 210-5.

58. Rubin, E.B., et al., *Molecular and phylogenetic analyses reveal mammalian-like clockwork in the honey bee (Apis mellifera) and shed new light on the molecular evolution of the circadian clock.* Genome Res, 2006. **16**(11): p. 1352-65.

59. Zhu, H., et al., *Cryptochromes define a novel circadian clock mechanism in monarch butterflies that may underlie sun compass navigation.* PLoS Biol, 2008. **6**(1): p. e4.

60. Zhu, H., et al., *The two CRYs of the butterfly.* Curr Biol, 2005. **15**(23): p. R953-4.

61. Stanewsky, R., et al., *The cryb mutation identifies cryptochrome as a circadian photoreceptor in Drosophila.* Cell, 1998. **95**(5): p. 681-92.

62. Ceriani, M.F., et al., *Light-dependent sequestration of TIMELESS by CRYPTOCHROME.* Science, 1999. **285**(5427): p. 553-6.

63. Krishnan, B., et al., *A new role for cryptochrome in a Drosophila circadian oscillator.* Nature, 2001. **411**(6835): p. 313-7.

64. Song, S.H., et al., *Formation and function of flavin anion radical in cryptochrome 1 blue-light photoreceptor of monarch butterfly.* J Biol Chem, 2007. **282**(24): p. 17608-12.

65. Gegear, R.J., et al., *Animal cryptochromes mediate magnetoreception by an unconventional photochemical mechanism.* Nature, 2010. **463**(7282): p. 804-7.

66. Adams, M.D., et al., *Initial assessment of human gene diversity and expression patterns based upon 83 million nucleotides of cDNA sequence.* Nature, 1995. **377**(6547 Suppl): p. 3-174.

67. Hsu, D.S., et al., *Putative human blue-light photoreceptors hCRY1 and hCRY2 are flavoproteins.* Biochemistry, 1996. **35**(44): p. 13871-7.

68. Kavakli, I.H. and A. Sancar, *Circadian photoreception in humans and mice.* Mol Interv, 2002. **2**(8): p. 484-92.

69. Semo, M., et al., *Melanopsin retinal ganglion cells and the maintenance of circadian and pupillary responses to light in aged rodless/coneless (rd/rd cl) mice.* Eur J Neurosci, 2003. **17**(9): p. 1793-801.

70. van der Horst, G.T., et al., *Mammalian Cry1 and Cry2 are essential for maintenance of circadian rhythms.* Nature, 1999. **398**(6728): p. 627-30.

71. Sancar, A., *Regulation of the mammalian circadian clock by cryptochrome.* J Biol Chem, 2004. **279**(33): p. 34079-82.

72. Green, C.B., J.S. Takahashi, and J. Bass, *The meter of metabolism.* Cell, 2008. **134**(5): p. 728-42.

73. Yagita, K., et al., *Nucleocytoplasmic shuttling and mCRY-dependent inhibition of ubiquitylation of the mPER2 clock protein.* EMBO J, 2002. **21**(6): p. 1301-14.

74. Ozturk, N., et al., *Structure and function of animal cryptochromes.* Cold Spring Harb Symp Quant Biol, 2007. **72**: p. 119-31.

75. Sancar, A., et al., *Circadian clock control of the cellular response to DNA damage.* FEBS Lett, 2010. **584**(12): p. 2618-25.

76. Daiyasu, H., et al., *Identification of cryptochrome DASH from vertebrates.* Genes Cells, 2004. **9**(5): p. 479-95.

77. Brudler, R., et al., *Identification of a new cryptochrome class. Structure, function, and evolution.* Mol Cell, 2003. **11**(1): p. 59-67.

78. Komori, H., et al., *Crystal structure of thermostable DNA photolyase: pyrimidine-dimer recognition mechanism.* Proc Natl Acad Sci U S A, 2001. **98**(24): p. 13560-5.

79. Sokolowsky, K., et al., *Spectroscopic and thermodynamic comparisons of Escherichia coli DNA photolyase and Vibrio cholerae cryptochrome 1.* J Phys Chem B, 2010. **114**(20): p. 7121-30.

80. Selby, C. and A. Sancar, *A cryptochrome/photolyase class of enzymes with single-stranded DNA-specific photolyase activity.* Proc Natl Acad Sci USA, 2006. **103**: p. 17696-17700.

81. Veluchamy, S. and J.A. Rollins, *A CRY-DASH-type photolyase/cryptochrome from Sclerotinia sclerotiorum mediates minor UV-A-specific effects on development.* Fungal Genet Biol, 2008. **45**(9): p. 1265-76.

82. Berrocal-Tito, G.M., et al., *Trichoderma atroviride PHR1, a fungal photolyase responsible for DNA repair, autoregulates its own photoinduction.* Eukaryot Cell, 2007. **6**(9): p. 1682-92.

83. Bluhm, B.H. and L.D. Dunkle, *PHL1 of Cercospora zeae-maydis encodes a member of the photolyase/cryptochrome family involved in UV protection and fungal development.* Fungal Genet Biol, 2008. **45**(10): p. 1364-72.

84. Hellingwerf, K.J., W.D. Hoff, and W. Crielaard, *Photobiology of microorganisms: how photosensors catch a photon to initialize signalling.* Mol Microbiol, 1996. **21**(4): p. 683-93.

85. Steglich, C., et al., *Genome-wide analysis of light sensing in Prochlorococcus.* J Bacteriol, 2006. **188**(22): p. 7796-806.

86.   Ozturk, N., et al., *Purification and characterization of a type III photolyase from Caulobacter crescentus.* Biochemistry, 2008. **47**(39): p. 10255-61.

87.   Hendrischk, A.K., et al., *A cryptochrome-like protein is involved in the regulation of photosynthesis genes in Rhodobacter sphaeroides.* Mol Microbiol, 2009. **74**(4): p. 990-1003.

88.   Fujihashi, M., et al., *Crystal structure of archaeal photolyase from Sulfolobus tokodaii with two FAD molecules: implication of a novel light-harvesting cofactor.* J Mol Biol, 2007. **365**(4): p. 903-10.

89.   Tamada, T., et al., *Crystal structure of DNA photolyase from Anacystis nidulans.* Nat Struct Biol, 1997. **4**(11): p. 887-91.

90.   Mees, A., et al., *Crystal structure of a photolyase bound to a CPD-like DNA lesion after in situ repair.* Science, 2004. **306**(5702): p. 1789-93.

91.   Deisenhofer, J., *DNA photolyases and cryptochromes.* Mutat Res, 2000. **460**(3-4): p. 143-9.

92.   Huang, Y., et al., *Crystal structure of cryptochrome 3 from Arabidopsis thaliana and its implications for photolyase activity.* Proc Natl Acad Sci U S A, 2006. **103**(47): p. 17701-6.

93.   Brautigam, C.A., et al., *Structure of the photolyase-like domain of cryptochrome 1 from Arabidopsis thaliana.* Proc Natl Acad Sci U S A, 2004. **101**(33): p. 12142-7.

94.   Bouly, J.P., et al., *Novel ATP-binding and autophosphorylation activity associated with Arabidopsis and human cryptochrome-1.* Eur J Biochem, 2003. **270**(14): p. 2921-8.

95.   Zoltowski, B.D., et al., *Structure of full-length Drosophila cryptochrome.* Nature, 2011. **480**(7377): p. 396-9.

96.   Hitomi, K., et al., *Functional motifs in the (6-4) photolyase crystal structure make a comparative framework for DNA repair photolyases and clock cryptochromes.* Proc Natl Acad Sci U S A, 2009. **106**(17): p. 6962-7.

97.   Glas, A.F., et al., *Crystal structure of the T(6-4)C lesion in complex with a (6-4) DNA photolyase and repair of UV-induced (6-4) and Dewar photolesions.* Chemistry, 2009. **15**(40): p. 10387-96.

98.   Maul, M.J., et al., *Crystal structure and mechanism of a DNA (6-4) photolyase.* Angew Chem Int Ed Engl, 2008. **47**(52): p. 10076-80.

99.   Busza, A., et al., *Roles of the two Drosophila CRYPTOCHROME structural domains in circadian photoreception.* Science, 2004. **304**(5676): p. 1503-6.

100.   Pokorny, R., et al., *Recognition and repair of UV lesions in loop structures of duplex DNA by DASH-type cryptochrome.* Proc Natl Acad Sci U S A, 2008. **105**(52): p. 21023-7.

101.   Klar, T., et al., *Cryptochrome 3 from Arabidopsis thaliana: structural and functional analysis of its complex with a folate light antenna.* J Mol Biol, 2007. **366**(3): p. 954-64.

102. Ueda, T., et al., *Identification and characterization of a second chromophore of DNA photolyase from Thermus thermophilus HB27.* J Biol Chem, 2005. **280**(43): p. 36237-43.

103. Payne, G., et al., *The active form of Escherichia coli DNA photolyase contains a fully reduced flavin and not a flavin radical, both in vivo and in vitro.* Biochemistry, 1987. **26**(22): p. 7121-7.

104. Wang, H., et al., *Femtosecond dynamics of flavin cofactor in DNA photolyase: radical reduction, local solvation, and charge recombination.* J Phys Chem B, 2005. **109**(4): p. 1329-33.

105. Liu, Z., et al., *Dynamics and mechanism of cyclobutane pyrimidine dimer repair by DNA photolyase.* Proc Natl Acad Sci U S A, 2011. **108**(36): p. 14831-6.

106. Zhao, X., et al., *Reaction mechanism of (6-4) photolyase.* J Biol Chem, 1997. **272**(51): p. 32580-90.

107. Hitomi, K., et al., *Binding and catalytic properties of Xenopus (6-4) photolyase.* J Biol Chem, 1997. **272**(51): p. 32591-8.

108. Li, J., et al., *Dynamics and mechanism of repair of ultraviolet-induced (6-4) photoproduct by photolyase.* Nature, 2010. **466**(7308): p. 887-890.

109. Weber, S., *Light-driven enzymatic catalysis of DNA repair: a review of recent biophysical studies on photolyase.* Biochim Biophys Acta, 2005. **1707**(1): p. 1-23.

110. Donahue, B.A., et al., *Transcript cleavage by RNA polymerase II arrested by a cyclobutane pyrimidine dimer in the DNA template.* Proc Natl Acad Sci U S A, 1994. **91**(18): p. 8502-6.

111. Hanawalt, P.C., *Transcription-coupled repair and human disease.* Science, 1994. **266**(5193): p. 1957-8.

112. Otoshi, E., et al., *Respective roles of cyclobutane pyrimidine dimers, (6-4)photoproducts, and minor photoproducts in ultraviolet mutagenesis of repair-deficient xeroderma pigmentosum A cells.* Cancer Res, 2000. **60**(6): p. 1729-35.

113. Sancar, A., et al., *Photolyase/cryptochrome family blue-light photoreceptors use light energy to repair DNA or set the circadian clock.* Cold Spring Harb Symp Quant Biol, 2000. **65**: p. 157-71.

114. Li, Q.H. and H.Q. Yang, *Cryptochrome signaling in plants.* Photochem Photobiol, 2007. **83**(1): p. 94-101.

115. Kleine, T., P. Lockhart, and A. Batschauer, *An Arabidopsis protein closely related to Synechocystis cryptochrome is targeted to organelles.* Plant J, 2003. **35**(1): p. 93-103.

116. Saxena, C., et al., *Ultrafast dynamics of resonance energy transfer in cryptochrome.* J Am Chem Soc, 2005. **127**(22): p. 7984-5.

117. Sancar, G.B. and A. Sancar, *Purification and characterization of DNA photolyases.* Methods Enzymol, 2006. **408**: p. 121-56.

118. Ritzefeld, M. and N. Sewald, *Real-Time Analysis of Specific Protein-DNA Interactions with Surface Plasmon Resonance.* J Amino Acids, 2012. **2012**: p. 816032.

119. Myszka, D.G., M.D. Jonsen, and B.J. Graves, *Equilibrium analysis of high affinity interactions using BIACORE.* Anal Biochem, 1998. **265**(2): p. 326-30.
120. Schaufler, L.E. and R.E. Klevit, *Mechanism of DNA binding by the ADR1 zinc finger transcription factor as determined by SPR.* J Mol Biol, 2003. **329**(5): p. 931-939.
121. Swinney, D.C., *Biochemical mechanisms of drug action: what does it take for success?* Nat Rev Drug Discov, 2004. **3**(9): p. 801-8.
122. Worthington, E.N., et al., *Purification and characterization of three members of the photolyase/cryptochrome family blue-light photoreceptors from Vibrio cholerae.* J Biol Chem, 2003. **278**(40): p. 39143-54.
123. Smith, C.A. and J.S. Taylor, *Preparation and characterization of a set of deoxyoligonucleotide 49-mers containing site-specific cis-syn, trans-syn-I, (6-4), and Dewar photoproducts of thymidylyl(3'-->5')-thymidine.* J Biol Chem, 1993. **268**(15): p. 11143-51.
124. Selby, C.P. and A. Sancar, *A cryptochrome/photolyase class of enzymes with single-stranded DNA-specific photolyase activity.* Proc Natl Acad Sci U S A, 2006. **103**(47): p. 17696-700.
125. Pfeifer, G.P., *Formation and processing of UV photoproducts: effects of DNA sequence and chromatin environment.* Photochem Photobiol, 1997. **65**(2): p. 270-83.
126. You, Y.H., et al., *Cyclobutane pyrimidine dimers are responsible for the vast majority of mutations induced by UVB irradiation in mammalian cells.* J Biol Chem, 2001. **276**(48): p. 44688-94.
127. Asimgil, H. and I.H. Kavakli, *Purification and characterization of five members of photolyase/cryptochrome family from Cyanidioschyzon merolae.* Plant Sci, 2012. **185-186**: p. 190-8.
128. Rich, R.L. and D.G. Myszka, *Advances in surface plasmon resonance biosensor analysis.* Curr Opin Biotechnol, 2000. **11**(1): p. 54-61.
129. Day, Y.S. and D.G. Myszka, *Characterizing a drug's primary binding site on albumin.* J Pharm Sci, 2003. **92**(2): p. 333-43.
130. Henn, C., et al., *Catalytic enzyme activity on a biosensor chip: combination of surface plasmon resonance and mass spectrometry.* Anal Biochem, 2012. **428**(1): p. 28-30.
131. Sancar, G.B., F.W. Smith, and A. Sancar, *Binding of Escherichia coli DNA photolyase to UV-irradiated DNA.* Biochemistry, 1985. **24**(8): p. 1849-55.
132. Boon, E.M., J.E. Salas, and J.K. Barton, *An electrical probe of protein-DNA interactions on DNA-modified surfaces.* Nat Biotechnol, 2002. **20**(3): p. 282-6.
133. Fox, M.E., B.J. Feldman, and G. Chu, *A novel role for DNA photolyase: binding to DNA damaged by drugs is associated with enhanced cytotoxicity in Saccharomyces cerevisiae.* Mol Cell Biol, 1994. **14**(12): p. 8071-7.
134. Yang, K., S. Matsika, and R.J. Stanley, *6MAP, a fluorescent adenine analogue, is a probe of base flipping by DNA photolyase.* J Phys Chem B, 2007. **111**(35): p. 10615-25.

135.   Chen, C.F., et al., *Auditory P300, CT scans and cognitive state in Binswanger's disease.* Chin J Physiol, 1997. **40**(1): p. 19-24.

136.   Husain, I., et al., *Mechanism of damage recognition by Escherichia coli DNA photolyase.* J Biol Chem, 1987. **262**(27): p. 13188-97.

137.   Zikihara, K., et al., *Involvement of electron transfer in the photoreaction of zebrafish Cryptochrome-DASH.* Photochem Photobiol, 2008. **84**(4): p. 1016-23.

138.   Kottke, T., et al., *Blue-light-induced changes in Arabidopsis cryptochrome 1 probed by FTIR difference spectroscopy.* Biochemistry, 2006. **45**(8): p. 2472-9.

139.   Song, S.H., et al., *Absorption and fluorescence spectroscopic characterization of cryptochrome 3 from Arabidopsis thaliana.* J Photochem Photobiol B, 2006. **85**(1): p. 1-16.

140.   Berndt, A., et al., *A novel photoreaction mechanism for the circadian blue light photoreceptor Drosophila cryptochrome.* J Biol Chem, 2007. **282**(17): p. 13011-21.

141.   Ozgur, S. and A. Sancar, *Purification and properties of human blue-light photoreceptor cryptochrome 2.* Biochemistry, 2003. **42**(10): p. 2926-32.

142.   Petersen, J.L., D.W. Lang, and G.D. Small, *Cloning and characterization of a class II DNA photolyase from Chlamydomonas.* Plant Mol Biol, 1999. **40**(6): p. 1063-71.

143.   Matsuzaki, M., et al., *Genome sequence of the ultrasmall unicellular red alga Cyanidioschyzon merolae 10D.* Nature, 2004. **428**(6983): p. 653-7.

144.   Nozaki, H., et al., *A 100%-complete sequence reveals unusually simple genomic features in the hot-spring red alga Cyanidioschyzon merolae.* BMC Biol, 2007. **5**: p. 28.

145.   Fujiwara, T., et al., *Periodic gene expression patterns during the highly synchronized cell nucleus and organelle division cycles in the unicellular red alga Cyanidioschyzon merolae.* DNA Res, 2009. **16**(1): p. 59-72.

146.   Nishida, K., et al., *Cell cycle-regulated, microtubule-independent organelle division in Cyanidioschyzon merolae.* Mol Biol Cell, 2005. **16**(5): p. 2493-502.

147.   Koichiro Tamura, D.P., Nicholas Peterson, Glen Stecher, Masatoshi Nei and Sudhir Kumar. *MOLECULAR EVOLUTIONARY GENETICS ANALYSIS*. 1993-2012 2008-03-11].

148.   Johnson, J.L., et al., *Identification of the second chromophore of Escherichia coli and yeast DNA photolyases as 5,10-methenyltetrahydrofolate.* Proc Natl Acad Sci U S A, 1988. **85**(7): p. 2046-50.

149.   Joe Sambrook, D.W.R., *Molecular Cloning: A Laboratory Manual*. 3rd ed. Vol. 1. 1989: Cold Spring Harbor, N.Y.

150.   http://merolae.biol.s.u-tokyo.ac.jp/. *Cyanidioschyzon merolae Genome Project*. 2008-06-04 10:06:30 JST 2008-02-12].

151.   Sancar, A., F.W. Smith, and G.B. Sancar, *Purification of Escherichia coli DNA photolyase.* J Biol Chem, 1984. **259**(9): p. 6028-32.

152.   Hara, R., J. Mo, and A. Sancar, *DNA damage in the nucleosome core is refractory to repair by human excision nuclease.* Mol Cell Biol, 2000. **20**(24): p. 9173-81.

153.   Partch, C.L. and A. Sancar, *Cryptochromes and circadian photoreception in animals.* Methods Enzymol, 2005. **393**: p. 726-45.
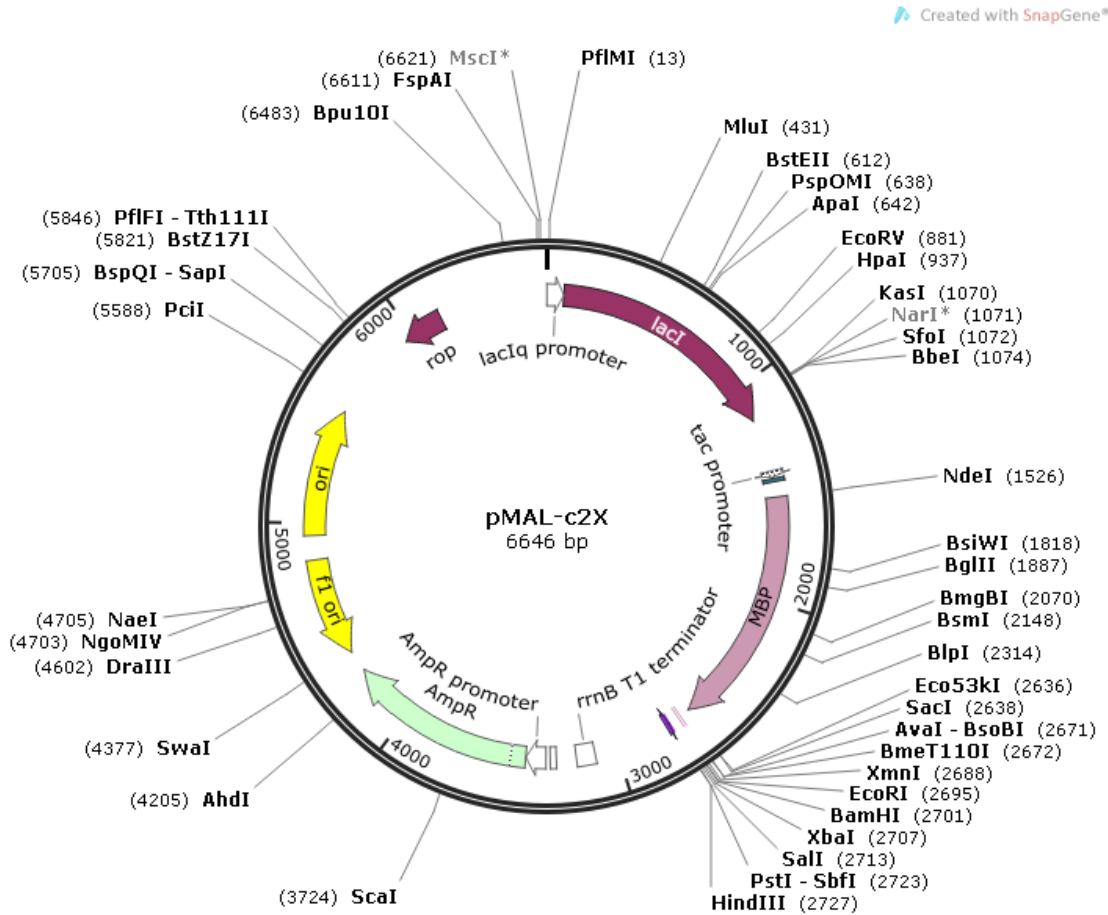
CURRICULUM VITAE

Hande Asimgil was born in Istanbul, Turkey, on March 6, 1980. She received her B.Sc. degree in Food Engineering from Middle East Techical University, Ankara in 2002. She received her M.Sc degree in Molecular Biology and Genetics from Istanbul Technical University (ITU) in 2006. She also worked as a teaching and research assistant at ITU. From September 2007 to December 2012, she worked as teaching and research assistant at Koç University. She worked on several projects during her Ph.D study funded by TUBITAK entitled as "Structure and function of Cryptochrome", Career Project, funded by TUBİTAK-212 (08/2006-02/2010), "Detection of interaction constants between biological clock proteins by Surface Plasmon Resonance" funded by TUBITAK-110T423 (01/2011-10/2012), *KU and "*Function of blue light photoreceptor Cryptochrome in Red Algae *Cyanidioschyzon merolae*" funded by TUBITAK-(04/2011-05/2014), KU. She has published articles in prestigious journals such as Plant Science and PLOS ONE.
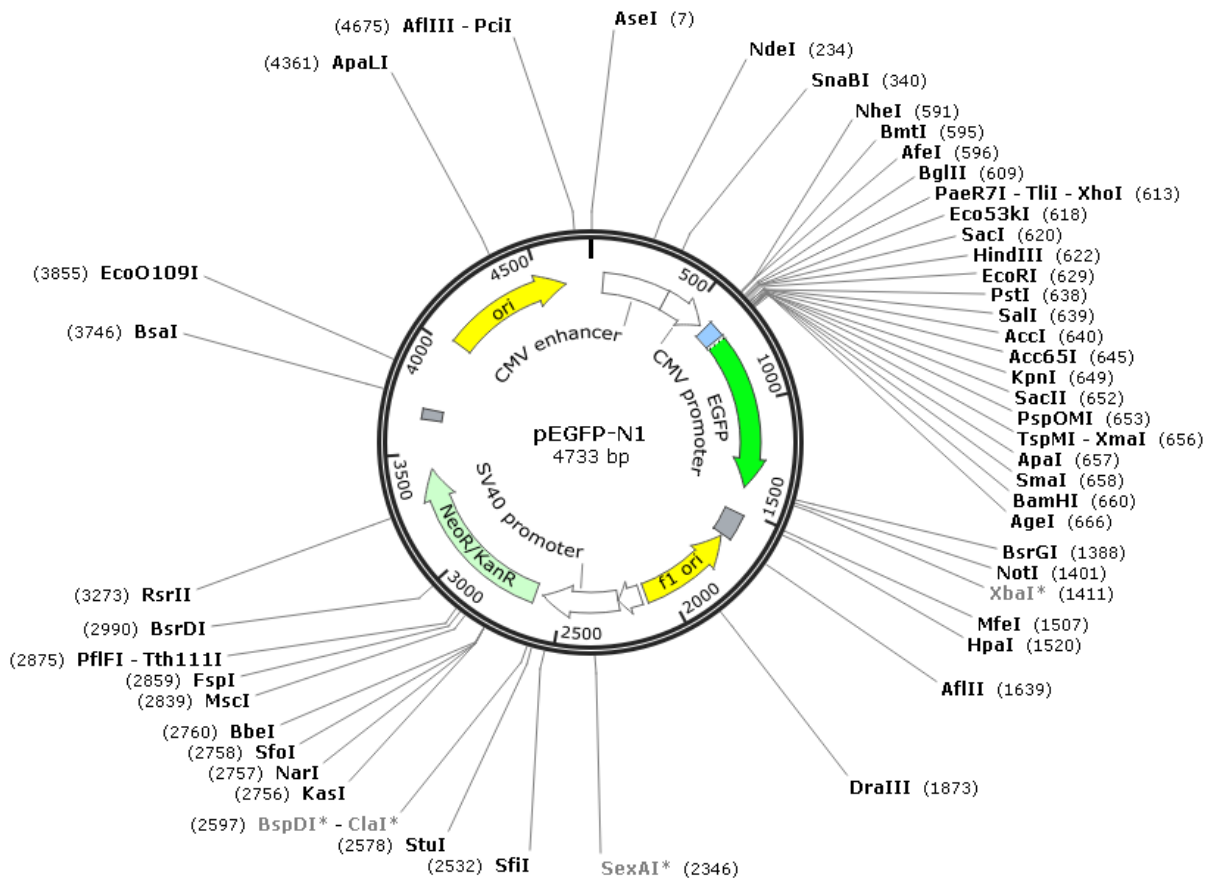
She will continue her academic career as a Postdoctoral Associate in Chemical and Biological Engineering Department at Koç University where she will focus to identify novel transcription factors that regulates circadian rhythm in human.

She plays tennis and she is also a former member of Turkish National Tennis Team.

Appendix A: Map of Expression Vectors

Created with SnapGene®

(4675) **AflIII - PciI**

(4361) **ApaLI**

AseI (7)

NdeI (234)

SnaBI (340)

NheI (591)
BmtI (595)
AfeI (596)
BglII (609)
PaeR7I - TliI - XhoI (613)
Eco53kI (618)
SacI (620)
HindIII (622)
EcoRI (629)
PstI (638)
SalI (639)
AccI (640)
Acc65I (645)
KpnI (649)
SacII (652)
PspOMI (653)
TspMI - XmaI (656)
ApaI (657)
SmaI (658)
BamHI (660)
AgeI (666)

BsrGI (1388)
NotI (1401)
XbaI* (1411)
MfeI (1507)
HpaI (1520)

AflII (1639)

(3855) **EcoO109I**

(3746) **BsaI**

ori

CMV enhancer

EGFP
CMV promoter

pEGFP-N1
4733 bp

SV40 promoter

NeoR/KanR

f1 ori

4500
5000
1000
1500
2000
2500
3000
3500
4000

(3273) **RsrII**

(2990) **BsrDI**

(2875) **PflFI - Tth111I**
(2859) **FspI**
(2839) **MscI**

(2760) **BbeI**
(2758) **SfoI**
(2757) **NarI**
(2756) **KasI**

(2597) BspDI* - ClaI*
(2578) **StuI**
(2532) **SfiI**

SexAI* (2346)

DraIII (1873)

Appendix B: DNA and Protein Markers

DNA Molecular Weight Marker

GeneRuler™ 1 kb DNA Ladder
O'GeneRuler™ 1 kb DNA Ladder, ready-to-use

bp	ng/0.5 µg	%
10000	30.0	6.0
8000	30.0	6.0
6000	70.0	14.0
5000	30.0	6.0
4000	30.0	6.0
3500	30.0	6.0
3000	70.0	14.0
2500	25.0	5.0
2000	25.0	5.0
1500	25.0	5.0
1000	60.0	12.0
750	25.0	5.0
500	25.0	5.0
250	25.0	5.0

1% TopVision™ LE GQ Agarose (#R0491)

0.5 µg/lane, 8 cm length gel,
1X TAE, 7 V/cm, 45 min
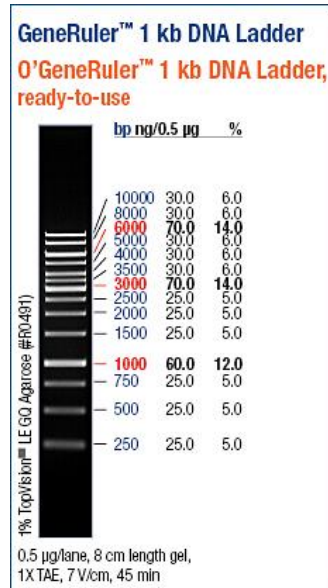
The ladder is a mixture of chromatography-purified individual DNA fragments.

PageRuler Prestained Protein Ladders

kDa
~170
~130
~100
~70
~55
~40
~35
~25
~15
~10

Gel | Blot

4-20% Tris-glycine SDS-PAGE
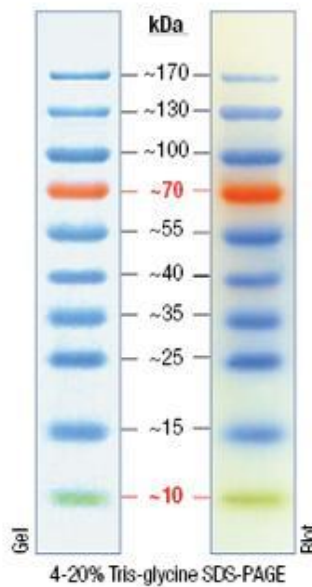
Protein Molecular Weight Marker

Appendix C: Lab Equipments

Autoclaves	: CL-40S/SDP (60L) ALP autoclave
Centrifuges	: 4K15, Sigma Laboratory
	: Microfuge 14-15, Sigma Laboratory
Deep freezes and refrigerators	: Heto Polar Bear 4410 ultra freezer, JOUAN Nordic A/S, catalog# 003431.
	: 2021 D deep freezer, Arcelik.
	: 1061 M refrigerator, Arcelik.
Electrophoresis equipments	: E-C Mini Cell Primo EC320, E-C Apparatus.
	: Mini-PROTEAN 3 Cell and Single-Row AnyGel Stand, Catalog# 165-3321,Bio-Rad.
Gel documentation system	: UVIpro GAS7000, UVItec Limited.
Ice Machine	: AF 10, Scotsman.
Shaker	: Innova 4300 incubator shaker
Magnetic stirrer	: Heidolph MR 3001
Pipettes	: Pipetteman P10, P 100, P1000, Eppendorf
pH meter	: Inolab pH level 1, order# 1A10-1113,
Power supply	: PowerPac Basic (300V,400mA,75W) Biorad
Pure water systems	: DV25 PureLab Option ELGA
Spectrophotometer	: W-1700 PharmaSpec, Shimadzu Corporation.
Vortexing machine	: Reax Top, Heidolph2.2.